STABILITY ANALYSIS OF INDIAN SUMMER MONSOON FLOW

AND

MECHANISMS OF THE GROWTH OF MONSOON DEPRESSIONS

A THESIS SUBMITTED FOR

THE DEGREE OF

DOCTOR OF PHILOSOPHY

OF THE

GUJARAT UNIVERSITY

BY

SUSHIL KUMAR DASH

PHYSICAL RESEARCH LABORATORY

AHMEDABAD 380 009

FEBRUARY 1982

TO

MY PARENTS

CERTIFICATE

I hereby declare that the work presented in this Thesis is original and has not formed the basis for the award of any degree or diploma by any University or Institution.

Sushil Kumar Dash

SUSHIL KUMAR DASH
(Author)

Certified by:

R N Keshavamurty

R.N. KESHAVAMURTY
(Professor-in-charge)

Ahmedabad

February 24, 1982

ACKNOWLEDGEMENTS

The research presented in this Thesis has been carried out under the valuable and expert guidance of Professor R.N. Keshavamurty. I wish to express here my deep sense of gratitude to him for his keen interest in my progress and his encouragement in my endeavours. I am also grateful to him for his critical reading of the manuscript and constructive comments.

I am very grateful to Professor P.R. Pisharoty with whom I had a number of helpful and illuminating discussions. I am also grateful to Professor S.P. Pandya for his kind interest and encouragement during the course of this research.

My sincere thanks are due to Dr. Man-Kin Mak for his valuable suggestions during his visit to the Physical Research Laboratory. My heartfelt thanks are also due to Drs. V. Satyan, B.N. Goswami and H.S.S. Sinha for the many useful discussions I had with them.

My sincere thanks are due to Professors R.V. Pratap B. Buti, R.K. Varma, J.C. Parikh, K.H. Bhatt, A. Sen, A.C. Das, A.K. Sundaram, S.B. Khadkikar and to Drs. A.R. Prasanna and V.B. Sheorey. I acknowledge here the fruitful discussions I had with some of them.

During the preparation of this Thesis, I have been helped in a number of ways by Dr.N.N. Rao and

D.N. Patro. I wish to express here my thanks and appreciations to them. My sincere thanks are also due to Drs. Surjalal Sharma, Mannil Mohan, Kamalesh Kar, A.K. Ambastha, Rhama Venkataraman and Aswin Oza, D.K. Chakraborty, A.K. Choudhary, Aparna, Manab, Avinash, Harish,, Nautiyal, Kailash, Usha, Chitra, Subbaraman, Vishnu Mayya, S.V. Kasture and V.T. Viswanathan for their co-operation and help.

I express my heartfelt thanks to Mr. P.S. Shah and his colleagues for providing the computer facilities; Mrs. R.R. Bharucha, Mrs. Urmila Ghiya, Miss Swadha Majmudar and their colleagues for providing the library services; Mr. Shanti K. Bhavsar for neat copying of the diagrams and Mr. Nayan D. Dave and Mr. D.R. Ranpura for preparing excellent photographs of diagrams.

I gratefully acknowledge the help rendered by Mr. P.P. Narayanan for his timely and prompt typing of the Thesis with personal care. Thanks are also due to Mr. Babulal Bramhabhatt for neat cyclostyling of the Thesis.

I am greatly indebted to the University Grants Commission, India for the award of Teacher Fellowship which enabled me to carry out this research at the Physical Research Laboratory, Ahmedabad. I am also thankful to the Principal and Secretary of Stewart Science College, Cuttack to allow me to stay on leave which enabled

me to complete this Thesis.

Shefali has come in my life at the right moment of this research. Her constant companionship and warm encouragement has helped me a lot in completing this research and the Thesis writing in time. It's a pleasure to thank her here.

No list of acknowledgement is ever complete nor what is expressed ever adequate. To all who have helped me in various ways I offer my heartfelt thanks.

ABSTRACT OF THE THESIS

The low pressure systems which form over north Bay of Bengal during monsoon months are the main producing systems of the monsoon. These disturbances, to a large extent, control the rainfall over the central parts of India. The importance of monsoon rainfall and hence that of monsoon disturbances in agriculture is well known. As scientific problems in atmospheric physics, the mechanisms of formation and growth of these disturbances are at once fascinating and challenging. We propose to study these as problems of stability of the mean monsoon flow.

A number of investigations have been conducted on the stability of monsoon zonal flow. Instability studies of Mak (1975), Shukla (1977, 1978), Brode and Mak (1978), Keshavamurty et al. (1978), Keshavamurty et al. (1980), Satyan et al. (1980), Goswami et al. (1980) and Mishra and Salvekar (1980) are a few to mention. For mathematical simplicity in all these studies the basic state is idealized to be zonally uniform (independent of longitude). But the observed monsoon flow varies with longitude. It is our main objective to consider a more realistic monsoon flow by including the zonal non-uniformity in the stability analysis and to examine whether it

explains any hitherto unexplained phenomenon. This study gives the clue as to why the monsoon cyclogenesis is localised over eastern India. We consider a zonally non-uniform flow by superposing a finite amplitude stationary Rossby wave on the monsoon zonal flow.

We have also conducted systematic studies on the stability of monsoon zonal flow incorporating Ekman layer friction and latent heating. The method of analysis is quite different from earlier stability analyses. The zonal winds and the meridional dependence of geopotential perturbation are expressed by simple trigonometric series. By this approach to the stability analysis one does not have to depend on numerical techniques and the time taken on the computer is also reduced.

Stability analyses of the monsoon zonal flow:

Since the monsoon zonal flow has appreciable horizontal shear, a perturbation may grow by drawing on the kinetic energy of the basic flow. We have examined the role of barotropic instability in the growth of monsoon disturbances in Chapter 2 by conducting such analysis of July mean monsoon flow at 700 mb and 200 mb along 80°E longitude. A channel from 5°N to 30°N is

chosen with the beta-plane centred at the middle. The observed winds are accurately represented by Fourier Series. The meridional dependence of the geopotential perturbation is expressed by trigonometric series satisfying appropriate boundary conditions.

From the barotropic stability analysis it is found that the zonal currents at 700 mb and 200 mb yield slowly growing modes. The fastest growing mode at 700 mb has a horizontal scale of 2300 km, a doubling time of 8 days and an eastward phase speed of 2.5 m s^{-1}. The slow growth rates are perhaps due to small horizontal wind shears. They may grow much faster during strong monsoon epochs. At both the levels the amplitudes of disturbances are maximum around 21°N latitude.

In addition to the horizontal shear the zonal wind is observed to have vertical shear. Thus the available potential energy of the basic flow can also be a source for disturbances. In Chapter 3 both the wind shears are included while doing the stability analysis. Cumulus heating is also included in the model and the analysis is extended to five level model.

We start the combined barotropic-baroclinic stability analysis with a two-level quasi-geostrophic model. Using the linearised potential vorticity equations at 200 mb

and 700 mb and expressing the observed winds and the meridional dependence of the geopotential perturbation by trigonometric series the problem is reduced to an eigenvalue problem. This analysis yields no lower tropospheric growing mode with appreciable growth rate. However, perturbations at 200 mb grow slowly with doubling time of 9 days and with westward phase speed of 17 m s^{-1}. These rapidly propagating disturbances possibly correspond to easterly waves one observes in the upper troposphere. When Ekman layer friction is not included in the model, the growth rate is found to increase to 5 days at 200 mb.

We have also studied the effect of inclusion of cumulus heating into the two-level model. It is not our intention to carry out detailed parameterisation of cumulus heating. It is our object to study the effect of inclusion of a simple form of heating on the growth of these disturbances. Following Charney and Eliassen (1964) we have specified the convective heating only at the mid-tropospheric level. So far as the upper tropospheric disturbances are concerned, their characteristics are hardly affected by the cumulus heating. However, with the inclusion of heating into the model, lower tropospheric growing modes appear. Stability analyses are done with two different values of heating co-efficient. The amplitude

distributions show that the disturbances are mainly confined to the lower troposphere. The fastest growing disturbance has a scale length of 2400 km, doubling time of 2 days and eastward phase speed of 2.5 m s^{-1}. When the frictional dissipation is neglected the growth rates of disturbances are increased, but there is no preferred scale for the fastest growing disturbance. Thus combined barotropic-baroclinic stability analysis of monsoon zonal flow incorporating a simple form of cumulus heating yields growing modes which resemble monsoon disturbances.

The stability analysis is also extended to a five-level quasi-geostrophic model in order to have greater vertical resolution. In the absence of actual vertical distribution of heating we have experimented with three different types of distribution function. The total heating in each case is the same. As the level of maximum heating is raised the fastest growing disturbance is found to occur at higher levels. The fastest growing disturbance is confined to the lower troposphere when the heating is maximum at 600 mb or at 500 mb. These disturbances have doubling time of 1.5 days and they move eastward with phase speed of 2 m s^{-1}. Unlike in the two-level model the doubling time hardly changes with the horizontal scale of the disturbance.

Stability of a stationary Rossby wave embedded in the monsoon zonal flow:

In the earlier stability analyses the basic flow was assumed to be zonally uniform. The stability of a flow pattern which varies with longitude can be carried out by superimposing a finite amplitude Rossby wave on the zonal flow (Lorenz, 1972). The purpose of Chapter 4 is to investigate the stability of monsoon zonal flow (with vertical shear) with a finite amplitude stationary baroclinic Rossby wave embedded in it. A two-level quasi-geostrophic model is used with a beta-plane centred at 18°N latitude. Calculations show that the realistic winds in the monsoon atmosphere can sustain a finite amplitude baroclinic stationary Rossby wave of wavelength about 30° longitude and the amplitude of the Rossby wave is mainly confined to the lower troposphere with a very small value in the upper troposphere. Such a stationary wave is observed over Bay of Bengal. These stationary waves can probably be induced by orographic influences, like the presence of Western Ghats over peninsular India. Gadgil (1977) has shown that the stationary wave over Bay of Bengal may be induced by the topography of peninsular India.

We studied stability of the above mentioned stationary Rossby wave embedded in the monsoon zonal flow

to small perturbations. Our analysis shows that the stationary Rossby wave is unstable. The growth rates of disturbances increase with the meridional velocity (amplitude). For each value of amplitude there is a minimum value of doubling time. When the amplitude is less than 9 m s^{-1} no disturbance grows. The doubling time of about 3 days corresponding to meridional velocity of 10 m s^{-1} is a reasonable doubling time for monsoon disturbances. Energy calculations show that the disturbance gets maximum energy from the kinetic energy of the basic wave. These growing modes are Rossby modes and they are almost stationary. Thus it is found from the analysis that the disturbances are stationary and grow with doubling time of 3 days. This may explain as to why the monsoon cyclogenesis is localised over eastern India. We have thus found a new mechanism for the formation of monsoon disturbances.

With a view to examine the role of baroclinicity in the growth of perturbations the stability analysis is also conducted in Chapter 5 by making the vertical wind shear zero. The growth rates of disturbances are found to increase in the absence of vertical wind shear.

In Chapter 6 we have re-examined the stability of the above mentioned stationary Rossby wave superposed on the monsoon zonal flow by retaining the divergence terms in

the basic equations. Hence, we use the two-level primitive equation model. In this system of equations the sound wave solutions are filtered, but the inertia-gravity waves are still there. This analysis yields two distinct types of growing modes. The Rossby modes, with frequencies much less than the coriolis parameter grow with almost the same doubling time as in the case of the earlier quasi-geostrophic model. These growing modes are almost stationary and the fastest mode has doubling time of about 3 days. Thus the characteristics of the Rossby modes do not change very much when we go to the primitive equation model. In addition to Rossby modes we find inertia-gravity modes whose frequencies are higher than or comparable to the coriolis parameter. The inertia-gravity modes also grow, but there is no preferred scale with maximum growth rate. The growth rate increases with the wavelength of the disturbance. This finding is of intriguing significance for numerical weather prediction where we generally try to eliminate gravity waves.

In Chapters 4, 5 and 6 the zonal wave numbers of the perturbation fields were restricted to be the multiples of the zonal wave number k_0 of the basic Rossby wave by taking $k = 0$. In Chapter 7 we intend to have a more general perturbation zonal wave number. We take $k = -k_0/2$ so that the condition for resonant interaction is satisfied.

The studies of previous three chapters reveal that the two-level primitive equation model does not yield any additional information regarding the Rossby modes. Hence we confine the present study to two-level quasi-geostrophic model only.

It is found that the Rossby modes grow, but the growth rate is slowed down compared to the case $k = 0$. Also the value of meridional velocity required for the growth of perturbation is more than in the previous case. This is also a significant finding.

By these studies of stability analyses of monsoon flows with horizontal and vertical shear, with cumulus heating and with a superposed stationary Rossby wave we have found out the dominant mechanisms of formation of monsoon disturbances. These are:

(i) combined barotropic-baroclinic instability of the zonal flow in the presence of cumulus heating and

(ii) instability of stationary Rossby wave superposed on the zonal flow.

CONTENTS

CHAPTER ONE

INTRODUCTION

The normal monsoon wind is observed to be westerly in the lower troposphere (Fig.1) and easterly in the upper troposphere (Fig.2). These winds are accompanied by cyclonic disturbances which form over north Bay of Bengal and move westnorthwestwards over central and north India. The pronounced rainfall over India is attributed to these monsoon disturbances. The mechanisms of formation and growth of these systems are among the most important scientific problems in atmospheric physics. We propose to study these as problems of stability of the mean

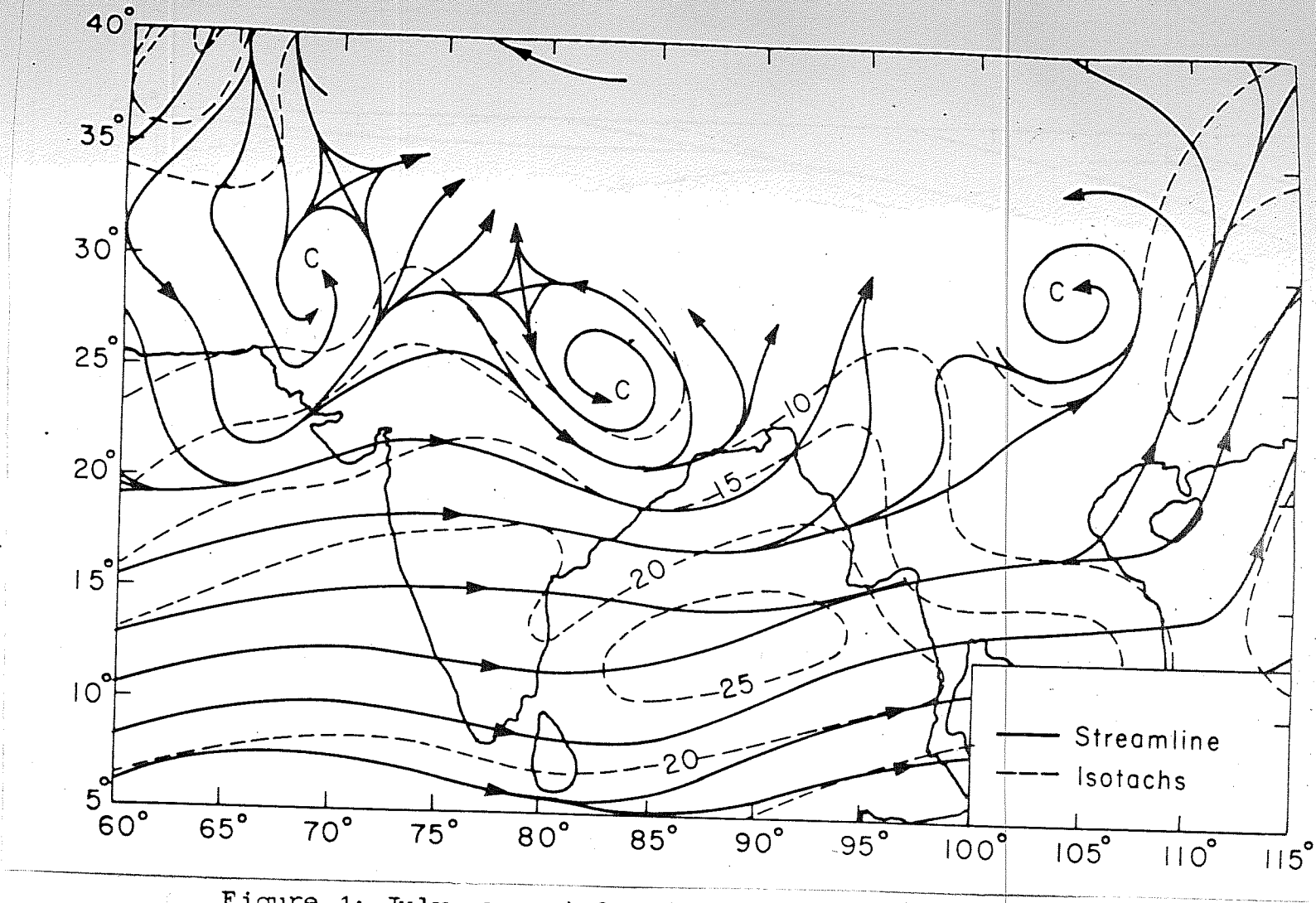

Figure 1: July mean wind at 850 mb (Meteorological Atlas of the International Indian Ocean Expedition, Vol.2, 1972)

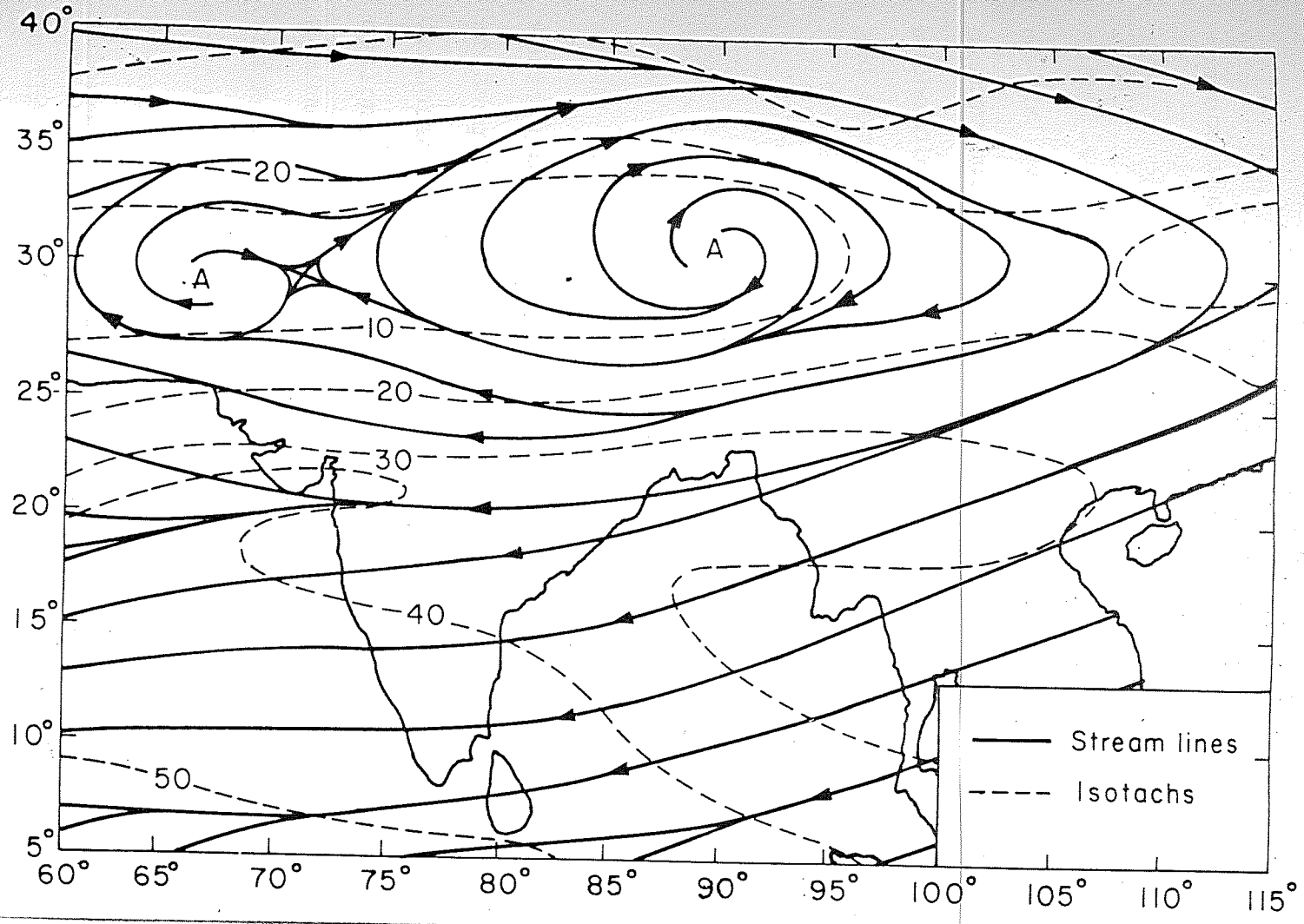

Figure 2: July mean wind at 200 mb (Meteorological Atlas of the International Indian Ocean Expedition, Vol.2, 1972).

monsoon flow.

Before going into the detailed study of the stability analysis we will discuss in this chapter some of the important observed characteristics of the monsoon disturbances. We shall also give a brief account of the methodology of stability analysis of atmospheric flows and some earlier important results.

A. MONSOON DISTURBANCES

During monsoon months cyclonic disturbances of various degrees of intensity form mainly over north Bay of Bengal. Low pressure systems are referred to as 'tropical depressions' when the surface winds in the cyclonic circulation range from 17 to 33 knots. When the maximum wind speed is between 34 and 47 knots the systems are known as 'moderate tropical storms' and those with still more speeds are termed as 'severe tropical storms'. Weaker systems with wind speeds less than 17 knots are referred to as 'lows'. These definitions are also used in the India Meteorological Department. Monsoon depressions rarely attain the intensity of tropical storms. In the pre and post monsoon seasons tropical storms form over the Indian seas.

1.1 Region and frequency of formation of monsoon disturbances:

The data published by India Meteorological Department reveals that monsoon disturbances form mainly over the Bay of Bengal, Arabian Sea and even over land. But the maximum number of cyclonic disturbances, about 75 per cent of the total, form over the Bay of Bengal and only 15 per cent of the total form over the Arabian Sea (Table 1).

In June, July and August depressions and storms usually form over the Bay of Bengal, north of 18°N latitude and west of 92°E latitude. In September, however, the formation extends southwards, upto 14°N latitude. In Arabian sea the region of formation is within about 5° of the coast north of 12°N latitude. These systems normally form in June (I.M.D., 1979). More often midtropospheric cyclones form over northeastern Arabian Sea. Depressions that develop over land areas are confined mostly to northwest India. Apart from depressions and storms, weaker lows appear in all the areas mentioned above, but mostly north of 20°N latitude. Only a few of the lows intensify into depressions and still fewer into storms and severe storms.

Regarding interannual variability of monsoon disturbances there appears to be no regularity in the

Table 1

Number of cyclonic disturbances (1891-1970). Originating over Bay of Bengal, Arabian Sea and over land.

	June			July			August			September		
	C	D	S	C	D	S	C	D	S	C	D	S
Bay of Bengal	106	47	35	145	84	38	158	106	26	173	109	32
Arabian Sea	33	12	15	12	6	3	4	1	2	14	6	5
Land area	13	5	1	40	26	1	42	24	0	22	16	1

C - Total number of Cyclonic Disturbances

D - Depressions

S - Cyclonic Storms

(Tracks of Storms and Depressions in the Bay of Bengal and the Arabian Sea, India Meteorological Department, 1979)

number of cyclonic disturbances. The number has a wide range of 8 in 1957 to 23 in 1927. The number of cyclonic storms has varied from a minimum of 1 in 1949 to a maximum of 10 in each of the years 1893, 1926 and 1930. The average number of cyclonic disturbances and storms per year is about 16 and 6 respectively (I.M.D., 1979). Marked variations in the decade frequencies of the cyclonic disturbances are observed, though no cycles are apparent.

A majority of depressions last for about 2 to 5 days and very few exist beyond 6 days (Table 2). Cyclonic storms usually weaken on coming over land and the cyclonic disturbances moving across the country are mainly depressions. When depressions weaken, the remnant lows remain for a day or two before filling up completely.

1.2 Tracks of depressions and cyclones:

Most of the depressions and storms forming over the Bay of Bengal follow almost a well defined track towards westnorthwest. Systems developing in July move mainly westnorthwestwards over the Bay and across the country (Figs. 3 and 4). The August depressions move more northwestwards. In relatively higher latitudes the movement is more towards north. The tracks of the disturbances of these two months are usually confined to a narrow belt,

Table 2

Life period of Bay depressions and storms (1901-1960)

Life period No. of days	Percentage of depressions and storms		
	July	August	September
1	9	7	4
2	11	17	11
3	37	17	18
4	16	21	20
5	13	17	18
6	7	10	10
7	5	6	7
8	2	1	8
9	0	4	4

(Srinivasan, Raman and Mukherji, 1971)

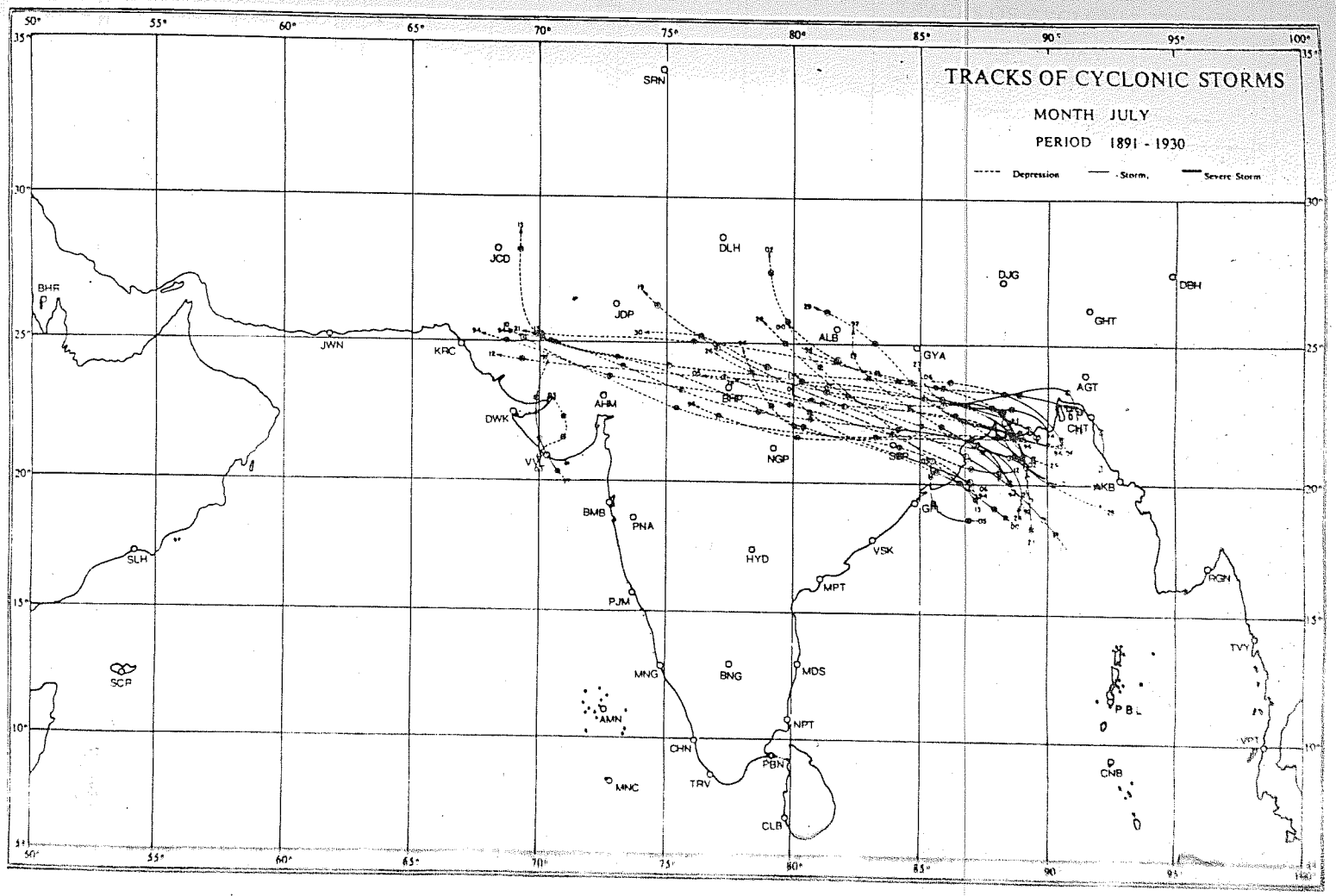

Figure 3: (Tracks of Storms and Depressions in the Bay of Bengal and the Arabian Sea, 1877-1970, India Meteorological Department, 1979).

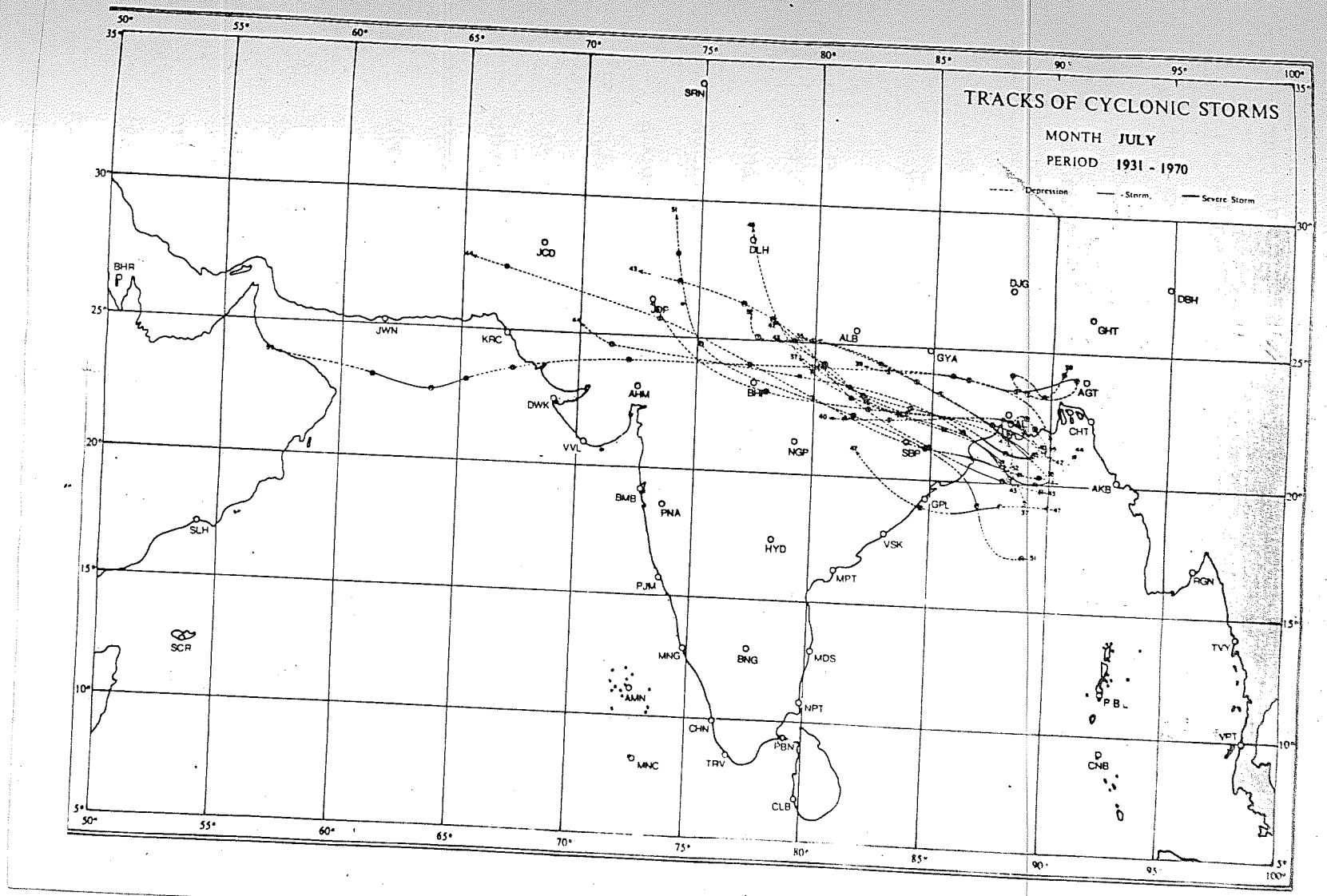

Figure 4: (Tracks of Storms and Depressions in the Bay of Bengal and the Arabian Sea, 1877-1970, India Meteorological Department, 1979).

but in June and September the tracks are more spread out (I.M.D., 1979). One of the interesting observations is the recurvature of the course of the disturbances forming in June and September. Some of these systems, usually forming at lower latitudes (even at 20°N) start with a northerly course and then recurve to have north to north-east course. Disturbances developing in the Arabian Sea in June maintain a northwestward and northward course.

In the formative stage over the Bay the depressions may move slowly, but coming over the central parts of peninsular India they may have speeds upto 30 km hr^{-1}. The average speed of July depressions is 5 to 10 km hr^{-1} or about 1.5 to 3.0 m s^{-1} to the east of 85°E longitude, but more (about 10 to 20 km hr^{-1}) to the west. In other months the speeds of depressions are less, but the general characteristics are more or less the same. The Arabian Sea systems of June have almost same speeds of 5 to 10 km hr^{-1} (Rao, 1976).

The basic monsoon current in the lower troposphere is westerly, but the monsoon disturbances propagate generally in the westnorth-west direction. This westward propagation of monsoon depressions can be explained (Krishnamurti et al., 1975) recognising that a pronounced field of low level convergence lies to the west of the

depression. This was examined by Krishnamurti et al. (1976) in a number of simple numerical prediction experiments. The barotropic non-divergent model and quasi-geostrophic model were found inadequate to account for the westward phase speed. Using a multi-level primitive equation model and considering features like air-sea interaction, parameterization of cumulus convection, large scale condensation, heat balance of the earth's surface and smoothed orography, they carried out a somewhat reasonable 48 hour real data forecast.

1.3 Structure of monsoon depressions:

On the synoptic charts the closed isobars of monsoon depressions are not circular, but nearly elliptic with alongation in westnorthwest direction (Fig. 5). This implies that the pressure gradient to south of the depression centre is more than to the west (Rao, 1976).

Many case studies are done on the vertical and horizontal structure of monsoon depressions. The studies of Sharma and Srinivasan (1971), Keshavamurty (1972), Krishnamurti et al. (1975), Sikka and Paul (1975), Godbole (1977) are a few to mention. Studies of Krishnamurti et al. (1975) suggest that the horizontal scale of depression is about 2000 km and the vertical scale is about 10 km.

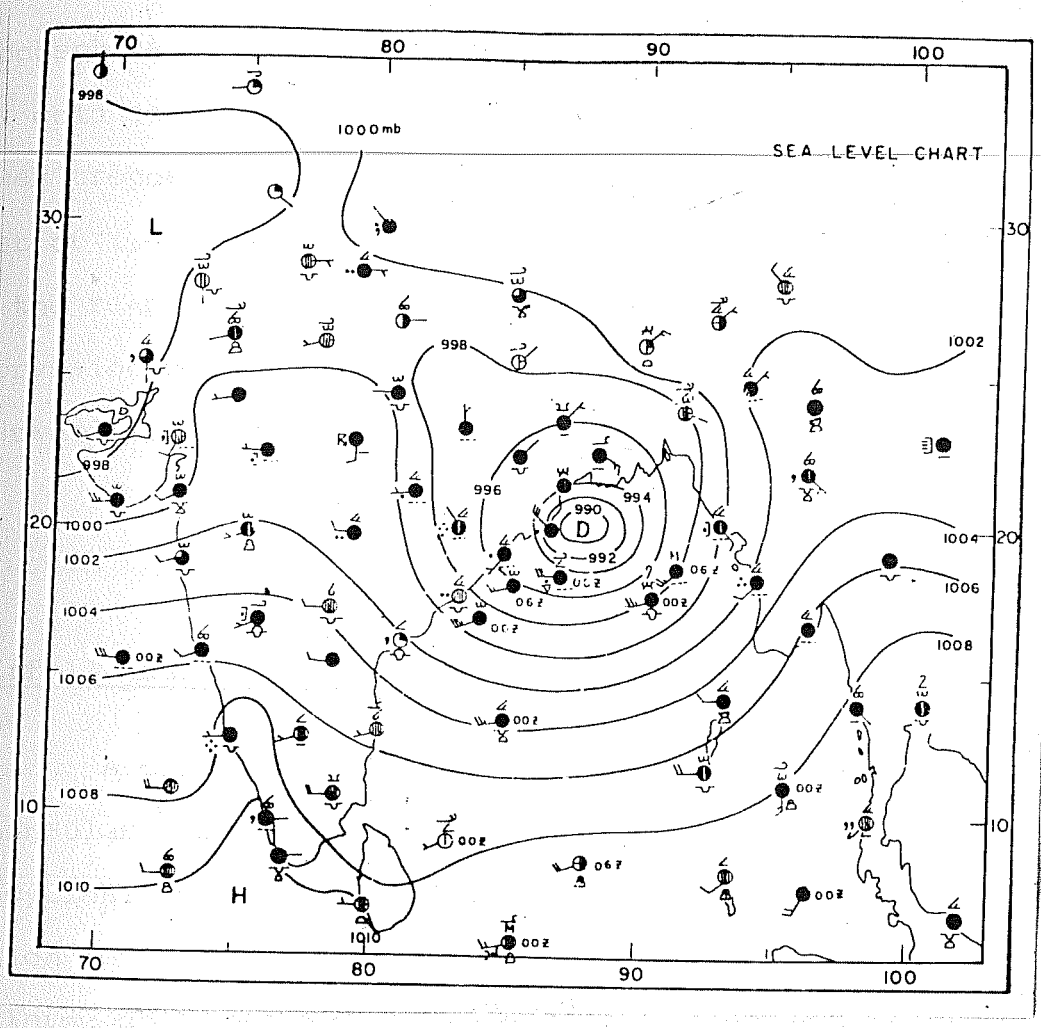

Figure 5: Synoptic Charts 0300 GMT, 1 August 1967. (Southwest Monsoon, Rao, Y.P., 1976).

They found that a narrow vertical tube of cyclonic vorticity with a horizontal scale of about 1000 km and extending upto 9 km is a characteristic feature of this circulation. The vortex has a very well defined cold core in the lower troposphere and a warm core above 500 mb. To the west of the cold core there exists a very intense warm core in the lower troposphere. Vertical motions show rising motion west of i.e. ahead of the trough line and descending motion to the rear. Studies of Keshavamurty (1972) show that the depression centre is either nearly vertical or has a small westward tilt with height.

1.4 Rainfall associated with monsoon disturbances:

A considerable proportion of monsoon rainfall over peninsular India is intimately associated with the movement of cyclonic disturbances from the Bay of Bengal. The region between 20°N and 30°N latitudes is characterised by large scale cyclonic vorticity, moisture convergence and upward motion. Hence rainfall due to depressions is maximum in this region.

Monsoon rainfall has its own characteristics. It is known to occur in spells. It is observed that after

the passage of a depression the monsoon usually weakens and there is period of lull for a few days. Thereafter the monsoon revives, another depression forms and the preceding pattern of rainfall is roughly repeated. This type of 'pulsation' in the monsoon rainfall is probably due to the day to day variations of the position of the 'monsoon trough'.

The rainfall around a depression centre is usually heavy and continuous over a well defined area and almost negligible beyond this area. Pisharoty and Asnani (1957) have studied the extent of this maximum rainfall area. They have found that falls of heavy rain are confined to an area lying to the lefthand side of the track. On any particular morning for instance, the heavy rainfall area extends to about 480 km ahead and to about 480 km behind the centre of the depression on that morning, measured respectively along the expected and past track of the depression. The width of the area is about 400 km and extends to the left of the track. Out of this belt, about 30 per cent of the area is almost the maximum over which there may be heavy rainfall in 24 hours.

Another rain belt often develops far to the west and outside the depression field, which is fairly distinct from that in the southwest sector. Its origin is mainly due to the convergence between northwest flow, northeast/

easterly flow around the depression and westerlies to south, in the lower troposphere (Raman and Banerjee, 1970).

Sometimes a depression in the Bay of Bengal is observed to trigger another low pressure area or mid-tropospheric cyclone (Miller and Keshavamurty, 1968) along the west coast of India.

Considerable amount of rainfall also occurs in association with low pressure areas which marginally differ from the definition of depressions.

1.5 Formation of depressions:

Although the formation of depressions and storms is not yet fully understood, in general depressions develop out of the following situations. In most cases, a diffuse pressure field develops over north Bay of Bengal and nearby areas, before a cyclonic disturbance forms. The pressure gradient to the south of the trough becomes fairly strong and the monsoon trough shifts southwards to the head Bay. Sometimes appearance of an upper air cyclonic circulation at any level upto mid-troposphere leads to depression formation. Diffuse lows that travel across Burma into north and adjoining central Bay may develop into depressions. Ramanna (1969) finds that more than

17 per cent of the depressions can be regarded as having formed out of the remnants of typhoons of China Seas moving across Burma.

Basing on synoptic studies several possible mechanisms of intensification of low pressure systems into monsoon depressions have been given by different researchers. Roy and Roy (1930), Ramanathan and Ramkrishnan (1933) and Desai and Koteswaram (1951) applied frontal models in order to explain the formation and intensification of depressions. After the introduction of upper air soundings in India doubts were raised about the existence of fronts and this concept was dropped.

Koteswaram and George (1958) examined the role of upper tropospheric perturbations in the formation of monsoon depressions in the Bay of Bengal. They hypothesised that cyclonic development at sea level occurs when and where an area of positive vorticity advection in the upper troposphere becomes superimposed upon a pre-existing trough at sea level. This mechanism has similarity with that found by Petterssen (1955) for extra-tropical cyclogenesis. However, there are cases of intensification without any of these concepts being accepted. Thus, the mechanism may be true in few individual cases. Of late, satellite photographs and radiation data have also been

used for the study of formation of depressions. However, the dynamics of the formation of monsoon disturbances is still not completely understood.

B. STABILITY ANALYSIS OF ATMOSPHERIC FLOWS

The monsoon disturbances can be treated as fluctuations in the basic monsoon flows and can be understood in terms of small amplitude stability analysis of an idealised flow. This notion is due to the early pioneering works such as those of Charney (1947) and Eady (1949). Most stability theories idealize the basic state as zonally uniform flow. These studies can reveal the mechanisms of instability and the general character of the observed fluctuations. On these lines the development of monsoon disturbances has also been studied by many workers.

A number of studies have been undertaken on the instability of atmospheric flows in mid-latitudes. A few important model results are briefly mentioned in the following paragraphs. These studies have immense bearing on the stability analysis of monsoon flows.

1.6 A few note-worthy models:

The pioneering studies of Charney (1947) and Eady (1949) showed that the atmospheric disturbances in mid-latitudes could be explained as a manifestation of the baroclinic instability of the zonal winds. Both considered continuously stratified atmosphere, where the basic wind U is independent of 'y', the vertical shear is constant and the viscosity is neglected. Due to the inclusion of beta-effect, Charney's model is considered to be more realistic model of baroclinic instability. The phase speeds of the unstable modes in Charney's model are very close to the minimum value of zonal wind whereas those of Eady's model are close to the mean zonal wind. However, the energy conversion mechanism is identical in both the models.

Kuo (1949) studied the dynamic instability of two-dimensional nondivergent flow in a barotropic atmosphere. He included the variation of westerly wind with latitude and took two different types of symmetric (with respect to some central latitude) wind profiles. In the first zonal wind profile the disturbances disappear at the boundaries of a limited channel and in the second profile the belt is extended to infinity in both directions. He found that the degree of instability depends on the

sharpness of the velocity profile. His study reveals the necessary condition for the instability of a zonal flow. This condition states that for neutral and amplified waves with phase velocities between the maximum and the minimum wind velocity in the belt there must be critical points where the absolute vorticity has an extreme value. Without the existence of these critical points the perturbations are damped. If the above condition is satisfied and the perturbation phase velocity is equal to the current velocity at the critical point, then the disturbance is neutral. On the other hand if the above condition is satisfied and the perturbation phase velocity is less than the critical velocity and greater than the minimum zonal wind, then the disturbances are amplified.

A simple two-level baroclinic model was used by Phillips (1954) to study the kinematic features of the unstable baroclinic waves in mid-latitudes. His basic winds at the two levels were independent of 'y', but he included the latitudinal variation of the perturbations. His study reveals that the quasi-geostrophic baroclinic waves are associated with weak meridional circulations which, in combination with the horizontal eddy flux of momentum, prescribes the main features of the observed surface zonal wind ditribution.

The stability analysis of zonal flow with both horizontal and vertical shear was conducted by Charney and Stern (1962). They developed stability criteria for the case of an internal jet. According to their study the internal jet is stable if the gradient of potential voritcity in isentropic surfaces does not vanish. The vanishing of the potential vorticity gradient is a sufficient condition for stability and a necessary condition for instability.

The stability with respect to quasi-geostrophic disturbances of atmospheric and oceanic currents containing both horizontal and vertical shear was investigated by, Pedlosky (1964) for both a continuously stratified layer and a two-layer model. He derived certain necessary conditions for instability. According to his study the potential vorticity gradient of the basic flow must be both positive and negative in the domain of interest for instability to occur in the two-layer model.

1.7 Some instability studies of the monsoon flow:

In the last decade a large number of theoretical studies have been conducted with a view to understand the mechanisms of the growth of monsoon disturbances. A

majority of researchers have considered a zonally uniform basic flow (independent of longitude) for the stability analysis. The characteristics of growing perturbations are compared with those of observed monsoon disturbances. Since the observed mean monsoon flow has appreciable horizontal and vertical wind shears there are possibilities for a perturbation to grow by drawing on zonal kinetic energy as well as zonal available potential energy.

Keshavamurty (1972) has shown that the monsoon depressions do not have the eastward tilt with height necessary for baroclinic growth. His studies (Keshavamurty, 1971) on momentum transport by the disturbances show that the latter may derive energy from the kinetic energy of the basic flow. This suggests that barotropic instability may be one of the mechanisms for the initial formation of monsoon depressions. In fact Keshavamurty et al. (1978) from their study of composite monsoon depressions have obtained north-north-east to south-south-west tilt in the monsoon depressions in the lower levels. Thus disturbances may draw upon zonal kinetic energy for their growth. A multi-level baroclinic stability analysis of monsoon zonal flow (Keshavamurty et al., 1978) showed that the flow is stable. Shukla (1977) from energy calculations has shown that the conversion from zonal available

potential energy to perturbation available potential energy is small and hence the baroclinic instability mechanism is not important. Studies of Goswami et al. (1980) show that baroclinicity has very little effect on the growth of disturbances. However, Mishra and Salvekar (1980) have shown that growth due to baroclinic instability plays an important role, at least in the formative stage of a monsoon depression.

Shukla (1977) studied the barotropic-baroclinic instability of the monsoon flow field using a ten-layer quasi-geostrophic model. He found only an upper tropospheric growing mode at 150 mb. This was essentially a barotropic mode. Shukla (1978) also performed CISK-barotropic-baroclinic instability analysis of the monsoon flow by numerically integrating the linearized perturbation equations for a three-layer quasi-geostrophic model. He found that the maximum growth rate occurs for the smallest scale. The mechanism for scale selection was therefore not clear. Satyan et al. (1980) concluded that the inclusion of cumulus heating into combined barotropic-baroclinic stability analysis of the mean zonal flow can induce cyclogenesis. They have got growing modes in the lower troposphere which compare reasonably well with observed monsoon disturbances in horizontal scale length, growth rate, phase speed and horizontal structure.

Mak (1975) and Brode and Mak (1978) have conducted the stability analysis of the Southwest monsoon flow having both zonal and meridional components. According to their studies, the basic meridional wind component is responsible for the relatively large amplitude of the mid-tropospheric cyclones (MTC) at the mid-troposphere and controls the length scale of the disturbance. The large easterly shear in the zonal wind contributes greatly to the growth rate of the MTC. Satyan et al. (1977) conducted stability analysis of the mean monsoon zonal flow with a long stationary wave superimposed on it and obtained monsoon-like disturbances. In another study Satyan et al. (1980) have found that with the inclusion of both cumulus heating and meridional wind into the model the instability of the monsoon zonal flow is much more pronounced.

1.8 Stability of a stationary Rossby wave embedded in a zonal flow:

The stability analysis of a flow pattern which varies with longitude can be carried out by superimposing a finite amplitude Rossby wave on the zonal flow. Lorenz (1972) investigated the barotropic instability of zonal flow with a superposed Rossby wave.

Gill (1974) generalized Lorenz's findings and identified Rayleigh instability and resonant triad regimes. Duffy (1975) reexamined the barotropic instability of stationary Rossby wave and found additional modes corresponding to stable inertia-gravity modes. Merkine and Israeli (1978) conducted the stability analysis of a stationary baroclinic Rossby wave embedded in a baroclinic zonal flow and applied the results to mountain induced cyclogenesis. Lin (1980) carried out a detailed parameter study of the stability of Rossby waves in a baroclinic zonal flow and applied the results to planetary scale waves that transport heat. All these studies are confined to the midlatitudes. We intend to study stability of a stationary Rossby wave superposed on the monsoon zonal flow.

CHAPTER TWO

BAROTROPIC INSTABILITY

The monsoon zonal wind (Fig.6) is observed to have appreciable horizontal and vertical shears. For a perturbation to grow on this basic flow there are mainly two sources of energy. From the quasi-geostrophic energy equations it can be shown that kinetic energy of the mean flow, represented by its horizontal shear $\frac{\partial U}{\partial y}$ is converted to the perturbation kinetic energy through the Reynold's stress $(-\overline{u'v'})$. Similarly available potential energy of the basic flow represented by its vertical shear $\frac{\partial U}{\partial p}$ is converted to the perturbation available potential energy through the eddy flow of heat.

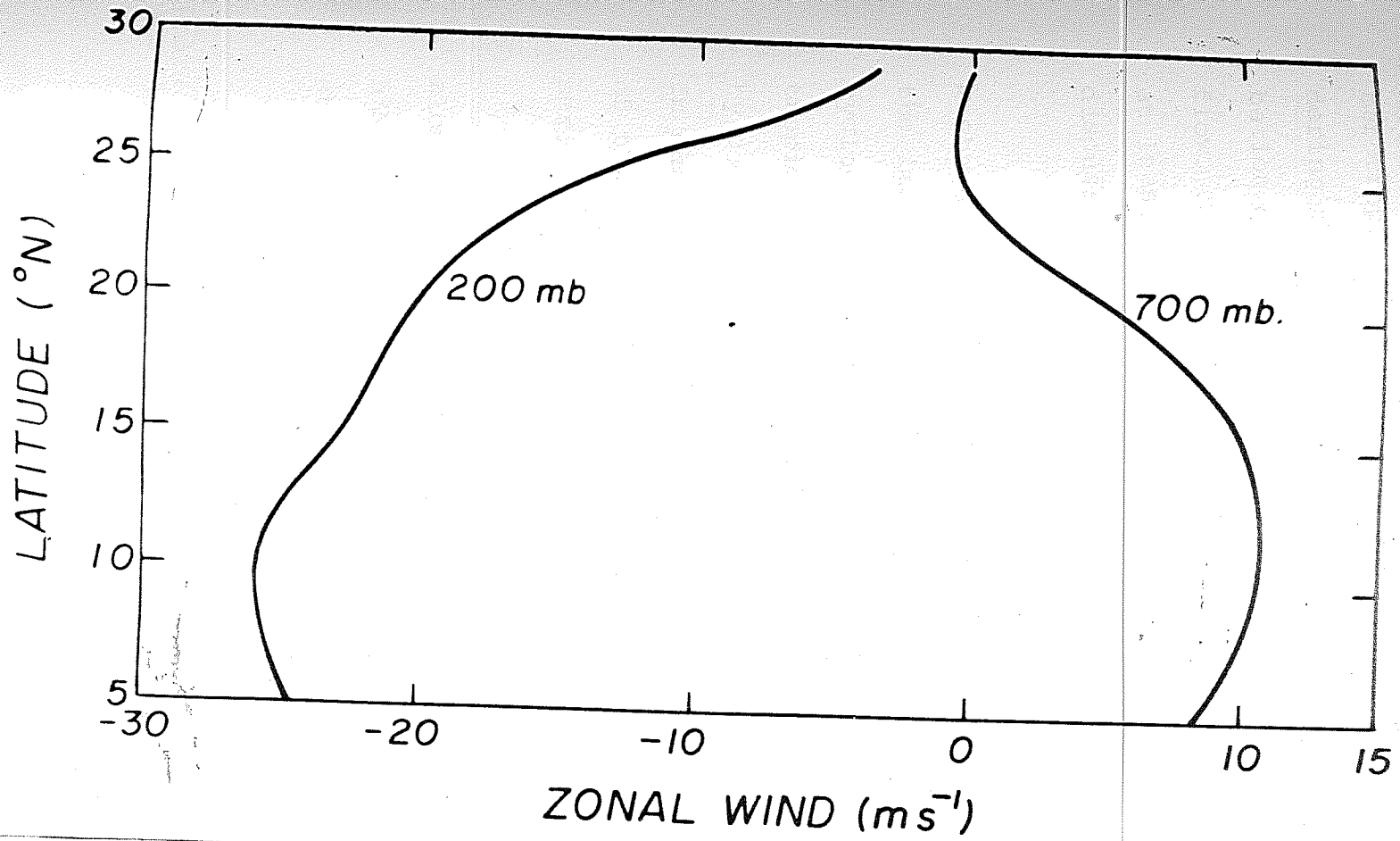

Figure 6: July mean zonal wind profiles, U_1 and U_3 (m s^{-1}) at 200 mb and 700 mb respectively.

Initially, in this chapter we will conduct the barotropic stability analysis of the mean flow by considering the horizontal wind shear only. Thus a perturbation may grow by drawing on kinetic energy of the zonal flow. To include the vertical wind shear in the model at least two levels are necessary and that will be discussed in Chapter 3.

Studies of Keshavamurty (1971), Shukla (1977), Keshavamurty et al. (1978) and Goswami et al. (1980) show the importance of barotropic instability in the monsoon cyclogenesis. We intend to reexamine the role of barotropic instability in the growth of monsoon disturbances by conducting the stability analysis in a different way. In our study the mean wind and the meridional dependence of the geopotential perturbation are expressed by Fourier series.

We have used the July mean zonal wind (Fig.6) along 80°E longitude as the basic wind and a channel from 5°N to 30°N latitude is selected with a beta-plane centred at the middle.

2.1 Linearisation of vorticity equation:

In a barotropic model, pressure and temperature surfaces coincide. Hence all pressure surfaces will be parallel and the wind does not have vertical shear. According to scale analysis, to a first approximation the flow in a barotropic atmosphere is governed by the vorticity equation

$$\frac{\partial \zeta}{\partial t} + \underline{V} \cdot \nabla (\zeta + f) = 0. \qquad (2.1)$$

With beta-plane approximation the above equation can be rewritten as

$$\left(\frac{\partial}{\partial t} + u\frac{\partial}{\partial x} + v\frac{\partial}{\partial y}\right)\zeta + \beta v = 0 \qquad (2.2)$$

where $\underline{V} = \hat{i}u + \hat{j}v$.

The above equation is to be linearized before conducting the stability analysis. The linearisation is done by perturbation method as follows.

Each field variable is expressed as summation of a basic part (zonal and time mean) and a perturbation

$$X = [\bar{X}] + X' \qquad (2.3)$$

where $\left|\frac{X'}{[\bar{X}]}\right| \ll 1.$

The square bracket and the bar represent zonal average and time mean respectively. Thus $[X] = \frac{1}{2\pi a}\int_0^{2\pi a} X\,dx$ and $\bar{X} = \frac{1}{T}\int_0^T X\,dt$.

In the present case of barotropic stability analysis we write

$$u = U + u' \quad \text{where} \quad U \equiv [\bar{u}]$$

$$v = v'$$

$$\phi = [\bar{\phi}] + \phi'$$

and

$$\zeta = [\bar{\zeta}] + \zeta'.$$

To linearise the vorticity equation first the above variables are substituted in (2.2) and we get

$$\left\{\frac{\partial}{\partial t} + (U + u')\frac{\partial}{\partial x} + v'\frac{\partial}{\partial y}\right\}\left([\bar{\zeta}] + \zeta'\right) + \beta v' = 0. \tag{2.4}$$

The vorticity equation in basic state variables is

$$\left(\frac{\partial}{\partial t} + U\frac{\partial}{\partial x}\right)[\bar{\zeta}] = 0.$$

The above equation is deducted from (2.4) and then simplified to get the perturbation vorticity equation. While simplifying it is to be noted that the zonal wind is assumed to be independent of longitude. Finally neglecting the product of the perturbation terms we get the following perturbation vorticity equation.

$$\left(\frac{\partial}{\partial t} + U\frac{\partial}{\partial x}\right)\zeta' + v'\left(\beta - \frac{\partial^2 U}{\partial y^2}\right) = 0. \quad (2.5)$$

The wind is assumed to be geostrophic. Hence

$$v' \equiv \frac{1}{f_0}\frac{\partial \phi'}{\partial x}$$

and $$\zeta' \equiv \frac{1}{f_0}\nabla^2\phi'$$

where f_0 corresponds to the middle of the channel. Hence in terms of geopotential perturbation (2.5) can be rewritten as

$$\left(\frac{\partial}{\partial t} + U\frac{\partial}{\partial x}\right)\nabla^2\phi' + \frac{\partial \phi'}{\partial x}\left(\beta - \frac{\partial^2 U}{\partial y^2}\right) = 0. \quad (2.6)$$

Here the term $\left(\beta - \frac{\partial^2 U}{\partial y^2}\right)$ is essential for barotropic instability.

2.2 The model:

We have expressed the zonal wind (Fig. 6) at each level by the Fourier series

$$U(y) = b_0 + \sum_{j=1}^{J} b_j \cos j\frac{2\pi y}{M} + \sum_{j=1}^{J} q_j \sin j\frac{2\pi y}{M} \quad (2.7)$$

where M is the number of points where the wind is given. The co-efficients b_0, b_j and q_j are obtained by harmonic analysis and the wind is accurately represented by the series (2.7). Using (2.7) $\left(\beta - \frac{\partial^2 U}{\partial y^2}\right)$ is calculated and it is found that this term changes its sign somewhere near 21°N latitude at both 700 mb and 200 mb. Thus the necessary condition (Kuo, 1949) of barotropic instability is satisfied by the lower and upper tropospheric zonal winds. We use normal mode analysis to reduce the problem to an eigenvalue problem and assume solution of of the type

$$\phi' = \phi(y) \exp\{ik(x-ct)\} \qquad (2.8)$$

for the geopotential perturbation. We look for modes characterised by a wavenumber k for which 'c' is complex. If $C \equiv C_r + iC_i$ then the disturbance will grow when $C_i > 0$. Substituting (2.8) in (2.6) one gets

$$(U-c)\left(-k^2\phi + \frac{\partial^2\phi}{\partial y^2}\right) + \left(\beta - \frac{\partial^2 U}{\partial y^2}\right)\phi = 0 . \qquad (2.9)$$

For the meridional dependence of amplitude we assume

$$\phi(y) = \sum_{n=1}^{N} A_n \sin \frac{n\pi}{D}(y - y_s) . \qquad (2.10)$$

This satisfies the boundary conditions, $\phi' = 0$ at

$y = y_s$, the southern boundary of the channel and ϕ' $= 0$ at $y = y_N$, the northern boundary. The width of the channel $D = y_N - y_s$. Substituting (2.10) in (2.9), we get

$$\sum_{n=1}^{N} \left[(U_m - c)(\eta_{m,n} - k^2 \gamma_{m,n}) + \left(\beta - \frac{\partial^2 U_m}{\partial y^2}\right) \gamma_{m,n} \right] A_n = 0 \qquad (2.11)$$

where $$\gamma_{m,n} = \sin \frac{n\pi}{D} (y_m - y_s) \qquad (2.12)$$

and $$\eta_{m,n} = -\frac{n^2\pi^2}{D^2} \sin \frac{n\pi}{D} (y_m - y_s)$$

and the subscript 'm' is put to identify a particular latitude in the channel. Eq. (2.11) is true at each latitude in the channel i.e. for each integral value of 'm'. The channel is divided into 'm' equal parts and we have an equation of the type (2.11) for each part. Thus 'm' number of homogeneous algebraic equations are obtained and these can be rewritten in the matrix form

$$(\underset{\sim}{B} - c\,\underset{\sim}{D})\,(\underset{\sim}{A}) = 0 .$$

The elements $b_{m,n}$ and $d_{m,n}$ of matrices $\underset{\sim}{B}$ and $\underset{\sim}{D}$ respectively, appearing in the above equation are defined as follows.

$$b_{m,n} = \left(\beta - \frac{\partial^2 U_m}{\partial y^2} - k^2 U_m\right)\gamma_{m,n} + U_m \eta_{m,n}$$

$$d_{m,n} = \eta_{m,n} - k^2 \gamma_{m,n}$$

$\underset{\sim}{A}$ is a column matrix with elements An. $\underset{\sim}{B}$ and $\underset{\sim}{D}$ are real, but $\underset{\sim}{A}$ may be complex. To convert the above matrix equation into eigenvalue form

$$\left(\underset{\sim}{B}\cdot\underset{\sim}{D}^{-1} - c\,\underset{\sim}{I}\right)\left(\underset{\sim}{D}\cdot\underset{\sim}{A}\right) = 0 \,. \qquad (2.13)$$

$\underset{\sim}{B}$ and $\underset{\sim}{D}$ should be square matrices. This is accomplished by making m = N. Here $\underset{\sim}{I}$ is the unit matrix. Solutions of (2.13) give the eigenvalues 'c' and the eigenvectors $(\underset{\sim}{D}.\underset{\sim}{A})$. The real part of 'c' gives the phase speed of the disturbance and its doubling time i.e. the time in which the amplitude becomes double of initial value is calculated from the relation $\tau_d = \frac{\ln 2}{k c_i}$.

We have increased N and hence the sizes of the square matrices and solved (2.13) for each value of N. When N is sufficiently large the solutions obtained are close to the 'true' solutions. N and the corresponding doubling times are plotted in Fig.(7). It is evident that the doubling time remains constant for N $>$ 30. Hence we have truncated the series (2.10) at N = 30. From the

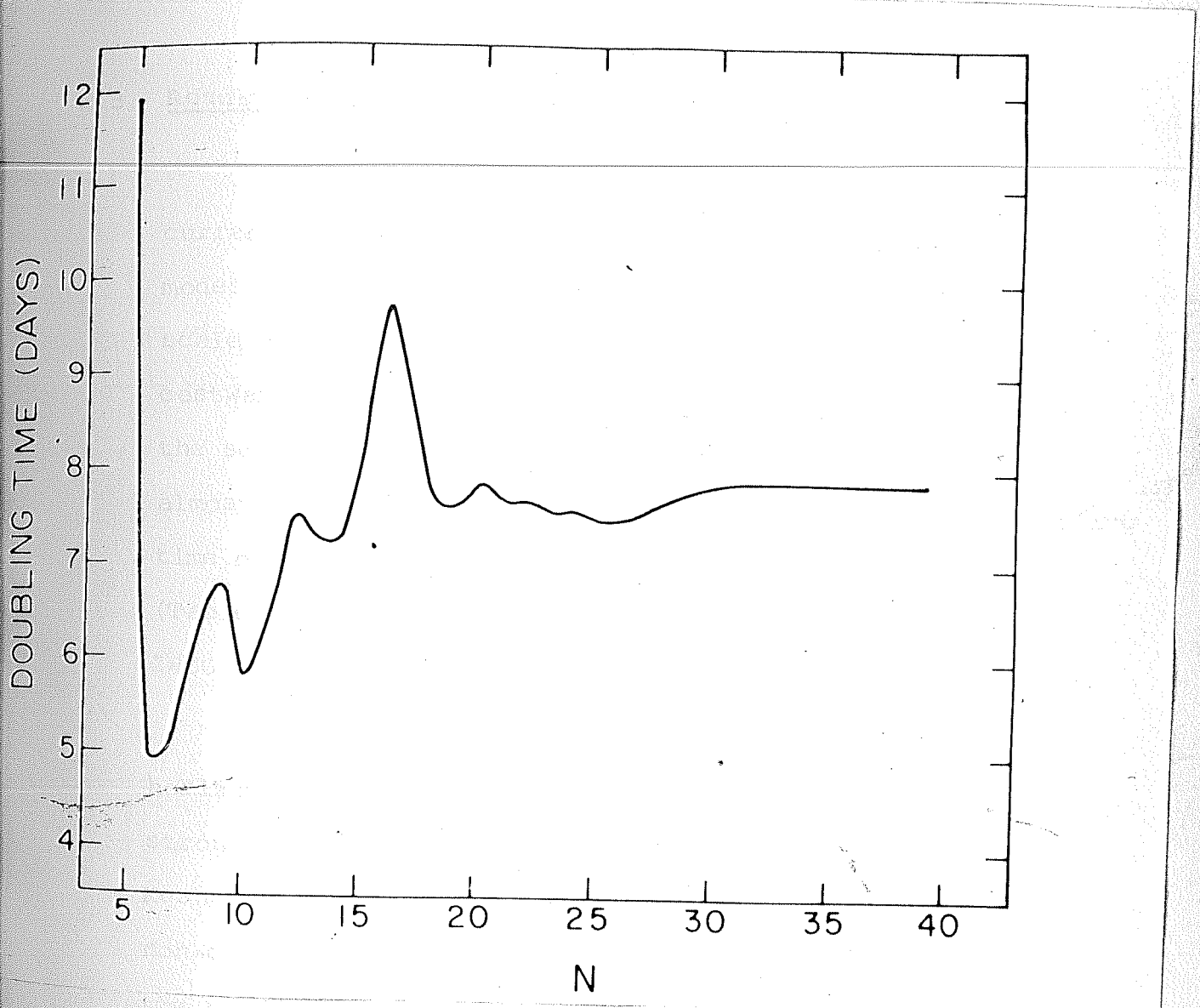

Figure 7: Variation of doubling time (τ_d in days) with the maximum number of terms (N) in series (2.10) in barotropic model at 700 mb.

eigenvectors, the coefficients An and hence the meridional structures of the disturbances are obtained using (2.10).

2.3 Results and Conclusions:

From the analysis it is found that the zonal currents at 700 mb and 200 mb (Fig.6) yield slow growing modes. The fastest growing mode at 700 mb has a horizontal scale of 2300 km, a doubling time of 8 days (Fig.8) and an eastward phase speed of 2.5 m s^{-1} (Table 3). At 200 mb the scale length vs. doubling time curve is seen to be almost flat. The fastest growing disturbance has a doubling time of 6.5 days and a westward phase speed of 17 m s^{-1} (Table 4). Its scale length lies between 2000 km and 2800 km.

The slow growth rates are perhaps due to small horizontal wind shears. They may grow much faster during strong monsoon epochs. These results agree with those of Keshavamurty et al. (1978). Since we have considered a non-divergent barotropic model, the perturbations ride on the basic current. The amplitude structure (Fig.9) shows that at both the levels the amplitudes are maximum at 21-22°N latitudes, which is observed to be the region of substantial cyclogenesis.

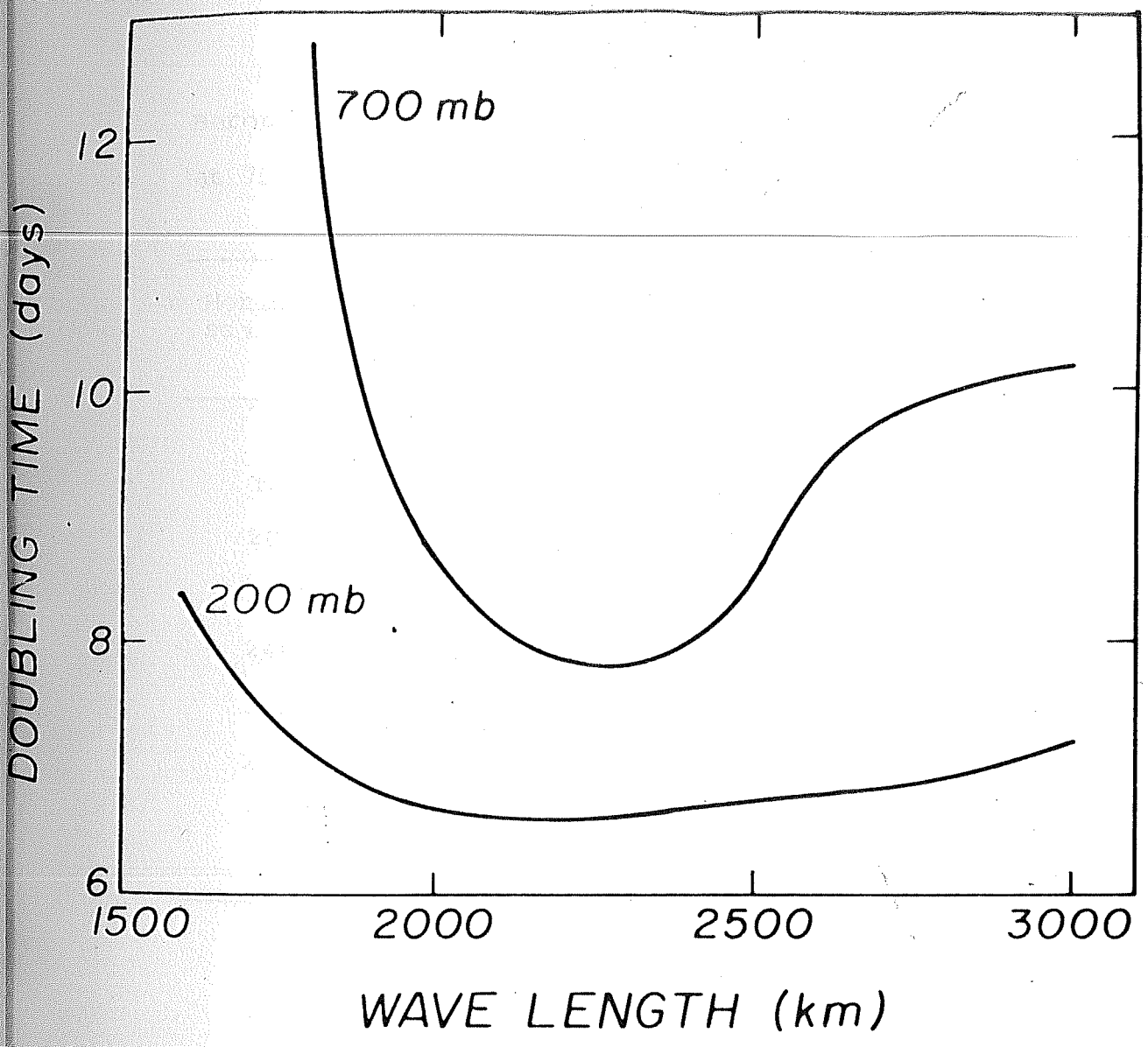

Figure 8: Scale dependence of the growth of barotropically unstable modes.

Table 3

Barotropic instability: Characteristics of growing modes at 700 mb.

Horizontal scale length (km)	Phase speed c_r ($m\ s^{-1}$)	Doubling time τ_d (days)	Maximum ϕ	Position of maximum ϕ (°N)
1800	2.7	12.7	180	21
2000	2.6	8.7	200	21
2200	2.5	7.9	210	21
2400	2.3	8.0	230	21
2600	2.2	9.4	250	21
2800	1.7	10.0	320	21
3000	1.5	10.5	320	21

Table 4

Barotropic instability:

Characteristics of growing modes at 200 mb.

Horizontal Scale length (km)	Phase speed C_r ($m\ s^{-1}$)	Doubling Time τ_d (days)	Maximum Φ	Position of maximum Φ (°N)
1800	- 17.4	7.1	130	22
2000	- 17.4	6.7	140	22
2200	- 17.3	6.6	140	22
2400	- 17.3	6.7	150	22
2600	- 17.3	6.8	150	22
2800	- 17.3	6.9	150	22
3000	- 17.3	7.2	160	22

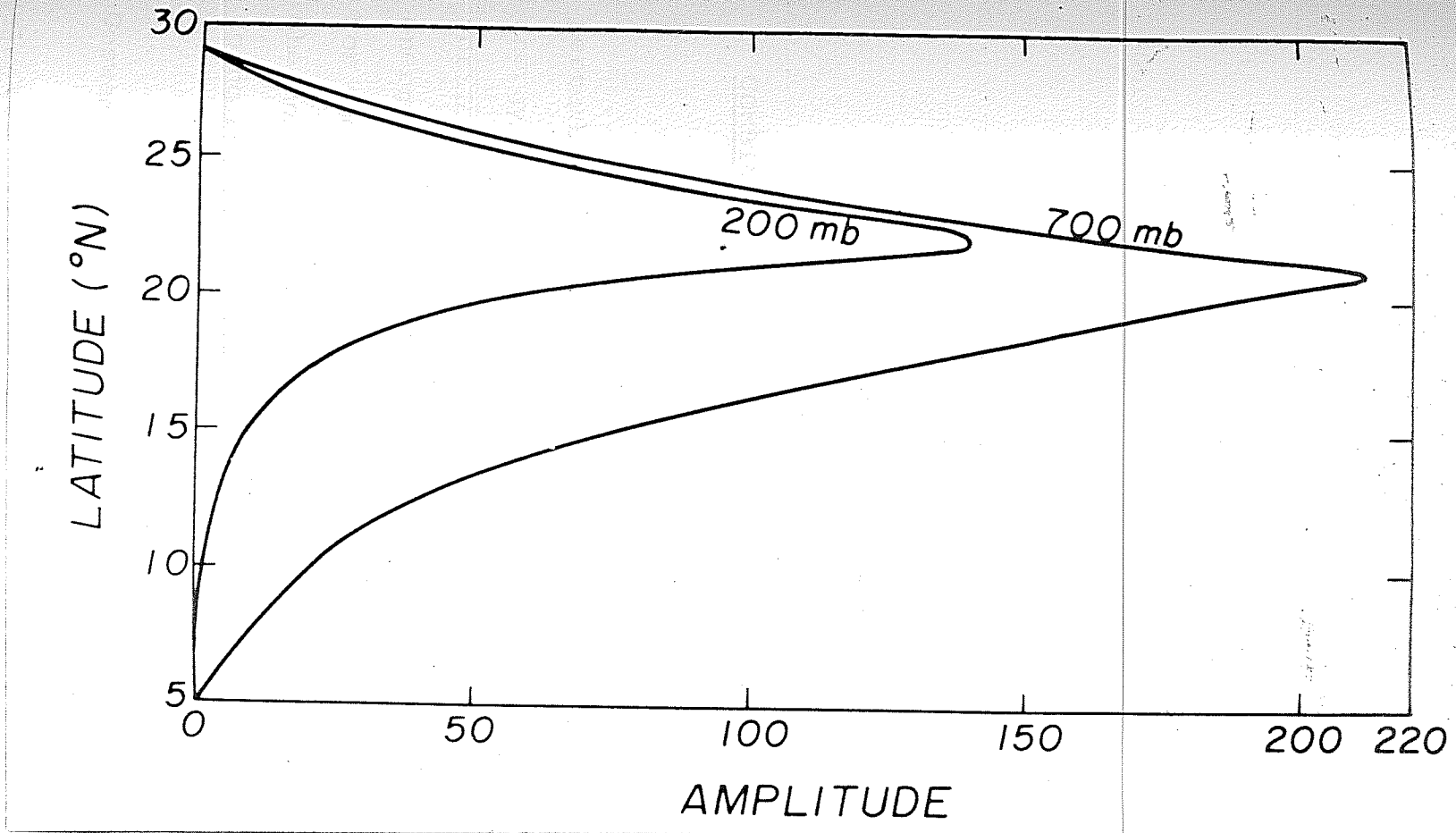

Figure 9: Amplitude structure of the fastest growing disturbance of Fig. 8.

CHAPTER THREE

COMBINED BAROTROPIC-BAROCLINIC STABILITY ANALYSIS

In the barotropic model discussed in Chapter 2, perturbations could grow by feeding on zonal kinetic energy. But the zonal wind (Fig. 6) is observed to have vertical shear also. Thus there is available potential energy of the basic flow, which can also be a source for the disturbances. So it is reasonable to consider the horizontal as well as the vertical wind shear while doing stability analysis.

Shukla (1977, 1978), Satyan et al. (1980) and Goswami et al. (1980) have considered both the horizontal

and vertical wind shears in their stability analyses of monsoon zonal flow. Since the monsoon atmosphere is conditionally unstable and there is always cyclonic vorticity present in the lower layers, Keshavamurty (1971) stressed the role of CISK in the growth of monsoon disturbances. Krishnamurty et al. (1975), from their study of the structure of monsoon depression have also suggested that CISK mechanism may be important. Shukla (1978) and Satyan et al. (1980) included cumulus heating in their models and the characteristics of the computed disturbances agreed reasonably with those of the monsoon disturbances.

In this chapter we have conducted the combined barotropic-baroclinic stability analysis of the monsoon zonal flow represented by the July mean zonal wind along 80°E longitude. As in the case of barotropic-stability analysis we express the zonal winds and the meridional dependence of the geopotential perturbation by trigonometic series. We also consider the same channel from 5°N to 30°N and a beta-plane centred at the middle.

Section 3.2 deals with combined barotropic-baroclinic stability analysis with a two-level quasi-geostrophic model. The cumulus heating is included in this model in Section 3.3. Finally in Section 3.4 we

have extended the analysis to a five-level quasi-geostrophic model.

3.1 Two-level quasi-geostrophic model:

In this section we will conduct the stability analysis of the zonal flow (Fig. 6) having horizontal and vertical wind shears, using a two-level quasi-geostrophic model.

3.1.1 Linearisation of potential vorticity equations:

To include baroclinicity in the model thermodynamic energy equation will be used in addition to the vorticity equation. Using the quasi-geostrophic vorticity and thermodynamic energy equations

$$\frac{\partial \zeta}{\partial t} = -\underline{V}\cdot\nabla(\zeta+f) + f_0 \frac{\partial \omega}{\partial p} \qquad (3.1)$$

and

$$\frac{\partial}{\partial t}\left(\frac{\partial \phi}{\partial p}\right) = -\underline{V}\cdot\nabla\left(\frac{\partial \phi}{\partial p}\right) - \sigma\omega - \frac{R\dot{Q}}{pC_p} \qquad (3.2)$$

respectively the quasi-geostrophic potential vorticity equation can be derived. Using beta-plane approximation

the above equations can be rewritten as

$$\left(\frac{\partial}{\partial t} + u\frac{\partial}{\partial x} + v\frac{\partial}{\partial y}\right)\zeta + \beta v - f_0\frac{\partial \omega}{\partial p} = 0 \qquad (3.3)$$

and

$$\left(\frac{\partial}{\partial t} + u\frac{\partial}{\partial x} + v\frac{\partial}{\partial y}\right)\frac{\partial \phi}{\partial p} + \sigma\omega = -\frac{R\dot{Q}}{pC_p} \qquad (3.4)$$

respectively where the symbols have their usual meaning.

In two-level model one writes the vorticity equations (3.3) at levels 1 and 3 and the thermodynamic energy equation (3.4) at level 2 and then ω_2 is eliminated to get the potential vorticity equations at levels 1 and 3.

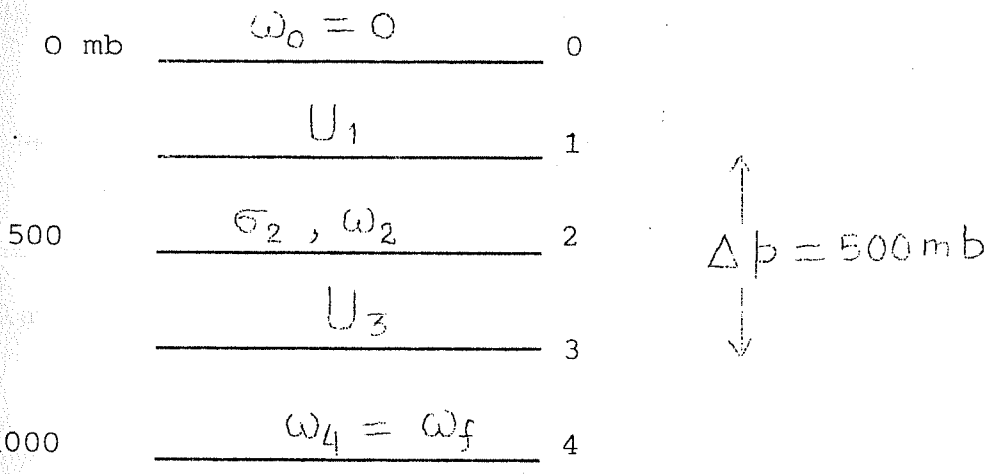

$\left(\frac{\partial \omega}{\partial p}\right)_{1,3}$ and $\left(\frac{\partial \phi}{\partial p}\right)_2$ are evaluated by finite difference approximation.

Thus

$$\left(\frac{\partial \omega}{\partial p}\right)_1 = \frac{\omega_2 - \omega_0}{\Delta p} = \frac{\omega_2}{\Delta p}$$

$$\left(\frac{\partial \omega}{\partial p}\right)_3 = \frac{\omega_4 - \omega_2}{\Delta p} = \frac{\omega_f - \omega_2}{\Delta p}$$

and

$$\left(\frac{\partial \phi}{\partial p}\right)_2 = \frac{\phi_3 - \phi_1}{\Delta p}$$

where the vertical boundary conditions used are $\omega_0 = 0$ at $p = 0$ and $\omega_4 = \omega_f$ at $p = p_0$.

Using subscripts 1, 2 and 3 for different variables at the respective levels the vorticity equations at levels 1 and 3 are

$$\left(\frac{\partial}{\partial t} + u_1 \frac{\partial}{\partial x} + v_1 \frac{\partial}{\partial y}\right)\zeta_1 + \beta v_1 - \frac{f_0}{\Delta p}\omega_2 = 0 \qquad (3.5)$$

and

$$\left(\frac{\partial}{\partial t} + u_3 \frac{\partial}{\partial x} + v_3 \frac{\partial}{\partial y}\right)\zeta_3 + \beta v_3 - \frac{f_0}{\Delta p}(\omega_f - \omega_2) = 0. \qquad (3.6)$$

Similarly the thermodynamic energy equation at level 2 is

$$\left(\frac{\partial}{\partial t} + u_2 \frac{\partial}{\partial x} + v_2 \frac{\partial}{\partial y}\right)\frac{\phi_3 - \phi_1}{\Delta p} + \sigma_2 \omega_2 = -\frac{R \dot{Q}_2}{p_2 c_p}. \qquad (3.7)$$

We use the identities

$$\underline{V}_2 \cdot \nabla \frac{\phi_3 - \phi_1}{\Delta p} \equiv \underline{V}_1 \cdot \nabla \frac{\phi_3 - \phi_1}{\Delta p} \equiv \underline{V}_3 \cdot \nabla \frac{\phi_3 - \phi_1}{\Delta p} \quad (3.8)$$

so that (3.7) can be written in either of the following ways

$$\left(\frac{\partial}{\partial t} + u_1 \frac{\partial}{\partial x} + v_1 \frac{\partial}{\partial y}\right) \frac{\phi_3 - \phi_1}{\Delta p} + \sigma_2 \omega_2 = -\frac{R \dot{Q}_2}{p_2 c_p} \quad (3.9)$$

$$\left(\frac{\partial}{\partial t} + u_3 \frac{\partial}{\partial x} + v_3 \frac{\partial}{\partial y}\right) \frac{\phi_3 - \phi_1}{\Delta p} + \sigma_2 \omega_2 = -\frac{R \dot{Q}_2}{p_2 c_p} \quad (3.10)$$

Eq.(3.9) is multiplied by $f_0/(\sigma_2 \Delta p)$ and then added to (3.5) to eliminate ω_2 . Similarly (3.10) is multiplied by $f_0/(\sigma_2 \Delta p)$ and substracted from (3.6). Hence we get the quasi-geostrophic potential vorticity equations at levels 1 and 3.

$$\left(\frac{\partial}{\partial t} + u_1 \frac{\partial}{\partial x} + v_1 \frac{\partial}{\partial y}\right) \left\{\zeta_1 + \frac{S_2}{f_0}(\phi_3 - \phi_1)\right\} + \beta v_1 = -\frac{R \Delta p S_2}{f_0 p_2 c_p} \dot{Q}_2 \quad (3.11)$$

and

$$\left(\frac{\partial}{\partial t} + u_3 \frac{\partial}{\partial x} + v_3 \frac{\partial}{\partial y}\right) \left\{\zeta_3 - \frac{S_2}{f_0}(\phi_3 - \phi_1)\right\} + \beta v_3 - \frac{f_0}{\Delta p} \omega_f = \frac{R \Delta p S_2}{f_0 p_2 c_p} \dot{Q}_2 \quad (3.12)$$

respectively, where $S_2 \equiv f_0^2/\{\sigma_2(\Delta p)^2\}$. The above equations are linearised as in Section 2.1 and we get the resulting perturbation potential vorticity equations at levels 1 and 3.

$$\left(\frac{\partial}{\partial t} + U_1\frac{\partial}{\partial x}\right)\left\{\nabla^2\phi_1' + S_2(\phi_3' - \phi_1')\right\}$$

$$+ f_0 v_1'\left\{\beta - \frac{\partial^2 U_1}{\partial y^2} - S_2(U_3 - U_1)\right\} = -\frac{R\,\Delta p\, S_2}{p_2\, c_p}\dot{Q}_2' \qquad (3.13)$$

and

$$\left(\frac{\partial}{\partial t} + U_3\frac{\partial}{\partial x}\right)\left\{\nabla^2\phi_3' - S_2(\phi_3' - \phi_1')\right\} - \frac{f_0^2}{\Delta p}\omega_f'$$

$$+ f_0 v_3'\left\{\beta - \frac{\partial^2 U_3}{\partial y^2} + S_2(U_3 - U_1)\right\} = \frac{R\,\Delta p\, S_2}{p_2\, c_p}\dot{Q}_2' \qquad (3.14)$$

In this section we will consider the case $\dot{Q}_2' = 0$.

3.1.2 The model:

In this two-level quasi-geostrophic model we have considered the Ekman layer friction by assuming that the vertical velocity at the lower boundary is due only to frictional pumping through the Ekman layer (Charney and Eliassen, 1949). Thus

$$\omega_f' = -0.8\,\rho\, g\sqrt{\frac{K}{2}}\; f_0^{-3/2}(\sin 2\alpha_s)\,\nabla^2\phi_3' \qquad (3.15)$$

Factor 0.8 is there so that the geostrophic vorticity at the bottom boundary is 0.8 times its value at level 3. Here K is the eddy diffusivity and α_s is the angle between the isobars and the surface wind.

The upper boundary condition is $\omega_0' = 0$ at $p = 0$, but we have conducted the stability analysis with two separate lower boundary conditions; $\omega_4' = \omega_f'$ (with Ekman layer friction) and $\omega_4' = 0$ (without surface frictional dissipation) at $p = p_0$.

As in Chapter 2, wavelike solutions of geopotential perturbation are considered at both the levels. Thus

$$\phi_{1,3}' = \phi_{1,3}(y) \exp\{ik(x-ct)\} \qquad (3.16)$$

where

$$\phi_1(y) = \sum_{n=1}^{N} A_n \sin \frac{n\pi}{D}(y - y_s)$$

and

$$\phi_3(y) = \sum_{n=1}^{N} A_{N+n} \sin \frac{n\pi}{D}(y - y_s) \qquad (3.17)$$

For convenience we have used the same symbol A, with different subscripts (N+n) for the co-efficients of the second series. Zonal winds U_1 and U_3 are accurately represented by Fourier series (2.7).

Substituting for ϕ_1' and ϕ_3' in (3.13) and (3.14)

and using (3.15) we get the following equations for the upper and lower level respectively.

$$\sum_{n=1}^{N}\Big[\Big\{U_{1m}\eta_{m,n}+\Big(\beta-\frac{\partial^2 U_{1m}}{\partial y^2}-k^2U_{1m}-s_2U_{3m}\Big)\gamma_{m,n}\Big\}A_n - c\Big\{\eta_{m,n}-(k^2+s_2)\gamma_{m,n}\Big\}A_n+s_2U_{1m}\gamma_{m,n}A_{N+n} - c\,s_2\gamma_{m,n}A_{N+n}\Big]=0 \tag{3.18}$$

$$\sum_{n=1}^{N}\Big[s_2U_{3m}\gamma_{m,n}A_n-c\,s_2\gamma_{m,n}A_n+\Big\{U_{3m}\eta_{m,n}+\Big(\beta-\frac{\partial^2U_{3m}}{\partial y^2}-k^2U_{3m}-s_2U_{1m}\Big)\gamma_{m,n}\Big\}A_{N+n}+\frac{i}{k}F\big(k^2\gamma_{m,n}-\eta_{m,n}\big)A_{N+n}-c\Big\{\eta_{m,n}-(k^2+s_2)\gamma_{m,n}\Big\}A_{N+n}\Big]=0 \tag{3.19}$$

$\gamma_{m,n}$ and $\eta_{m,n}$ are defined in (2.12) and

$$F=\frac{0.8fg}{\Delta p}\sqrt{\frac{Kf_0}{2}}\,\sin(2\alpha_s) \tag{3.20}$$

As in Section 2.2 we put the subscript 'm' to identify a particular latitude in the channel and following the justification given there we consider N number of equations from each level and then arrange the terms of the 2N number of resulting algebraic equations to get a matrix equation like (2.13). But here $\underset{\sim}{B}$ is a complex matrix.

Denoting its real and imaginary parts by $\underset{\sim}{B}^r$ and $\underset{\sim}{B}^i$ respectively, we get the eigenvalue equation

$$\left(\underset{\sim}{B}^r \cdot \underset{\sim}{D}^{-1} + i\,\underset{\sim}{B}^i \cdot \underset{\sim}{D}^{-1} - c\,\underset{\sim}{I}\right)\left(\underset{\sim}{D}\cdot\underset{\sim}{A}\right) = 0 \qquad (3.21)$$

$\underset{\sim}{B}^r$, $\underset{\sim}{B}^i$ and $\underset{\sim}{D}$ are real square matrices of size 2N x 2N. As discussed in Chapter 2, the eigenvalues give the phase speed and the growthrate of the disturbances, whereas the eigenfumctions are used to calculate the amplitudes.

The non zero elements $b^r_{m,n}$, $b^i_{m,n}$ and $d_{m,n}$ of matrices $\underset{\sim}{B}^r$, $\underset{\sim}{B}^i$ and $\underset{\sim}{D}$ respectively appearing in (3.21) are defined as follows.

$$b^r_{m,n} = U_{1m}\eta_{m,n} + \left(\beta - \frac{\partial^2 U_{1m}}{\partial y^2} - k^2 U_{1m} - s_2 U_{3m}\right)\gamma_{m,n}$$

$$b^r_{m,N+n} = s_2 U_{1m}\gamma_{m,n}$$

$$b^r_{N+m,n} = s_2 U_{3m}\gamma_{m,n}$$

$$b^r_{N+m,N+n} = U_{3m}\eta_{m,n} + \left(\beta - \frac{\partial^2 U_{3m}}{\partial y^2} - k^2 U_{3m} - s_2 U_{1m}\right)\gamma_{m,n}$$

$$b^i_{N+m,N+n} = \frac{F}{k}\left(k^2\gamma_{m,n} - \eta_{m,n}\right)$$

$$d_{m,n} = \eta_{m,n} - \left(k^2 + s_2\right)\gamma_{m,n}$$

$$d_{m,N+n} = s_2 \gamma_{m,n}$$

$$d_{m+N,n} = s_2 \gamma_{m,n}$$

$$d_{N+m,N+n} = \eta_{m,n} - (k^2 + s_2)\gamma_{m,n}$$

where both m and n vary from 1 to N. It is to be noted that wherever U appears with two subscripts, the first one refers to the level and the second to the latitude.

3.1.3 Results:

The analysis yields no lower tropospheric mode with appreciable growth rate. However, perturbations at 200 mb grow slowly with doubling time of 9 days and with westward phase speed of about 17 m s^{-1} (Table 5). These rapidly propagating disturbances possibly correspond to easterly waves one observes in the upper troposphere. When surface friction is not included in the model, the growth rate is found to increase. In the absence of cumulus heating and surface friction the doubling time of the fastest growing disturbance at 200 mb is 5 days.

Table 5

Two-level model:

Characteristics of growing modes with maximum amplitude at 200 mb

Horizontal scale length (km)	Phase speed C_r (m s^{-1})	Doubling time τ_d (days)	200 mb Maximum Φ_1	200 mb Position of maximum Φ_1 (°N)	700 mb Maximum Φ_3	700 mb Position of maximum Φ_3 (°N)
2000	-17.4	10.7	130	22	1.2	22
2200	-17.3	9.6	130	22	1.5	22
2400	-17.3	9.2	130	22	1.7	22
2600	-17.3	9.0	140	22	2.0	21
2800	-17.3	9.1	140	22	2.3	21
3000	-17.3	9.2	140	22	2.6	21

3.2 Inclusion of cumulus heating:

The purpose of this section is to study the effect of inclusion of cumulus heating into the two-level model. It may be noted that we do not intend to carry out detailed parameterisation of cumulus heating. It is our object to study the effect of inclusion of a simple form of heating on the growth of disturbances. We have specified the convective heating only at mid-tropospheric level. Following Charney and Eliassen (1964) the rate of heating per unit mass can be written as

$$\dot{Q}' = H_f(p)\, C_p \left(\frac{p}{p_0}\right)^{R/c_p} \frac{\partial \theta}{\partial p}\, \omega_f' \qquad (3.22)$$

Here $H_f(p)$ is the vertical distribution function for heating and it is a measure of the rate of condensation of water vapour at the pressure level p. Using (3.15), (3.20) and (3.22), we can simplify the heating terms on the right hand side of (3.13) and (3.14) as

$$\frac{R\,\Delta p\, S_2}{p_2\, C_p}\, \dot{Q}_2' = F\, H_f\, \nabla^2 \phi_3' \qquad (3.23)$$

In the two-level model $H_f(p)$ is prescribed at 500 mb simply by a number. Following Ogura (1964) we have taken $H_f = 3.0$. To examine the effect of heating we have also done the analysis by reducing H_f by half.

Using (3.23) we can get matrix equation (3.21) from (3.13) and (3.14) as in Section 3.1.2. The elements of matrices $\underset{\sim}{B}^r$ and $\underset{\sim}{D}$ are same as defined in Section 3.1.2. But the elements of matrix $\underset{\sim}{B}^i$ are different and its non-zero elements are defined below.

$$b^i_{m,N+n} = \frac{1}{k} F H_f \left(k^2 \gamma_{m,n} - \eta_{m,n}\right)$$

$$b^i_{N+m,N+n} = \frac{1}{k} F (1 - H_f)\left(k^2 \gamma_{m,n} - \eta_{m,n}\right)$$

where m and n vary from 1 to N.

So far as the upper tropospheric disturbances are concerned, their characteristics are hardly affected (Tables 5 and 6) by the cumulus heating. However, with the inclusion of heating into the model lower tropospheric growing modes are found. When $H_f = 3.0$, the fastest growing disturbance has doubling time of 1.7 days and horizontal scale length of 2400 km (Fig. 10, $\omega'_4 = \omega'_f$). It has eastward phase speed of 2.5 m s^{-1} and the amplitude is maximum at 21°N (Table 7). The amplitude distribution (Fig. 11) shows that the disturbance is mainly confined to the lower troposphere. When the heating is reduced by half, the doubling time of the fastest growing mode is increased to 5 days (Fig. 12, $\omega'_4 = \omega'_f$), but other characteristics like the horizontal scale length, phase speed and the amplitude distribution are not affected

Table 6

Two-level model with cumulus heating: Characteristics of growing modes with maximum amplitude at 200 mb.

Heating co-efficients H_f	Horizontal scale length (km)	Phase speed C_r ($m\ s^{-1}$)	Doubling Time τ_d (Days)	200 mb Maximum Φ_1	200 mb Position of maximum Φ_1 (°N)	700 mb Maximum Φ_3	700 mb Position of maximum Φ_3 (°N)
1.5	2000	-17.4	10.8	130	22	1.2	22
	2200	-17.3	9.7	130	22	1.5	22
	2400	-17.3	9.2	130	22	1.7	22
	2600	-17.3	9.1	140	22	2.0	21
	2800	-17.3	9.2	140	22	2.3	21
	3000	-17.3	9.3	140	22	2.6	21
3.0	2000	-17.4	10.9	130	22	1.2	22
	2200	-17.3	9.8	130	22	1.5	22
	2400	-17.3	9.3	130	22	1.7	22
	2600	-17.3	9.2	140	22	2.0	21
	2800	-17.3	9.3	140	22	2.3	21
	3000	-17.3	9.4	140	22	2.6	21

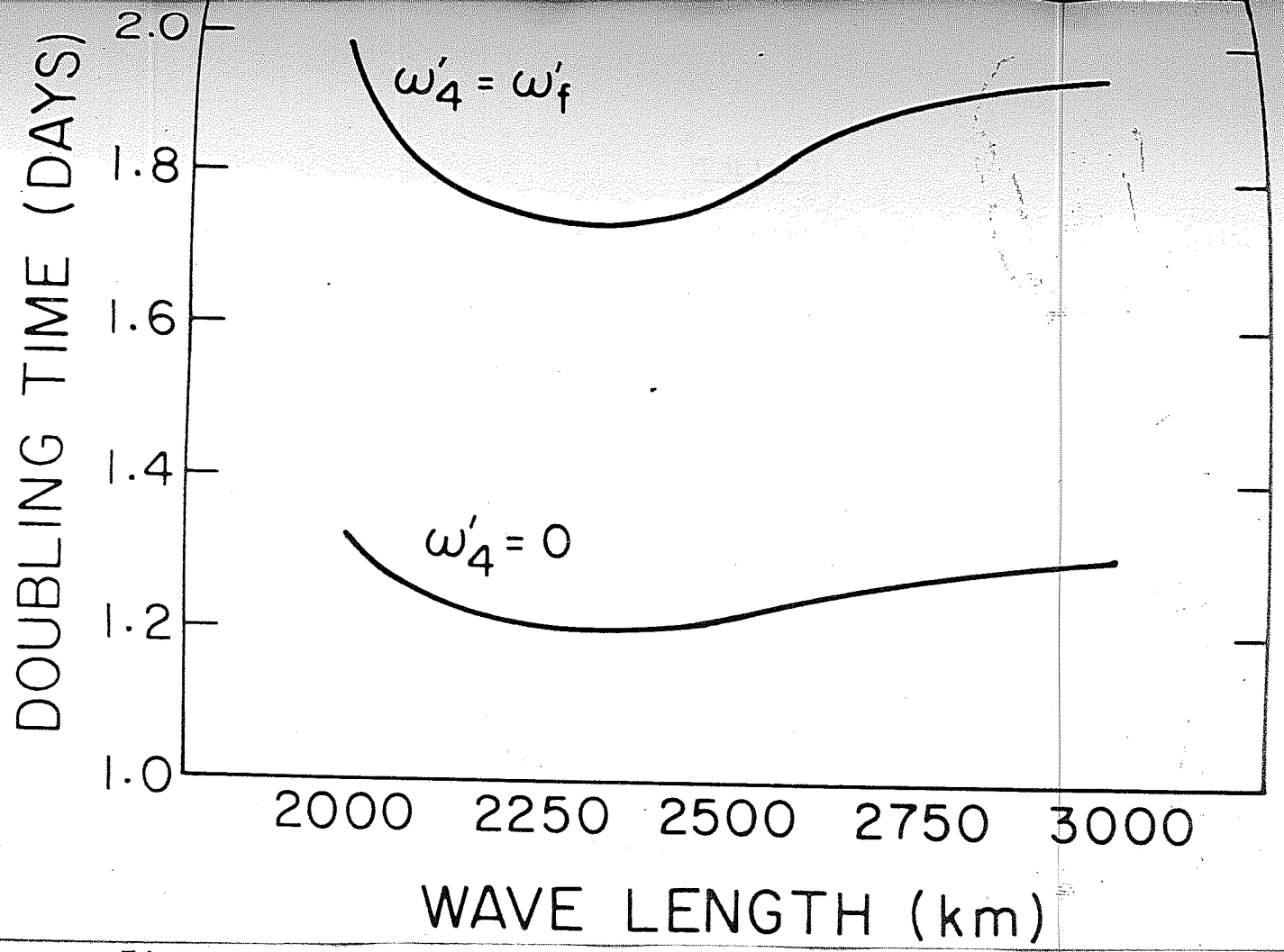

Figure 10: Scale dependence of the growth of unstable modes in two-level model when $H_f = 3.0$ ($\omega'_4 = \omega'_f$ indicates the inclusion of Ekman layer friction into the model)

Table 7

Two-level model with cumulus heating: Characteristics of growing modes with maximum amplitude at 700 mb.

Heating Coefficient H_f	Horizontal Scale length (km)	Phase Speed C_r (m s^{-1})	Doubling Time τ_d (days)	200 mb Maximum Φ_1	200 mb Position of maximum Φ_1 (°N)	700 mb Maximum Φ_3	700 mb Position of maximum Φ_3 (°N)
1.5	2000	2.5	7.9	9	21	190	21
	2200	2.5	5.4	10	21	190	21
	2400	2.4	5.3	11	21	210	21
	2600	2.3	6.6	13	21	220	21
	2800	2.3	7.7	13	20	210	19
	3000	2.4	7.7	15	18	230	18
3.0	2000	2.5	2.0	17	21	190	21
	2200	2.5	1.8	19	21	190	21
	2400	2.4	1.7	22	21	210	21
	2600	2.3	1.8	25	21	220	21
	2800	2.3	1.9	25	21	210	20
	3000	2.4	1.9	27	18	230	18

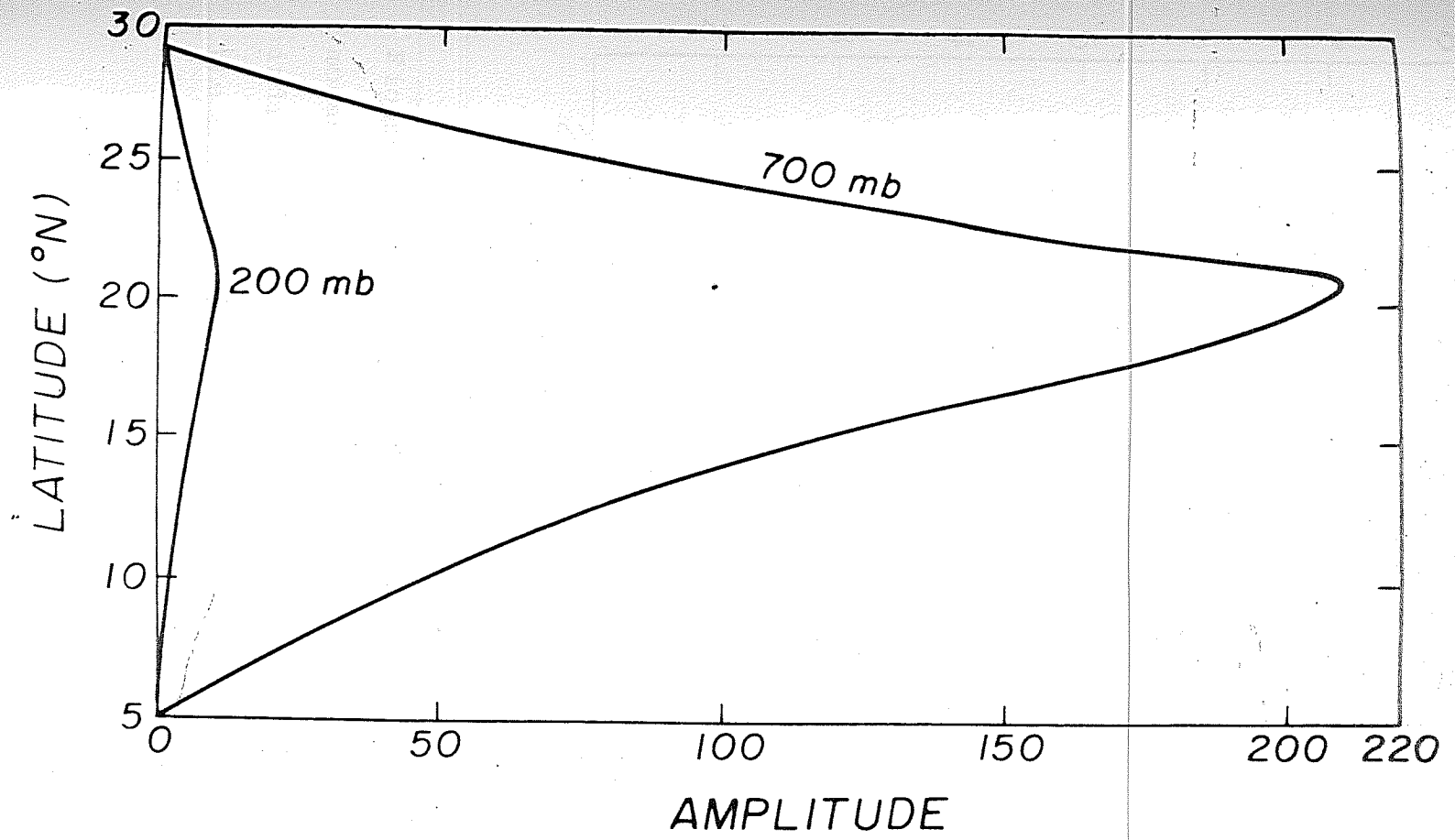

Figure 11: Amplitude structure of the fastest growing disturbance of Fig. 10 when $\omega_4' = \omega_f'$.

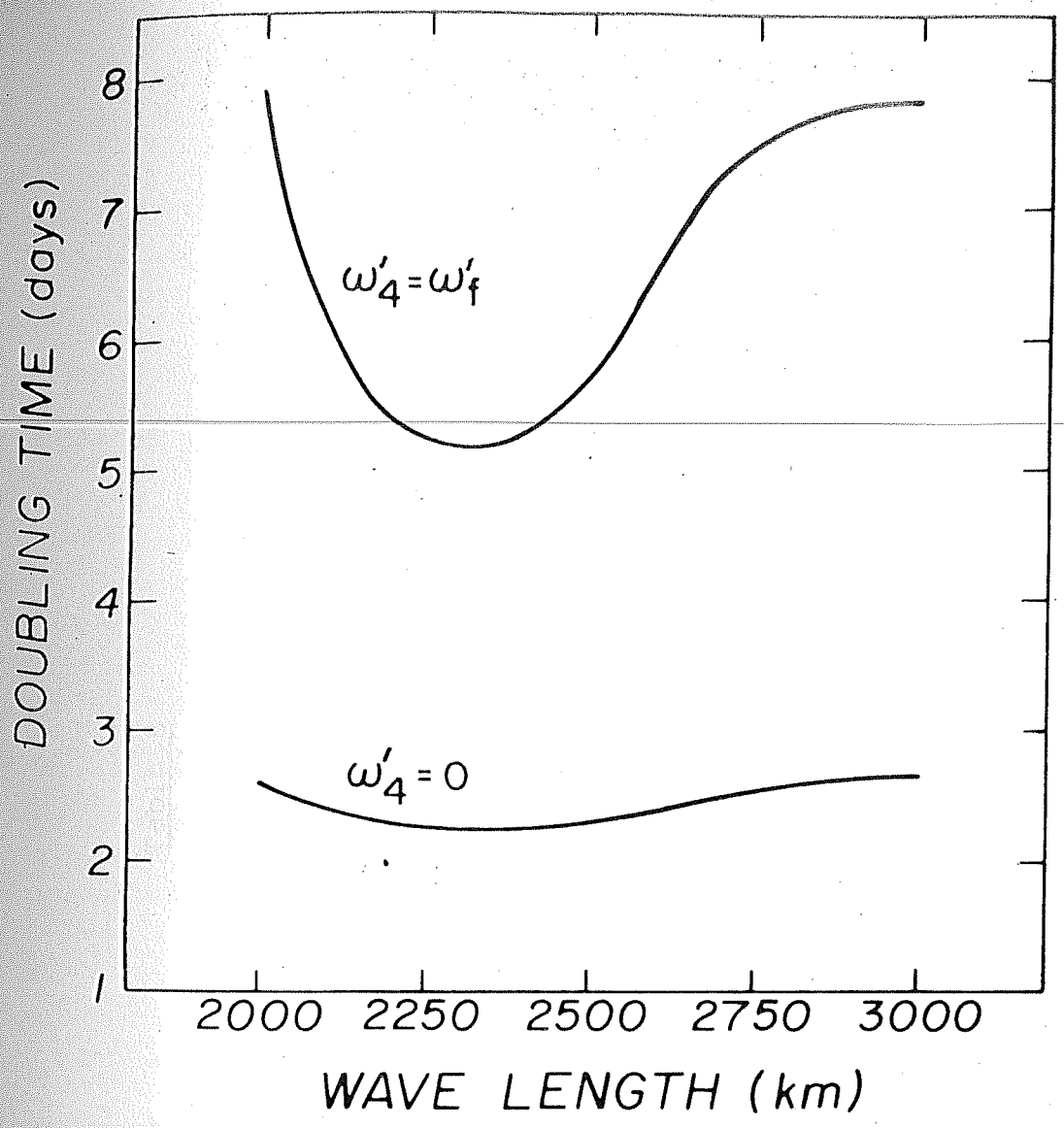

Figure 12: Scale dependence of the growth of unstable modes in two-level model when $H_f = 1.5$. ($\omega'_4 = \omega'_f$ indicates the inclusion of Ekman layer friction into the model).

Table 8

Two-level mode without frictional dissipation: Characteristics of growing modes with maximum amplitude at 700 mb.

Heating Coefficient H_f	Horizontal Scale length (km)	Phase Speed C_r (m s^{-1})	Doubling Time τ_d (days)	200 mb		700 mb	
				Maximum Φ_1	Position of maximum Φ_1 (°N)	Maximum Φ_3	Position of maximum Φ_3 (°N)
1.5	2000	2.5	2.63	9	21	190	21
	2200	2.5	2.27	10.	21	190	21
	2400	2.4	2.25	11	21	210	21
	2600	2.3	2.43	13	21	220	21
	2800	2.3	2.56	13	20	210	19
	3000	2.4	2.59	14	19	230	19
3.0	2000	2.5	1.32	17	21	190	21
	2200	2.5	1.21	18	21	190	21
	2400	2.4	1.20	21	21	210	21
	2600	2.3	1.24	24	21	220	21
	2800	2.3	1.28	25	20	210	19
	3000	2.4	1.29	27	18	230	18

(Table 7).

To see what happens when the frictional dissipation is neglected we have also done the stability analysis by using the surface boundary condition $\omega'_4 = 0$. It is found that the growth rates of the disturbances are increased compared to the previous case when $\omega'_4 = \omega'_f$. When $H_f = 3.0$ the doubling time is about 1 day and for $H_f = 1.5$, $\tau_d = 2$ days (Figs. 10 and 12). We find that there is no preferred scale for the fastest growing disturbance when the surface friction term is dropped. In this case the doubling time hardly changes with the horizontal scale of the disturbance. The phase speed and the amplitude distribution remain same in both the cases (Tables 7 and 8).

3.3 Five-level quasi-geostrophic model:

3.3.1 The model:

We have extended the stability analysis of monsoon zonal flow to a five-level quasi-geostrophic model in order to have greater vertical resolution. The atmosphere is divided into five layers and the different parameters to be prescribed at different levels are

shown below.

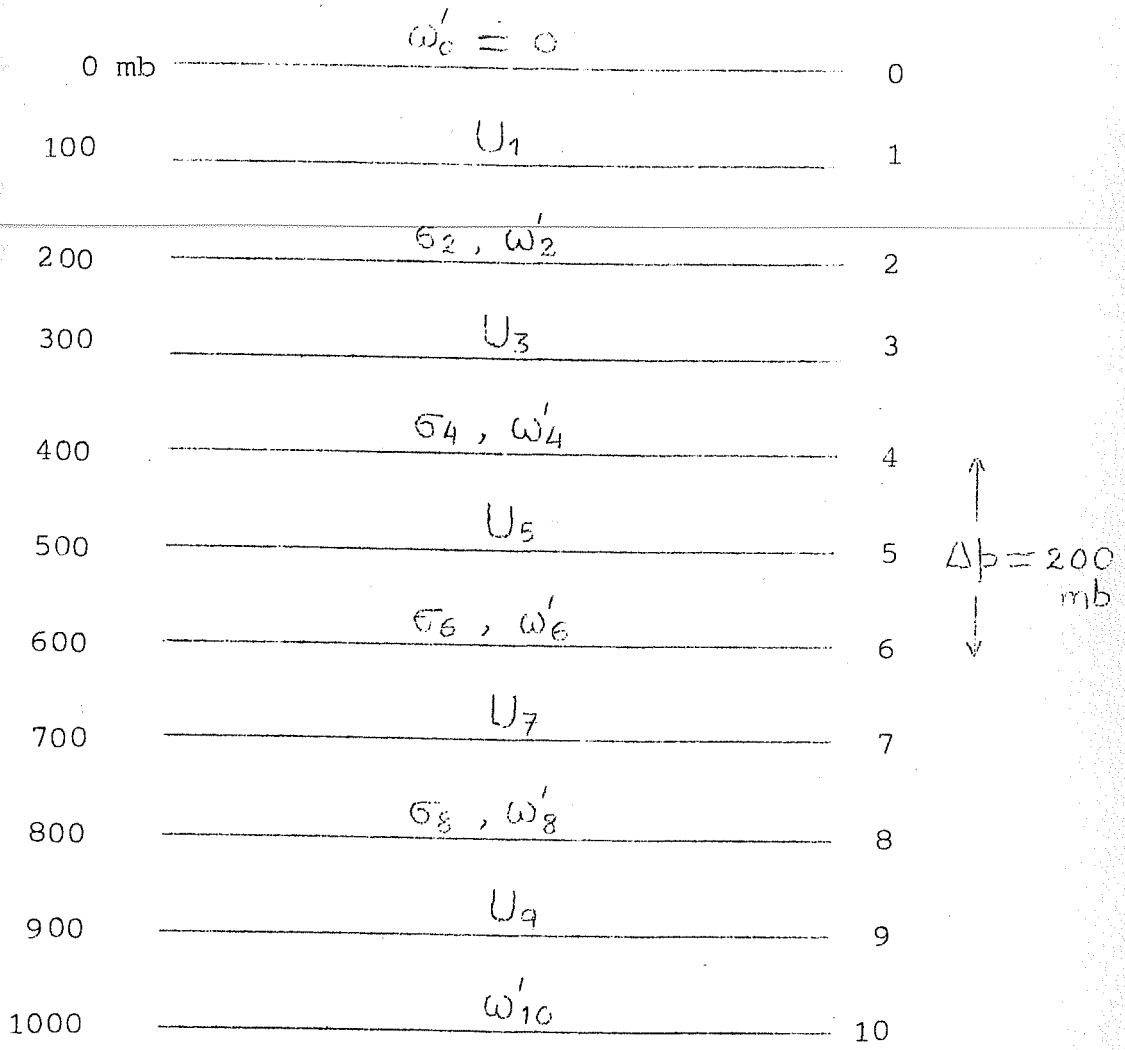

Static stability parameter σ at different levels are same as used by Keshavamurty et al. (1978). The quasi-geostrophic vorticity equations (3.3) at levels 1, 3, 5, 7 and 9 and the thermodynamic energy equations (3.4) at levels 2, 4, 6 and 8 are considered and the potential

vorticity equations at levels 1, 3, 5, 7 and 9 are derived as in Section 3.1.1 and then these equations are linearized as described before. Thus we get the following perturbation potential vorticity equations.

Level 1:

$$\left(\frac{\partial}{\partial t}+U_1\frac{\partial}{\partial x}\right)\left\{\zeta_1'+\frac{S_2}{f_0}(\phi_3'-\phi_1')\right\}$$
$$+v_1'\left\{\beta-\frac{\partial^2 U_1}{\partial y^2}-S_2(U_3-U_1)\right\}=-\frac{R\,\Delta p\,S_2}{f_0\,p_2\,c_p}\dot{Q}_2' \qquad (3.24)$$

Levels 3, 5 and 7:

$$\left(\frac{\partial}{\partial t}+U_l\frac{\partial}{\partial x}\right)\left\{\zeta_l'+\frac{S_{l+1}}{f_0}(\phi_{l+2}'-\phi_l')-\frac{S_{l-1}}{f_0}(\phi_l'-\phi_{l-2}')\right\}$$
$$+v_l'\left\{\beta-\frac{\partial^2 U_l}{\partial y^2}-S_{l+1}(U_{l+2}-U_l)+S_{l-1}(U_l-U_{l-2})\right\}$$
$$=-\frac{R\,\Delta p}{f_0 c_p}\left(\frac{S_{l+1}}{p_{l+1}}\dot{Q}_{l+1}'-\frac{S_{l-1}}{p_{l-1}}\dot{Q}_{l-1}'\right) \qquad (3.25)$$

where l = 3, 5, and 7 respectively.

Level 9:

$$\left(\frac{\partial}{\partial t}+U_9\frac{\partial}{\partial x}\right)\left\{\zeta_9'-\frac{S_8}{f_0}(\phi_9'-\phi_7')\right\}-\frac{f_0}{\Delta p}\omega_f'$$
$$+v_9'\left\{\beta-\frac{\partial^2 U_9}{\partial y^2}+S_8(U_9-U_7)\right\}=\frac{R\,\Delta p\,S_8}{f_0\,p_8\,c_p}\dot{Q}_8' \qquad (3.26)$$

As before we assume wavelike solution for the perturbation geopotential field at each level.

$$\phi_l' = \phi_l(y)\ \exp\{ik(x-ct)\} \tag{3.27}$$

where

$$\phi_l(y) = \sum_{n=1}^{N} A_{\left(\frac{l-1}{2}N+n\right)} \sin\frac{n\pi}{D}(y-y_s) \tag{3.28}$$

and $l = 1, 3, 5, 7$ and 9.

Also the zonal winds (Fig. 13) at levels 1, 3, 5, 7 and 9 are accurately represented by Fourier series (2.7). The rate of heating per unit mass and Ekman layer friction are given by (3.22) and (3.15) respectively. In the absence of actual vertical distribution of heating we have experimented with three different types of distribution functions $H_f(p)$ as shown in Fig. 14. For type (b) the distribution is parabolic with maximum heating at 500 mb. In case of (a) the heating is maximum at 600 mb and in type (c) the maximum release of latent heat is at a higher level, 400 mb. The total heating in each case is the same. Using (3.15), (3.20) and (3.22) one can simplify the heating terms on the right hand side of equations (3.24) to (3.26) and write

$$\frac{R\,\Delta p\,S_{l+1}}{p_{l+1}\,c_p}\,\dot{Q}'_{l+1} = F\,H_{f_{l+1}}\nabla^2\phi_{l+2} \tag{3.29}$$

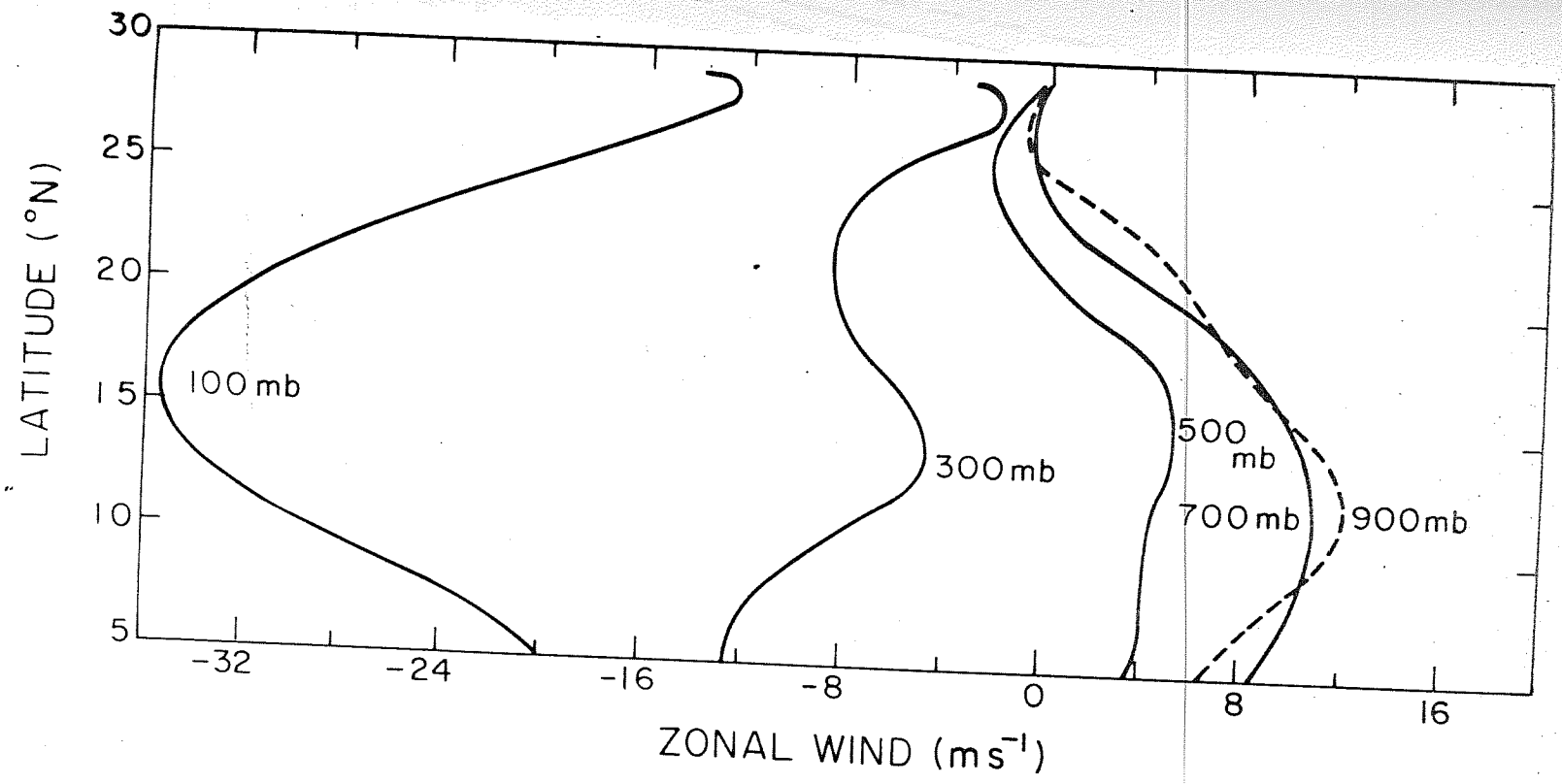

Figure 13: July mean zonal wind profiles U_1, U_3, U_5, U_7 and U_9 (m s^{-1}) at 100 mb, 300 mb, 500 mb, 700 mb and 900 mb respectively.

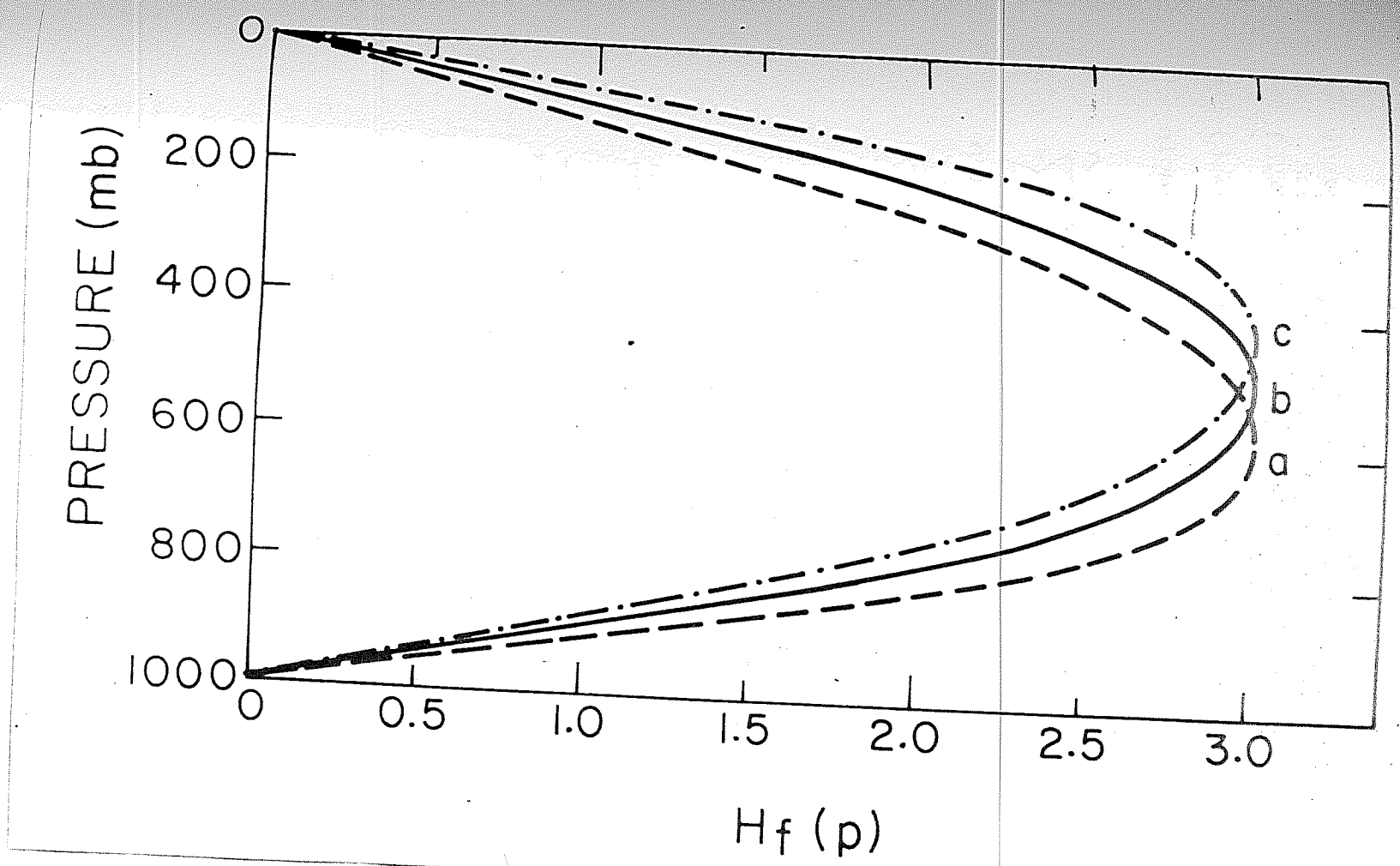

Figure 14: Three different types of heating distributions in the vertical included in the five-level model.

where l = 1, 3, 5 and 7. Using (3.15), (3.27), (3.28) and (3.29) in perturbation potential vorticity equations (3.24) to (3.26) and simplifying we get the following algebraic equations for levels 1, 3, 5, 7 and 9 respectively.

$$\sum_{n=1}^{N} \Big[\Big\{ U_{1m}\eta_{m,n} + \Big(\beta - \frac{\partial^2 U_{1m}}{\partial y^2} - k^2 U_{1m} - s_2 U_{3m}\Big)\gamma_{m,n} \Big\} A_n + s_2 U_{1m}\gamma_{m,n} A_{N+n} + \frac{i}{k} H_{f_2} F\big(k^2\gamma_{m,n} - \eta_{m,n}\big) A_{N+n} - c\Big\{\eta_{m,n} - (k^2 + s_2)\gamma_{m,n}\Big\} A_n - c\, s_2 \gamma_{m,n} A_{N+n} \Big] = 0 \tag{3.30}$$

$$\sum_{n=1}^{N} \Big[s_2 U_{3m}\gamma_{m,n} A_n + \Big\{ U_{3m}\eta_{m,n} + \Big(\beta - \frac{\partial^2 U_{3m}}{\partial y^2} - k^2 U_{3m} - s_2 U_{1m} - s_4 U_{5m}\Big)\gamma_{m,n} \Big\} A_{N+n} + s_4 U_{3m}\gamma_{m,n} A_{2N+n} - \frac{i}{k} H_{f_2} F\big(k^2\gamma_{m,n} - \eta_{m,n}\big) A_{N+n} + \frac{i}{k} H_{f_4} F\big(k^2\gamma_{m,n} - \eta_{m,n}\big) A_{2N+n} - c\, s_2 \gamma_{m,n} A_n - c\Big\{\eta_{m,n} - (k^2 + s_2 + s_4)\gamma_{m,n}\Big\} A_{N+n} - c\, s_4 \gamma_{m,n} A_{2N+n} \Big] = 0 \tag{3.31}$$

$$\sum_{n=1}^{N}\Big[s_4 U_{5m}\gamma_{m,n} A_{N+n} + \Big\{U_{5m}\eta_{m,n} + \Big(\beta - \frac{\partial^2 U_{5m}}{\partial y^2} - k^2 U_{5m} - s_4 U_{3m} - s_6 U_{7m}\Big)\gamma_{m,n}\Big\} A_{2N+n} + s_6 U_{5m}\gamma_{m,n} A_{3N+n} - \frac{i}{k} H f_4 F\big(k^2\gamma_{m,n} - \eta_{m,n}\big) A_{2N+n} + \frac{i}{k} H f_6 F\big(k^2\gamma_{m,n} - \eta_{m,n}\big) A_{3N+n} - c\, s_4 \gamma_{m,n} A_{N+n} - c\Big\{\eta_{m,n} - (k^2 + s_4 + s_6)\gamma_{m,n}\Big\} A_{2N+n} - c\, s_6 \gamma_{m,n} A_{3N+n}\Big] = 0 \qquad (3.32)$$

$$\sum_{n=1}^{N}\Big[s_6 U_{7m}\gamma_{m,n} A_{2N+n} + \Big\{U_{7m}\eta_{m,n} + \Big(\beta - \frac{\partial^2 U_{7m}}{\partial y^2} - k^2 U_{7m} - s_6 U_{5m} - s_8 U_{9m}\Big)\gamma_{m,n}\Big\} A_{3N+n} + s_8 U_{7m}\gamma_{m,n} A_{4N+n} - \frac{i}{k} H f_6 F\big(k^2\gamma_{m,n} - \eta_{m,n}\big) A_{3N+n} - c\, s_6 \gamma_{m,n} A_{2N+n} + \frac{i}{k} H f_8 F\big(k^2\gamma_{m,n} - \eta_{m,n}\big) A_{4N+n} - c\, s_8 \gamma_{m,n} A_{4N+n} - c\Big\{\eta_{m,n} - (k^2 + s_6 + s_8)\gamma_{m,n}\Big\} A_{3N+n}\Big] = 0 \qquad (3.33)$$

$$\sum_{n=1}^{N}\Big[s_8 U_{qm}\gamma_{m,n}A_{3N+n}+\Big\{U_{qm}\eta_{m,n}+\Big(\beta-\frac{\partial^2 U_{qm}}{\partial y^2}-k^2U_{qm}-s_8U_{7m}\Big)\gamma_{m,n}\Big\}A_{4N+n}+\frac{i}{k}F(1-Hf_8)\Big(k^2\gamma_{m,n}-\eta_{m,n}\Big)A_{4N+n}-cs_8\gamma_{m,n}A_{3N+n}-c\Big\{\eta_{m,n}-\gamma_{m,n}(k^2+s_8)\Big\}A_{4N+n}\Big]=0 \tag{3.34}$$

Eqs. (3.30) to (3.34) are true for each latitude denoted by subscript 'm'. For mathematical conveneience we make m = N as discussed in Section 2.2. We truncate the series (3.28) for N = 12 and thus we have 60 algebraic equations from the above sets of equations. For computational limitations we could not increase N more than 12. Finally arranging the terms we can get an eigenvalue equation in matrix form (3.21). It is evident that $\underset{\sim}{B}$, $\underset{\sim}{B}^i$ and $\underset{\sim}{D}$ are square matrices of size 60 x 60 and $\underset{\sim}{A}$ is a column matrix with 60 elements. Characteristics of growing modes are obtained by solving the eigenvalue equations by numerical algorithms.

The nonzero elements $b^r_{m,n}$, $b^i_{m,n}$, $d_{m,n}$ of matrices $\underset{\sim}{B}^r, \underset{\sim}{B}^i, \underset{\sim}{D}$ respectively are defined below where m and n both vary from 1 to N.

$$b^v_{m,n} = U_{1m}\,\eta_{m,n} + \left(\beta - \frac{\partial^2 U_{1m}}{\partial y^2} - k^2 U_{1m} - s_2 U_{3m}\right)\gamma_{m,n}$$

$$b^r_{m,N+n} = s_2\,U_{1m}\,\gamma_{m,n}$$

$$b^v_{N+m,n} = s_2\,U_{3m}\,\gamma_{m,n}$$

$$b^r_{N+m,N+n} = U_{3m}\,\eta_{m,n} + \left(\beta - \frac{\partial^2 U_{3m}}{\partial y^2} - k^2 U_{3m} - s_2 U_{1m} - s_4 U_{5m}\right)\gamma_{m,n}$$

$$b^r_{N+m,2N+n} = s_4\,U_{3m}\,\gamma_{m,n}$$

$$b^r_{2N+m,N+n} = s_4\,U_{5m}\,\gamma_{m,n}$$

$$b^r_{2N+m,2N+n} = U_{5m}\,\eta_{m,n} + \left(\beta - \frac{\partial^2 U_{5m}}{\partial y^2} - k^2 U_{5m} - s_4 U_{3m} - s_6 U_{7m}\right)\gamma_{m,n}$$

$$b^r_{2N+m,3N+n} = s_6\,U_{5m}\,\gamma_{m,n}$$

$$b^r_{3N+m,\,2N+n} = s_6\, U_{7m}\, r_{m,n}$$

$$b^r_{3N+m,\,3N+n} = U_{7m}\,\eta_{m,n} + \left(\beta - \frac{\partial^2 U_{7m}}{\partial y^2} - k^2 U_{7m} - s_6 U_{5m} - s_8 U_{9m}\right) r_{m,n}$$

$$b^r_{3N+m,\,4N+n} = s_8\, U_{7m}\, r_{m,n}$$

$$b^r_{4N+m,\,3N+n} = s_8\, U_{9m}\, r_{m,n}$$

$$b^r_{4N+m,\,4N+n} = U_{9m}\,\eta_{m,n} + \left(\beta - \frac{\partial^2 U_{9m}}{\partial y^2} - k^2 U_{9m} - s_8 U_{7m}\right) r_{m,n}$$

$$b^i_{m,N+n} = \frac{1}{k} H_{f_2} F\left(k^2 r_{m,n} - \eta_{m,n}\right)$$

$$b^i_{N+m,N+n} = -\frac{1}{k} H_{f_2} F\left(k^2 r_{m,n} - \eta_{m,n}\right)$$

$$b^i_{N+m,2N+n} = \frac{1}{k} H_{f_4} F\left(k^2 r_{m,n} - \eta_{m,n}\right)$$

$$b^i_{2N+m,2N+n} = -\frac{1}{k} H_{f_4} F\left(k^2 r_{m,n} - \eta_{m,n}\right)$$

$$b^i_{2N+m,3N+n} = \frac{1}{k} H_{f_6} F\left(k^2 r_{m,n} - \eta_{m,n}\right)$$

$$\dot{b}^{i}_{3N+m,\,3N+n} = -\frac{1}{k} H_{f_6} F \left(k^2 \gamma_{m,n} - \eta_{m,n}\right)$$

$$\dot{b}^{i}_{3N+m,\,4N+n} = \frac{1}{k} H_{f_8} F \left(k^2 \gamma_{m,n} - \eta_{m,n}\right)$$

$$\dot{b}^{i}_{4N+m,\,4N+n} = \frac{1}{k} F \left(1 - H_{f_8}\right)\left(k^2 \gamma_{m,n} - \eta_{m,n}\right)$$

$$d_{m,n} = \eta_{m,n} - \left(k^2 + s_2\right) \gamma_{m,n}$$

$$d_{m,N+n} = s_2 \gamma_{m,n}$$

$$d_{N+m,n} = s_2 \gamma_{m,n}$$

$$d_{N+m,N+n} = \eta_{m,n} - \left(k^2 + s_2 + s_4\right) \gamma_{m,n}$$

$$d_{N+m,\,2N+n} = s_4 \gamma_{m,n}$$

$$d_{2N+m,\,N+n} = s_4 \gamma_{m,n}$$

$$d_{2N+m,\,2N+n} = \eta_{m,n} - \left(k^2 + s_4 + s_6\right) \gamma_{m,n}$$

$$d_{2N+m,\,3N+n} = s_6 \gamma_{m,n}$$

$$d_{3N+m,\,2N+n} = s_6 \gamma_{m,n}$$

$$d_{3N+m,\,3N+n} = \eta_{m,n} - \left(k^2 + s_6 + s_8\right) \gamma_{m,n}$$

$$d_{3N+m,\,4N+n} = s_8 \gamma_{m,n}$$

$$d_{4N+m,\,3N+n} = s_8 \gamma_{m,n}$$

$$d_{4N+m,\,4N+n} = \eta_{m,n} - \left(k^2 + s_8\right) \gamma_{m,n}$$

3.3.2 Results:

When the cumulus heating is maximum at 600 mb the fastest growing mode has maximum amplitude at 700 mb. These disturbances grow to double their amplitudes in about 1.5 days and they move eastwards with phase speed of about 2 m s^{-1}. As shown in Table 9, at 700 mb the amplitudes are maximum at 22°N.

When the level of maximum heating is raised to 500 mb the fastest growing mode has maximum amplitude somewhere between 500 mb and 700 mb. These perturbations have the same phase speed and almost the same growth rate as in the previous case. So far as the meridional distribution of amplitude is concerned the disturbances have maximum amplitude in the region 19°N to 22°N latitudes (Table 10).

Finally the level of maximum cumulus heating is raised to 400 mb. The analysis yields that the fastest growing mode has maximum amplitude at 500 mb. They have eastward phase speed less than 1 m s^{-1} and their growth rates are same as in the previous two cases. At 500 mb the magnitudes of these disturbances are maximum at 19-20°N latitudes (Table 11).

In all the above three cases the doubling times are almost independent of the horizontal scales of the

Table 9

Five-level model: Characteristics of fastest growing modes with maximum amplitude at 700 mb. Heating corresponds to distribution function (a) in Figure 14.

Horizontal Scale Length	Phase speed	Doubling Time	100 mb		300 mb		500 mb		700 mb		900 mb	
	c_r	τ_d	Maximum	position	Maximum	position	Maximum	position	Maximum	position	Maximum	position
(km)	(m s^{-1})	(days)	Φ_1	(°N)	Φ_3	(°N)	Φ_5	(°N)	Φ_7	(°N)	Φ_9	(°N)
2000	2.0	1.3	0.6	23	19	22	130	22	240	22	9	22
2200	1.9	1.3	0.9	22	25	22	160	22	260	22	13	22
2400	1.9	1.3	1.1	22	31	22	180	22	290	22	17	21
2600	1.8	1.4	1.5	22	38	22	210	22	310	22	22	21
2800	1.8	1.4	1.8	22	45	22	240	22	340	21	28	21
3000	1.8	1.4	2.2	22	58	22	270	22	370	21	35	20

Table 10

Five-level model: Characteristics of fastest growing modes with maximum amplitude at 700 mb. Heating corresponds to distribution function (b) in Figure 14.

Horizontal scale Length (km)	Phase speed C_r ($m\ s^{-1}$)	Doubling Time τ_d (days)	100 mb		300 mb		500 mb		700 mb		900 mb	
			Maximum Φ_1	Position (°N)	Maximum Φ_3	Position (°N)	Maximum Φ_5	Position (°N)	Maximum Φ_7	Position (°N)	Maximum Φ_9	Position (°N)
2000	2.0	1.4	0.8	22	20	22	130	22	240	22	9	22
2200	1.9	1.4	1.1	22	26	22	150	22	260	22	12	21
2400	1.9	1.4	1.4	22	32	22	180	22	290	22	16	21
2600	1.8	1.4	1.8	22	39	22	200	22	310	22	21	21
2800	1.8	1.4	2.3	22	47	22	230	22	330	21	27	20
3000	1.8	1.4	2.8	22	56	22	260	22	360	21	33	20

Table 11

Five-level model: Characteristics of fastest growing modes with maximum amplitude at 500 mb. Heating corresponds to distribution function (c) in Figure 14.

Horizontal Scale Length (km)	Phase Speed C_r (m s^{-1})	Doubling Time τ_d (days)	100 mb		300 mb		500 mb		700 mb		900 mb	
			Maximum Φ_1	Position (°N)	Maximum Φ_3	Position (°N)	Maximum Φ_5	Position (°N)	Maximum Φ_7	Position (°N)	Maximum Φ_9	Position (°N)
2000	0.7	1.3	1.9	20	46	20	240	20	5	19	0.2	19
2200	0.6	1.3	2.5	19	55	20	270	20	6	19	0.4	19
2400	0.5	1.3	3.2	19	66	19	300	19	8	18	0.6	19
2600	0.5	1.3	4.0	19	78	19	380	19	11	18	0.8	18
2800	0.4	1.3	5.0	19	92	19	360	19	14	18	1.3	18
3000	0.4	1.3	6.1	19	110	19	400	19	18	17	1.8	18

disturbances. There is no preferred scale for the fastest growing mode.

3.4 Summary and Conclusions:

In this chapter the stability analyses of mean zonal flow over 80°E are conducted by expressing the basic winds and the meridional dependence of the geopotential perturbation by trigonometric series. The two-level combined barotropic-baroclinic stability analysis gives no lower tropospheric mode with appreciable growth rate. Perturbations at 200 mb grow slowly and propagate westwards rapidly (17 m s^{-1}), and possibly correspond to observed easterly waves in the upper troposphere. When a simple form of cumulus heating is included in the two-level model the fastest growing disturbance has doubling time of 1.7 days and horizontal scale of 2400 km. This disturbance is mainly confined to the lower troposphere. These characteristics agree well with those of the monsoon depressions. When the surface friction is neglected the growth rates of disturbances increase and there is no preferred scale for the fastest growing disturbance.

In the five-level model as the level of maximum heating is raised the fastest growing disturbance is found to occur at higher levels. The fastest growing disturbance is

confined to the lower troposphere when the heating is maximum at 600 mb or at 500 mb. Unlike in the two-level model the doubling time hardly changes with the horizontal scale of disturbance.

CHAPTER FOUR

STABILITY OF A STATIONARY ROSSBY WAVE EMBEDDED IN THE MONSOON ZONAL FLOW: TWO-LEVEL QUASI-GEOSTROPHIC MODEL

Monsoon zonal flow with horizontal and vertical wind shears is found to be unstable under the influence of Conditional Instability of the Second Kind (CISK). In these studies (conducted in the earlier chapters) the basic flow is assumed to be zonally uniform. In this chapter we intend to investigate the stability of monsoon flow which is not zonally uniform. The stability analysis of such a flow pattern which varies with longitude can be carried out by superposing a finite

amplitude Rossby wave on the zonal flow. Lorenz (1972) investigated the barotropic instability of zonal flow in middle latitudes with a superposed Rossby wave. Subsequent studies by Gill (1974), Duffy (1975), Merkine and Israeli (1978) and Lin (1980) in this regard are also confined to the midlatitudes. In this chapter we will conduct the stability analysis of monsoon zonal flow (with vertical shear) with a finite amplitude stationary baroclinic Rossby wave embedded in it.

In Section 4.1 we calculate the wavelength and the relative amplitudes at lower and upper levels of a stationary Rossby wave which can be supported by the observed monsoon zonal winds. In section 4.2 the stability analysis is conducted using a two-level quasi-geostrophic model with a beta-plane centred at 18°N latitude. Later, in Chapter 6 the analysis is extended using a primitive equation model. Energy calculations are done in Section 4.3 to find out the sources of energy for perturbations to grow.

4.1 Stationary Rossby wave:

We consider a two-level quasi-geostrophic model and calculate the wavelength and the relative amplitudes at

the lower and upper levels of a stationary Rossby wave which can be supported by the observed monsoon zonal winds. For convenience the potential vorticity equations (3.11) and (3.12) at 250 mb and 750 mb respectively can be rewritten as

$$\left(\frac{\partial}{\partial t}+u_1\frac{\partial}{\partial x}+v_1\frac{\partial}{\partial y}\right)\left\{\zeta_1+\frac{s_2}{f_0}(\phi_3-\phi_1)\right\}+\beta v_1=0 \qquad (4.1)$$

$$\left(\frac{\partial}{\partial t}+u_3\frac{\partial}{\partial x}+v_3\frac{\partial}{\partial y}\right)\left\{\zeta_3-\frac{s_2}{f_0}(\phi_3-\phi_1)\right\}+\beta v_3=0 \qquad (4.2)$$

where the diabatic heating is not considered. The subscripts 1,2 and 3 correspond to pressure levels 250 mb, 500 mb and 750 mb respectively. The other symbols have their usual meaning. The basic flow is given by

$$\begin{aligned}\Phi_1 &= -f_0 U_1 y + f_0 A \sin k_0 x \\ \Phi_3 &= -f_0 U_3 y + f_0 B \sin k_0 x\end{aligned} \qquad (4.3)$$

where U_1 and U_3 are the realistic zonally averaged winds representing the upper and lower layers; A and B are the Rossby wave amplitudes and k_0 is the wave number of the stationary Rossby wave.

The basic flow (4.3) is geostrophic. Hence using the geostrophic relations we can express the wind components and the vertical component of relative vorticity

in terms of A, B and k_0 as given below.

$$u_1 = -\frac{1}{f_0}\frac{\partial \Phi_1}{\partial y} = U_1 \quad ; v_1 = \frac{1}{f_0}\frac{\partial \Phi_1}{\partial x} = k_0 A \cos k_0 x$$

$$u_3 = -\frac{1}{f_0}\frac{\partial \Phi_3}{\partial y} = U_3 \quad ; v_3 = \frac{1}{f_0}\frac{\partial \Phi_3}{\partial x} = k_0 B \cos k_0 x$$

$$\zeta_1 = \frac{1}{f_0}\nabla^2 \Phi_1 = -k_0^2 A \sin k_0 x \quad ; \zeta_3 = \frac{1}{f_0}\nabla^2 \Phi_3 = -k_0^2 B \sin k_0 x$$

Substituting these in (4.1) and collecting the coefficients of A and B we get

$$\left(\beta - s_2 U_3 - k_0^2 U_1\right) A + s_2 U_1 B = 0 \quad . \tag{4.4}$$

Similarly from (4.2) we get the following equation

$$s_2 U_3 A + \left(\beta - s_2 U_1 - k_0^2 U_3\right) B = 0 \quad . \tag{4.5}$$

For nontrivial solutions of Eqs. (4.4) and (4.5)

$$\begin{vmatrix} \beta - s_2 U_3 - k_0^2 U_1 & s_2 U_1 \\ s_2 U_3 & \beta - s_2 U_1 - k_0^2 U_3 \end{vmatrix} = 0$$

or,

$$k_0^4 U_1 U_3 - k_0^2 \left\{\beta\left(U_1 + U_3\right) - s_2\left(U_1^2 + U_3^2\right)\right\} + \beta\left\{\beta - s_2\left(U_1 + U_3\right)\right\} = 0 \quad .$$

This is a quadratic equation in k_o^2, which can be solved to get

$$k_o^2 = \frac{\beta(U_1+U_3) - S_2(U_1^2+U_3^2)}{2U_1U_3} \pm \frac{\left[\{\beta(U_1+U_3) - S_2(U_1^2+U_3^2)\}^2 - 4U_1U_3\beta\{\beta - S_2(U_1+U_3)\}\right]^{1/2}}{2U_1U_3} \quad (4.6)$$

In order to have an expression for the ratio of the relative amplitudes of Rossby waves one can use either of the equations (4.4) and (4.5). From (4.4) we get

$$\frac{B}{A} = \frac{k_o^2 U_1 + S_2 U_3 - \beta}{S_2 U_1} \quad (4.7)$$

Thus (4.3) will be solutions of (4.1) and (4.2) provided (4.6) and (4.7) are satisfied. Considering the mean zonal wind for July over 18° latitude we have taken $U_1 = -14$ m s^{-1} and $U_3 = 7.5$ m s^{-1}. From (4.6) we calculated $k_o = 1.84 \times 10^{-6}$ m^{-1}. Since we have taken the beta-plane centred at 18°N latitude, the wavelength in terms of longitude can be written as

$$L_S = \frac{360}{a\, k_o \cos(18^\circ)}$$

where 'a' is the radius of the earth. We get $L_S = 32°$ longitude, but to satisfy cyclic boundary conditions, we have assumed the wavelength of stationary wave to be 30°

longitude. Using this value of k_o in (4.7) we get $\frac{B}{A} \simeq 22$.

These calculations show that the realistic winds in the monsoon atmosphere can sustain a finite amplitude baroclinic stationary Rossby wave of wavelength about 30° longitude and the amplitude of the Rossby wave is mainly confined to the lower troposphere with a very small value in the upper troposphere. Such a stationary wave is in fact observed over Bay of Bengal. These stationary waves can probably be induced by orographic influences, like the presence of Western Ghats. Gadgil (1977) has shown that the stationary wave over the Bay of Bengal may be induced by the topography of peninsular India.

4.2 The stability analysis:

The purpose of this section is to examine whether the basic flow given by (4.3) is stable to small perturbations. In this chapter the stability analysis will be carried out with a two-level quasi-geostrophic model.

As usual the perturbation potential vorticity equations at levels 1 and 3 can be obtained from (4.1) and (4.2) respectively by linearising these equations by

perturbation method. Let us write a field variable as

$$X = [\bar{X}] + \bar{X}^* + X' \tag{4.8}$$

where the transient eddy $X' = X - \bar{X}$ and the stationary eddy $\bar{X}^* = \bar{X} - [\bar{X}]$. The bar and square bracket represent time average and zonal average respectively. Thus the field variables u, v and ϕ are written as

$$u = U + u' \quad , \text{ where } \quad [\bar{u}] \equiv U$$

$$v = \bar{v}^* + v'$$

and $$\phi = [\bar{\phi}] + \bar{\phi}^* + \phi'$$

Noting that U and $\bar{v}^*$ are independent of 'y' the potential vorticity equations (4.1) and (4.2) are linearised as in Section 1.1 to get the following quasi-geostrophic perturbation potential vorticity equations.

$$\mathcal{L}_1 \left\{ \bar{J}_1' + \frac{S_2}{f_0} (\phi_3' - \phi_1') \right\} + u_1' \left\{ \frac{\partial \bar{J}_1^*}{\partial x} + S_2 (\bar{v}_3^* - \bar{v}_1^*) \right\}$$

$$+ v_1' \left\{ \beta - S_2 (U_3 - U_1) \right\} = 0 \tag{4.9}$$

at level 1 and

$$\mathcal{L}_3 \left\{ \bar{J}_3' - \frac{S_2}{f_0} (\phi_3' - \phi_1') \right\} + u_3' \left\{ \frac{\partial \bar{J}_3^*}{\partial x} - S_2 (\bar{v}_3^* - \bar{v}_1^*) \right\}$$

$$+ v_3' \left\{ \beta + S_2 (U_3 - U_1) \right\} = 0 \tag{4.10}$$

at level 3.

Here the operator $\mathcal{L}_i \equiv \frac{\partial}{\partial t} + U_i \frac{\partial}{\partial x} + \bar{v}_i^* \frac{\partial}{\partial y}$; i = 1, 3.

The basic flow is geostrophic. As is evident from (4.3)

$$U_{1,3} = -\frac{1}{f_0} \frac{\partial \Phi_{1,3}}{\partial y}$$

Similarly

$$\bar{v}_1^* = \frac{1}{f_0} \frac{\partial \Phi_1}{\partial x} = k_0 A \cos k_0 x \qquad (4.11)$$

and $$\bar{v}_3^* = \frac{1}{f_0} \frac{\partial \Phi_3}{\partial x} = k_0 B \cos k_0 x$$

One can replace $k_0 A$ and $k_0 B$ by $\bar{v}_1$ and $\bar{v}_3$ which represent the amplitudes of the meridional wind. We have also calculated in Section 4.1 that $\frac{B}{A} \simeq 22$ for the stationary Rossby wave. Hence

$$\frac{B}{A} = \frac{\bar{v}_3}{\bar{v}_1} = 22 \qquad (4.12)$$

We propose to do normal mode analysis and following Lorenz (1972) assume solutions of the type

$$\phi_1' = \sum_{n=-\infty}^{\infty} \phi_n^{(1)} \exp\left[i(nk_0 x + kx + ly + \lambda t)\right]$$

and (4.13)

$$\phi_3' = \sum_{n=-\infty}^{\infty} \phi_n^{(3)} \exp\left[i(nk_0 x + kx + ly + \lambda t)\right]$$

where k_o, $\bar{k}$ and l are real and λ may be real or complex. The bracketed superscript denotes the level. Should the imaginary part of λ be negative, (4.13) will possess solutions which amplify with time. For side boundary conditions we impose cyclic continuity. It is to be noted that the wavelength of the stationary Rossby wave is 30° longitude and it satisfies the cyclic boundary condition. In this chapter the results discussed are for $\bar{k} = 0$.

Upon substituting (4.11) and (4.13) in (4.9) and (4.10) and collecting the co-efficients of $\exp\left[i\left(nk_o x + ly + \lambda t\right)\right]$ we get the equations

$$-\frac{1}{2} l \left\{ \bar{v}_1 \left(b_{n-1} - k_o^2 \right) + s_2 \bar{v}_3 \right\} \phi_{n-1}^{(1)} + a_n \left(\beta - b_n U_1 - s_2 U_3 \right) \phi_n^{(1)} - \frac{1}{2} l \left\{ \bar{v}_1 \left(b_{n+1} - k_o^2 \right) + s_2 \bar{v}_3 \right\} \phi_{n+1}^{(1)} + \frac{1}{2} l s_2 \bar{v}_1 \phi_{n-1}^{(3)} + s_2 a_n U_1 \phi_n^{(3)} + \frac{1}{2} l s_2 \bar{v}_1 \phi_{n+1}^{(3)} - \lambda \left\{ \left(b_n + s_2 \right) \phi_n^{(1)} - s_2 \phi_n^{(3)} \right\} = 0 \tag{4.14}$$

and

$$\frac{1}{2} l s_2 \bar{v}_3 \phi_{n-1}^{(1)} + s_2 a_n U_3 \phi_n^{(1)} + \frac{1}{2} l s_2 \bar{v}_3 \phi_{n+1}^{(1)} - \frac{1}{2} l \left\{ \left(b_{n-1} - k_o^2 \right) \bar{v}_3 + s_2 \bar{v}_1 \right\} \phi_{n-1}^{(3)} + a_n \left(\beta - b_n U_3 - s_2 U_1 \right) \phi_n^{(3)} - \frac{1}{2} l \left\{ \left(b_{n+1} - k_o^2 \right) \bar{v}_3 + s_2 \bar{v}_1 \right\} \phi_{n+1}^{(3)} - \lambda \left\{ \left(b_n + s_2 \right) \phi_n^{(3)} - s_2 \phi_n^{(1)} \right\} = 0 \tag{4.15}$$

where $a_n \equiv n k_o$ and $b_n \equiv n^2 k_o^2 + l^2$.

Varying n from $-\infty$ to ∞ one gets an infinite system of linear, homogeneous algebraic equations. Generally one is able to obtain a good approximation by summing the series (4.13) upto a finite number, N, thus obtaining 2(2N + 1) number of equations in 2(2N + 1) number of unknowns. When N is large enough such that λ_N has converged, a good approximation to the 'true' solution will have been obtained. By this process progressively decreasing zonal scales are included in the series and convergence is obtained when the smallest scale has been resolved. Since these equations are homogeneous, they result in an eigenvalue problem. The truncated system of Eqs. (4.14) and (4.15) can be rewritten in matrix notation as

$$\left(\underset{\sim}{P} - \lambda \underset{\sim}{Q}\right) \underset{\sim}{\Phi} = 0$$

or

$$\left(\underset{\sim}{P} \cdot \underset{\sim}{Q}^{-1} - \lambda \underset{\sim}{I}\right)\left(\underset{\sim}{Q} \cdot \underset{\sim}{\Phi}\right) = 0 \qquad (4.16)$$

where $\underset{\sim}{I}$ is a unit matrix. Matrix $\left(\underset{\sim}{P} \cdot \underset{\sim}{Q}^{-1}\right)$ is real, but the eigenvalues λ and eigenfunctions $\left(\underset{\sim}{Q} \cdot \underset{\sim}{\Phi}\right)$ are in general complex. If $\lambda = \lambda_r + i\lambda_i$, then the frequency of the disturbance is given by λ_r and the time in which the disturbance grows to double its initial amplitude is given by $\tau_d = \ln 2 / \lambda_i$. From the eigenfunctions

the amplitudes of different Fourier components ϕ_n can be obtained.

The nonzero elements $p_{j,k}$, $q_{j,k}$ of matrices $\underset{\sim}{P}$ and $\underset{\sim}{Q}$ are shown in Figs. 15 and 16. $\underset{\sim}{\Phi}$ is a column matrix of the form

$$\underset{\sim}{\Phi} \equiv \begin{pmatrix} \Phi_1 \\ \Phi_2 \\ \vdots \\ \Phi_{2N} \\ \Phi_{2N+1} \\ \Phi_{2N+2} \\ \vdots \\ \Phi_{4N+1} \\ \Phi_{4N+2} \end{pmatrix}$$

The nonzero elements $p_{j,k}$ and $q_{j,k}$ of $\underset{\sim}{P}$ and $\underset{\sim}{Q}$ are defined as follows. For convenience let us write

$$n = m - (N+1)$$

when m varies from 1 to (2N + 1) we define

$$p_{m,m} = a_n \left(\beta - b_n U_1 - s_2 U_3 \right)$$

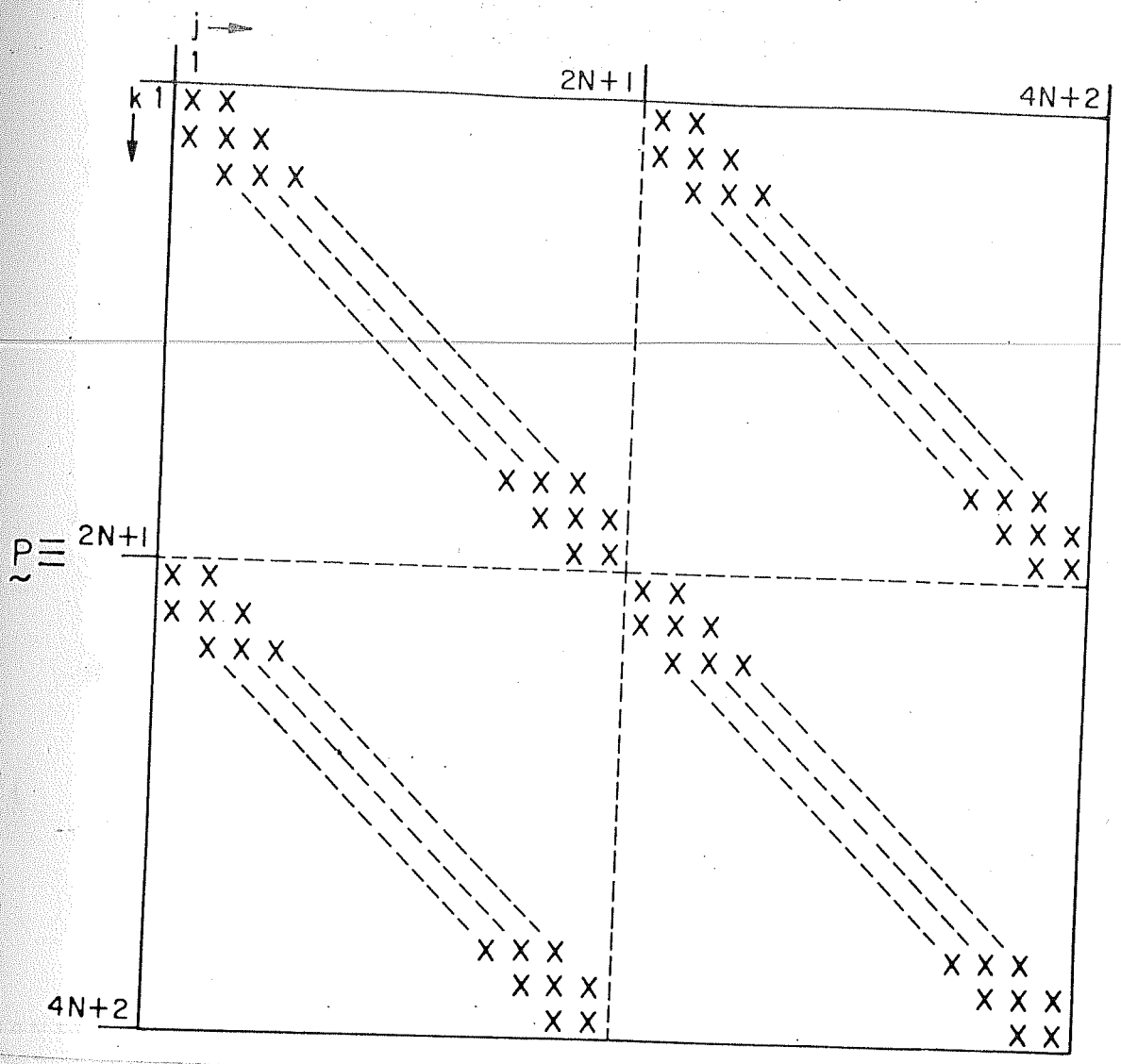

Figure 15: Nonzero elements of matrix $\underset{\sim}{P}$ appearing in Eq. (4.16). The cross marks denote the nonzero elements.

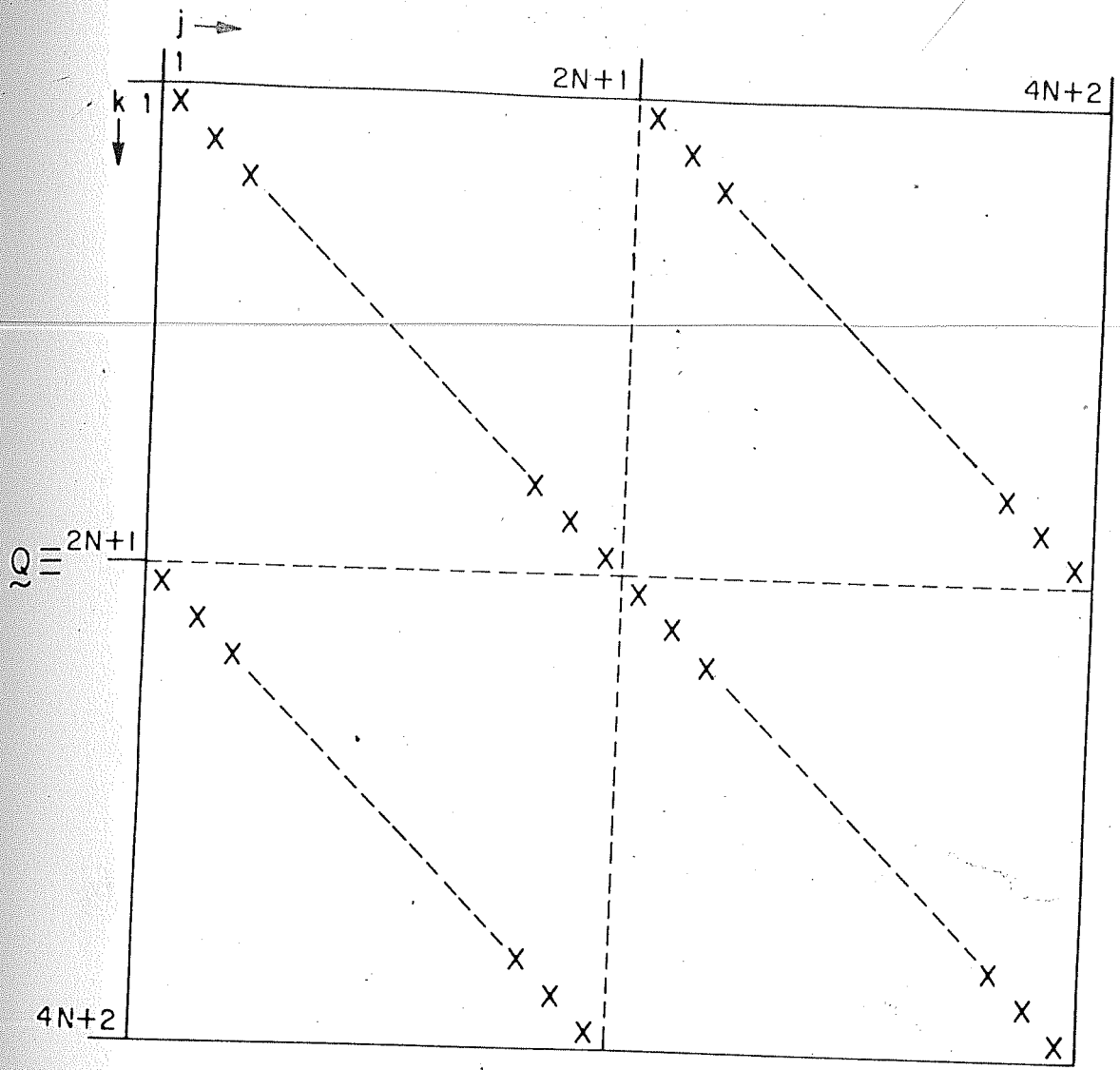

Figure 16: Nonzero elements of matrix $\underset{\sim}{Q}$ appearing in Eq. (4.16). The cross marks denote the nonzero elements.

$$p_{m,\,2N+m+1} = a_n s_2 U_1$$

$$p_{2N+m+1,\,m} = a_n s_2 U_3$$

$$p_{2N+m+1,\,2N+m+1} = a_n (\beta - b_n U_3 - s_2 U_1)$$

$$q_{m,m} = b_n + s_2$$

$$q_{m,\,2N+m+1} = -s_2$$

$$q_{2N+m+1,\,m} = -s_2$$

$$q_{2N+m+1,\,2N+m+1} = b_n + s_2$$

When m varies from 1 to 2N we have

$$p_{m,\,m+1} = -\frac{1}{2} l \left\{ \bar{v}_1 (b_{n+1} - k_a^2) + s_2 \bar{v}_3 \right\}$$

$$p_{m,\,2N+m+2} = \frac{1}{2} l s_2 \bar{v}_1$$

$$p_{2N+m+1,\,m+1} = \frac{1}{2} l s_2 \bar{v}_3$$

$$p_{2N+m+1,\,2N+m+2} = -\frac{1}{2} l \left\{ (b_{n+1} - k_0^2)\bar{v}_3 + s_2 \bar{v}_1 \right\}$$

Similarly when m varies from 2 to (2N + 1) we have

$$p_{m,\,m-1} = -\frac{1}{2} l \left\{ \bar{v}_1 (b_{n-1} - k_0^2) + s_2 \bar{v}_3 \right\}$$

$$p_{m,\,2N+m} = \frac{1}{2} l s_2 \bar{v}_1$$

$$p_{2N+m+1,\,m-1} = \frac{1}{2} l s_2 \bar{v}_3$$

$$p_{2N+m+1,\,2N+m} = -\frac{1}{2} l \left\{ (b_{n-1} - k_0^2)\bar{v}_3 + s_2 \bar{v}_1 \right\}$$

The elements φ_i of $\underset{\sim}{\Phi}$ are defined below. If $n = m - (N+1)$ and m varies from 1 to (2N + 1) we have

$$\varphi_m = \phi_n^{(1)}$$

and

$$\varphi_{2N+m+1} = \phi_n^{(3)}$$

In our analysis we have truncated the series (4.13) at N = 10. Gradually increasing the value of N we found that for N $>$ 4 there is no appreciable change in the eigenvalues and eigenfunctions. Figs. 19 and 20 show the eigenfunctions for different harmonics. It is seen that at both the levels the Fourier components of geopotential perturbation are large for the first few lower order harmonics and become very small as 'n' increases. Hence the truncation of series (4.13) at N = 10 is reasonable.

Stability analysis is done for different amplitudes of the basic Rossby wave by varying $\bar{v}_3$ from 5 m s^{-1} to 20 m s^{-1}. For each value of $\bar{v}_3$ the corresponding value of $\bar{v}_1$ is calculated from (4.12). For each amplitude of Rossby wave meridional wave number 'l' is varied from $k_o/12$ to k_o, satisfying the cyclic boundary conditions. For convenience we put $l = \frac{J}{12} k_o$ and vary J from 1 to 12 by steps of 1. In terms of wavelength $L_y = \frac{12}{J} L_s$, where L_y is the meridional scale length of disturbance and L_s is the wavelength of the stationary Rossby wave.

Characteristics of growing modes for different amplitudes of Rossby wave are reported in Tables 12 to 18. In all these tables the meridional scale length of disturbance is to be taken as $\frac{12}{J}$ times the wavelength

Table 12

Characteristics of growing modes in quasi-geostrophic model for $\bar{v}_3 = 9$ m s^{-1} (Meridional scale length of perturbation is $\frac{12}{J}$ times wavelength of the stationary Rossby wave).

$J = \frac{12\,l}{k_0}$	Frequency $\lvert\lambda_r\rvert$ (s^{-1})	Doubling time τ_d (days)
3	1.9×10^{-6}	8.5×10^{14}
4	3.4×10^{-21}	12.5
5	5.0×10^{-21}	6.5
6	1.0×10^{-21}	6.8
7	9.0×10^{-23}	1.9×10^{18}

Table 13

Characteristics of growing modes in quasi-geostrophic model for $\overline{v}_3 = 10$ m s^{-1} ($L_y = \frac{12}{J} L_s$)

$J = \frac{12\,l}{k_o}$	Frequency $\lvert\lambda_r\rvert$ (s^{-1})	Doubling time τ_d (days)
2	1.5×10^{-6}	2.6×10^{13}
3	5.2×10^{-21}	22.9
4	1.1×10^{-21}	4.7
5	5.3×10^{-21}	3.5
6	1.5×10^{-21}	3.2
7	8.5×10^{-22}	3.5
8	2.3×10^{-20}	6.0
9	1.3×10^{-21}	8.9×10^{16}

Table 14

Characteristics of growing modes in quasi-geostrophic model for $\overline{U}_3 = 12$ m s^{-1} $\left(L_y = \frac{12}{J} L_s\right)$.

$J = \frac{12\,l}{k_0}$	Frequency $\lvert\lambda_r\rvert$ (s^{-1})	Doubling time τ_d (days)
2	2.8×10^{-22}	6.6×10^{16}
3	5.1×10^{-22}	4.4
4	9.9×10^{-22}	2.7
5	1.3×10^{-21}	2.2
6	6.2×10^{-22}	1.9
7	3.8×10^{-22}	1.9
8	1.2×10^{-21}	2.0
9	9.9×10^{-22}	2.4
10	2.1×10^{-19}	5.4
11	5.4×10^{-24}	5.5×10^{16}

Table 15

Characteristics of growing modes in quasi-geostrophic model for $\bar{v}_3 = 14$ m s^{-1} ($L_y = \frac{12}{J} L_s$).

$J = \frac{12 l}{k_0}$	Frequency $\lvert \lambda r \rvert$ (s^{-1})	Doubling time τ_d (days)
1	1.7×10^{-6}	2.3×10^{14}
2	1.1×10^{-21}	9.1
3	4.8×10^{-22}	3.0
4	7.0×10^{-22}	2.1
5	5.2×10^{-22}	1.6
6	9.7×10^{-22}	1.5
7	9.7×10^{-22}	1.4
8	1.4×10^{-21}	1.4
9	2.3×10^{-21}	1.5
10	6.3×10^{-22}	1.9
11	9.1×10^{-22}	4.0
12	5.1×10^{-24}	2.1×10^{17}

Table 16

Characteristics of growing modes in quasi-geostrophic model for $\overline{v}_3 = 16$ m s^{-1}. ($L_y = \frac{12}{J} L_s$).

$J = \frac{12\,l}{k_0}$	Frequency $\lvert\lambda_r\rvert$ (s^{-1})	Doubling time τ_d (days)
1	5.8×10^{-22}	5.4×10^{17}
2	6.6×10^{-22}	4.9
3	8.0×10^{-22}	2.4
4	1.2×10^{-21}	1.7
5	3.2×10^{-22}	1.4
6	1.3×10^{-20}	1.2
7	2.7×10^{-21}	1.1
8	7.1×10^{-22}	1.1
9	1.5×10^{-22}	1.2
10	5.1×10^{-22}	1.4
11	5.1×10^{-22}	1.4
12	5.5×10^{-24}	3.1×10^{17}

Table 17

Characteristics of growing modes in quasi-geostrophic model for $\overline{\vartheta}_3 = 18$ m s^{-1}. ($L_y = \frac{12}{J} L_s$).

$J = \frac{12l}{k_0}$	Frequency $\lvert\lambda_r\rvert$ (s^{-1})	Doubling time τ_d (days)
1	1.7×10^{-23}	2.4×10^{19}
2	5.6×10^{-22}	3.7
3	1.1×10^{-22}	2.0
4	1.5×10^{-20}	1.4
5	8.9×10^{-22}	1.2
6	3.1×10^{-22}	1.0
7	3.1×10^{-22}	1.0
8	6.2×10^{-22}	0.9
9	1.3×10^{-21}	1.0
10	2.2×10^{-21}	1.1
11	3.2×10^{-22}	1.5
12	6.5×10^{-23}	5.3×10^{16}

Table 18

Characteristics of growing modes in quasi-geostrophic model for $\overline{v}_3 = 20$ m s^{-1} ($L_y = \frac{12}{J} L_s$).

$J = \frac{12 l}{k_0}$	Frequency $\lvert \lambda r \rvert$ (s^{-1})	Doubling time τ_d (days)
1	1.1×10^{-6}	4.2×10^{17}
2	6.0×10^{-22}	3.0
3	3.3×10^{-22}	1.7
4	1.1×10^{-22}	1.2
5	4.2×10^{-22}	1.0
6	2.7×10^{-22}	0.9
7	3.9×10^{-22}	0.8
8	8.9×10^{-23}	0.8
9	6.8×10^{-20}	0.9
10	1.9×10^{-22}	1.0
11	6.2×10^{-21}	1.3
12	3.1×10^{-22}	4.1×10^{18}

of the stationary Rossby wave. The frequencies of the above computed disturbances are found to be far less than the coriolis parameter. This suggests that these growing modes are Rossby modes. Also these disturbances are stationary. For each value of $\overline{v}_3$ the growing disturbances have maximum amplitude in the lower troposphere (Figs. 19 and 20, note the log scale). We see that the perturbation does not grow for lower tropospheric meridional velocity $\overline{v}_3$ less than 9 m s^{-1} (Fig. 17).

The doubling time of the disturbance depends very much on the Rossby wave amplitude (Fig. 18). The growth rate increases with the meridional velocity (amplitude). For each value of $\overline{v}_3$ there is a minimum value of doubling time and the minimum seems to shift towards higher l as $\overline{v}_3$ increases (Fig.17). In all these cases the growth rate is maximum for small values of 'l' ($l \leq k_o/2$) which corresponds to the results of barotropic stability analysis of Lorenz (1972). The doubling time of about 3 days corresponding to the value of $\overline{v}_3$ = 10 m s^{-1} is a reasonable doubling time for monsoon disturbances.

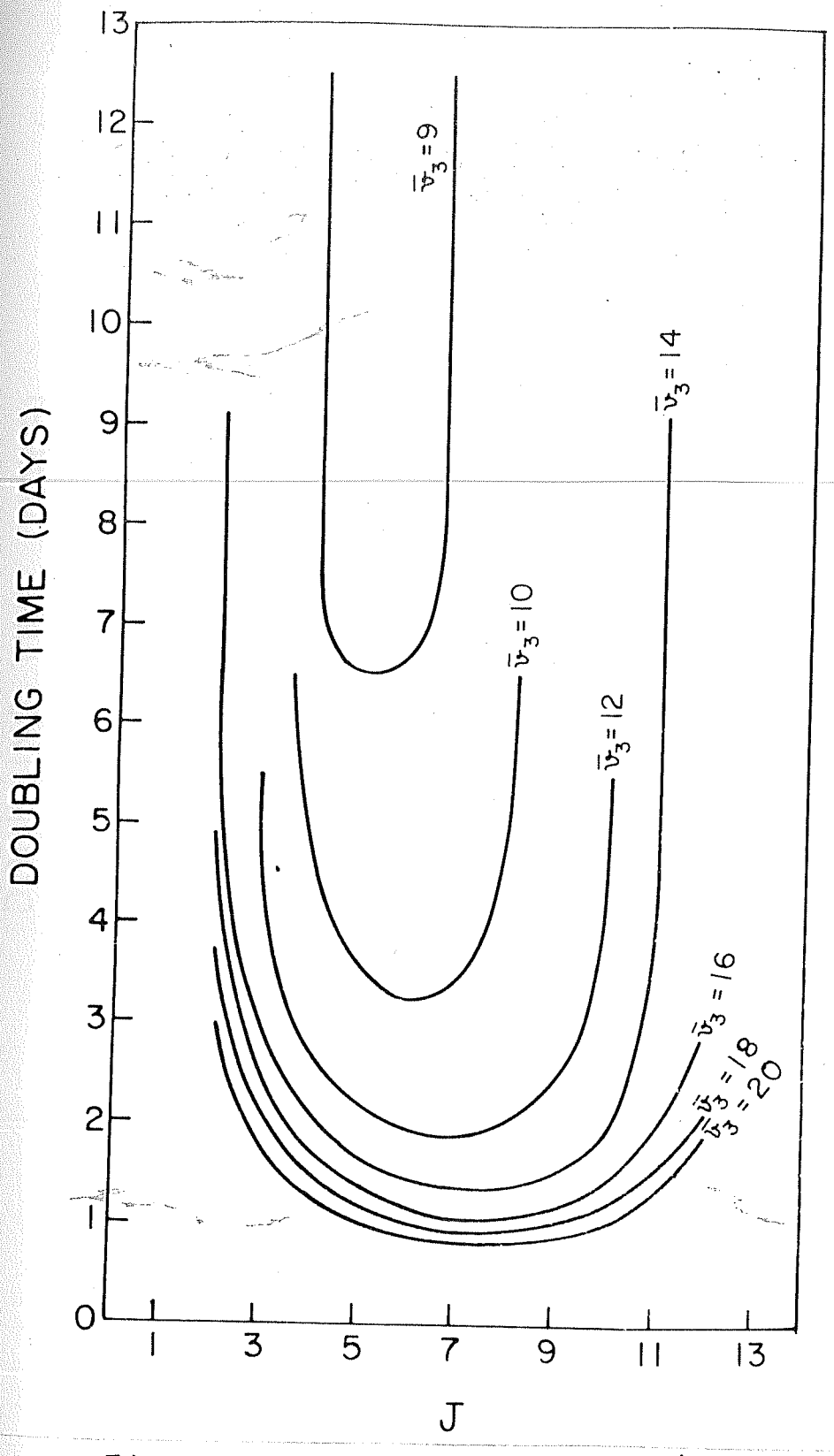

Figure 17: Meridional wavenumber $l = J k_0 / 12)$ dependence of the growth of Rossby modes in quasi-geostrophic model.

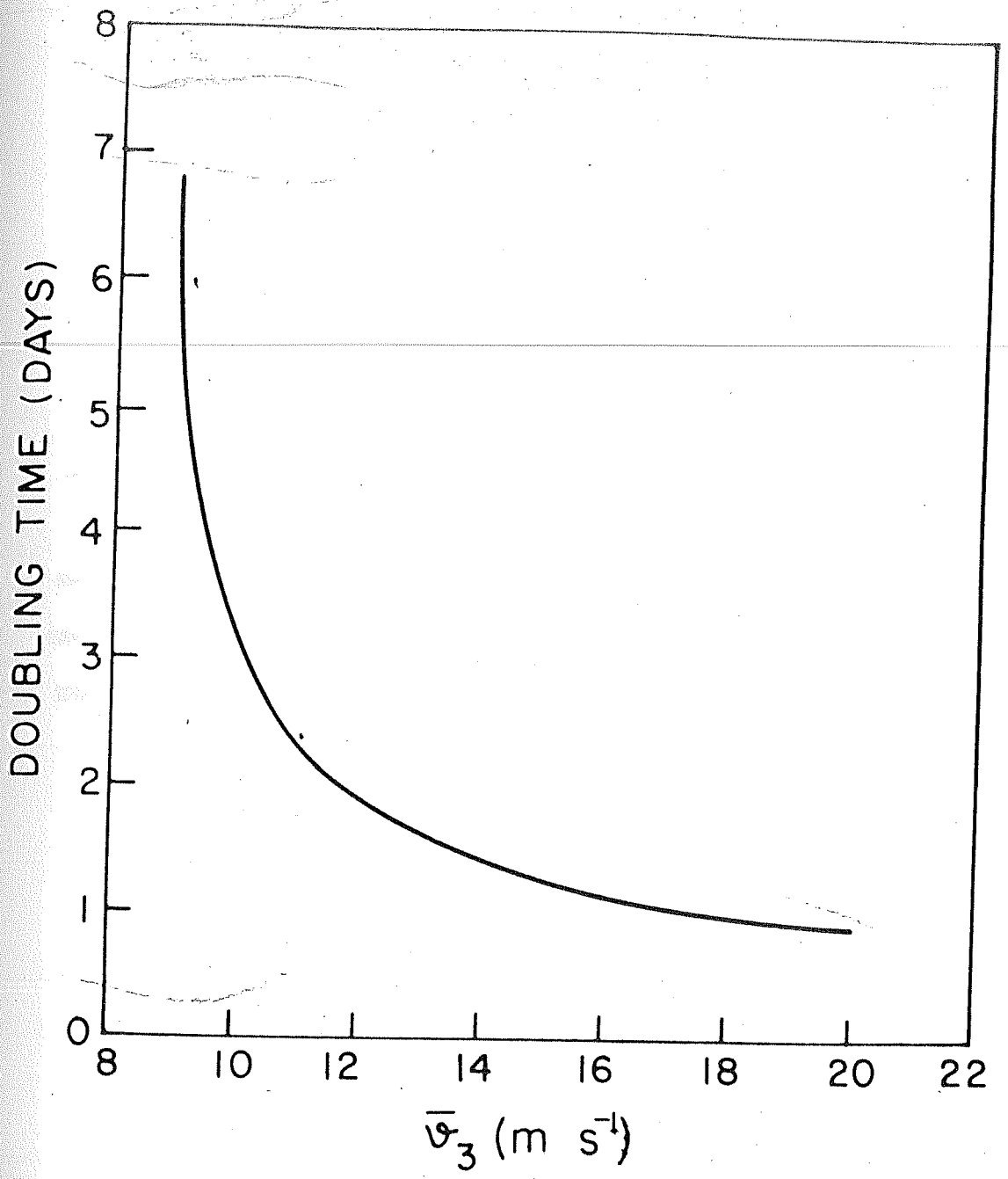

Figure 18: Meridional wind (amplitude) dependence of the growth of Rossby modes in quasi-geostrophic model.

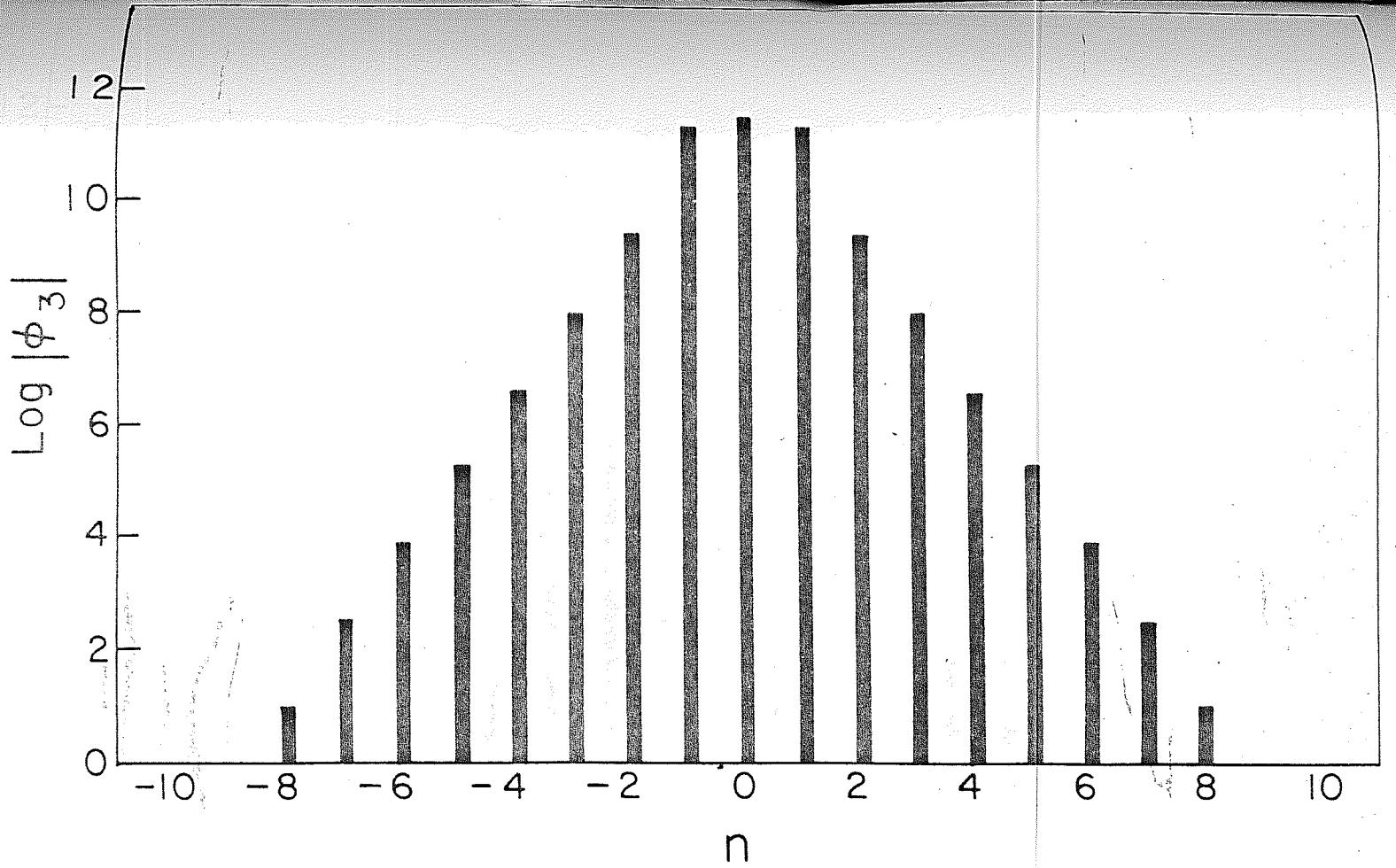

Figure 19: Fourier components of the lower tropospheric geopotential perturbation of the fastest growing Rossby mode for $\overline{v}_3$ = 10 (m s^{-1}) in Fig. 17.

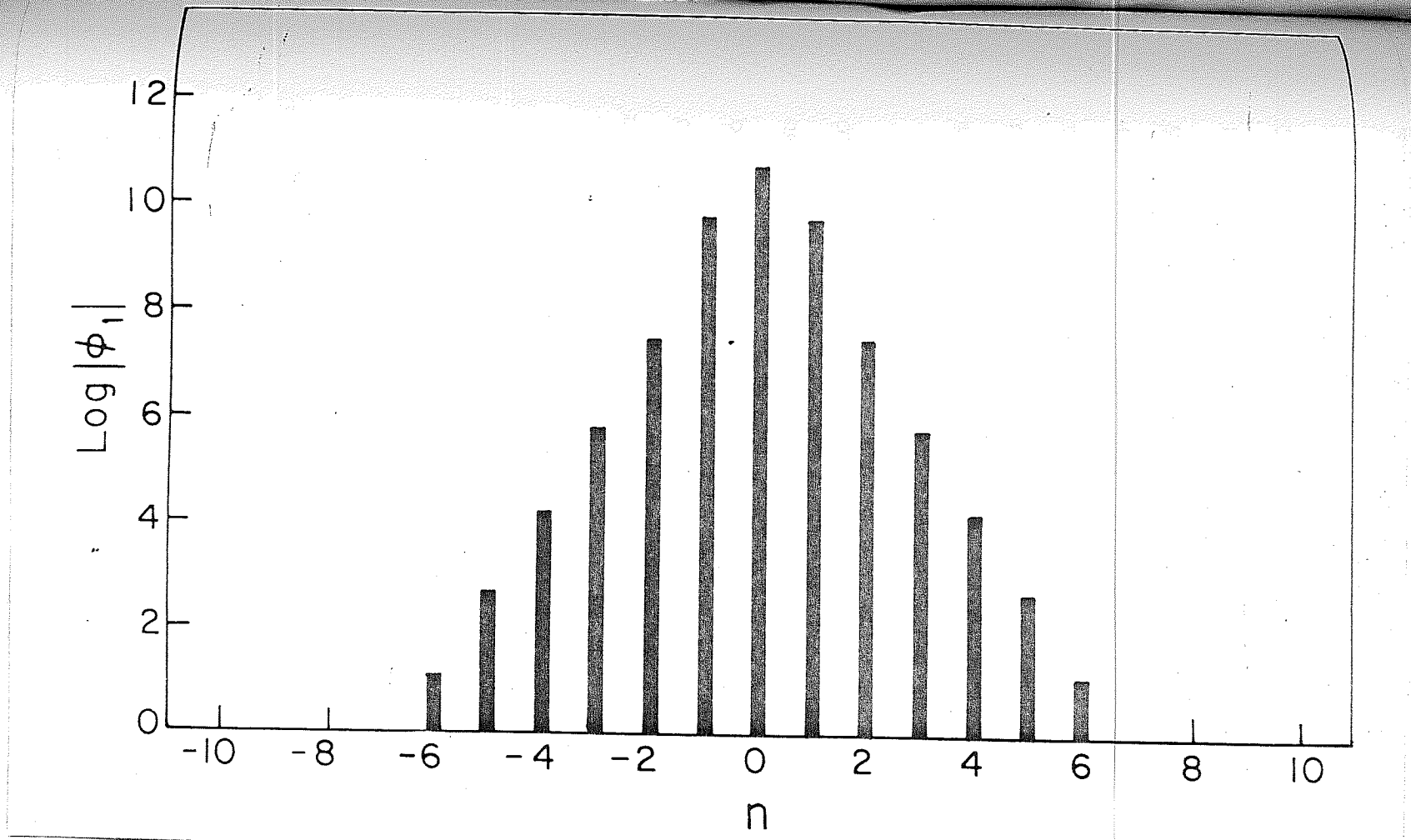

Figure 20: Fourier components of the upper tropospheric geopotential perturbation of the fastest growing Rossby mode for $\bar{v}_3 = 10$ (m s^{-1}) in Fig. 17.

4.3 Energy conversions:

In this study the zonal wind is assumed to be independent of latitude, but has vertical shear. Hence the possible sources of energy for the perturbation to grow are, available potential energy of the zonal flow, and kinetic energy and available potential energy associated with the basic Rossby wave. We have calculated the rates of energy conversions to see which of the above energies contribute the most to the growth of perturbations.

The rate of conversion among the different forms of energy can be calculated as follows. First we will derive the equation for the rate of change of the perturbation kinetic energy. Let us consider the x-component of the momentum equation and the continuity equation respectively.

$$\frac{\partial u}{\partial t} = -u\frac{\partial u}{\partial x} - v\frac{\partial u}{\partial y} - \omega\frac{\partial u}{\partial p} + fv - \frac{\partial \phi}{\partial x} \qquad (4.17)$$

$$\frac{\partial u}{\partial x} + \frac{\partial v}{\partial y} + \frac{\partial \omega}{\partial p} = 0 \qquad (4.18)$$

Multiplying (4.18) by u and adding to (4.17) we get

$$\frac{\partial u}{\partial t} = -\frac{\partial u^2}{\partial x} - \frac{\partial}{\partial y}(uv) - \frac{\partial}{\partial p}(u\omega) + fv - \frac{\partial \phi}{\partial x} \qquad (4.19)$$

Similarly let us consider the y-component of the momentum equation.

$$\frac{\partial v}{\partial t} = -u\frac{\partial v}{\partial x} - v\frac{\partial v}{\partial y} - \omega\frac{\partial v}{\partial p} - fu - \frac{\partial \phi}{\partial y} \qquad (4.20)$$

Multiplying (4.18) by v and adding to (4.20), we get

$$\frac{\partial v}{\partial t} = -\frac{\partial}{\partial x}(uv) - \frac{\partial}{\partial y}(v^2) - \frac{\partial}{\partial p}(\omega v) - fu - \frac{\partial \phi}{\partial y} \qquad (4.21)$$

Equations (4.19) and (4.21) are linearised as in Section 4.2 to get

$$\frac{\partial u'}{\partial t} = -\frac{\partial}{\partial x}(2Uu') - \frac{\partial}{\partial y}(Uv' + u'\bar{v}^*) - \frac{\partial}{\partial p}(U\omega') + fv' - \frac{\partial \phi'}{\partial x} \qquad (4.22)$$

$$\frac{\partial v'}{\partial t} = -\frac{\partial}{\partial x}(u'\bar{v}^* + Uv') - \frac{\partial}{\partial y}(2\bar{v}^* v') - \frac{\partial}{\partial p}(\omega'\bar{v}^*) - fu' - \frac{\partial \phi'}{\partial y} \qquad (4.23)$$

To get the equation for the rate of change of kinetic energy of perturbation, (4.22) and (4.23) are multiplied by u' and v' respectively and then added. Terms containing f will cancel each other and we get

$$u'\frac{\partial u'}{\partial t}+v'\frac{\partial v'}{\partial t} = -u'\frac{\partial}{\partial x}(2Uu') - u'\frac{\partial}{\partial y}(Uv'+u'\bar{v}^*)$$
$$-u'\frac{\partial}{\partial p}(U\omega') - v'\frac{\partial}{\partial x}(u'\bar{v}^*+Uv')$$
$$-v'\frac{\partial}{\partial y}(2\bar{v}^*v') - v'\frac{\partial}{\partial p}(\omega'\bar{v}^*)$$
$$-u'\frac{\partial\phi'}{\partial x} - v'\frac{\partial\phi'}{\partial y}$$

The right hand side of the above equation can be simplified by taking note of the following facts.

We have assumed the zonal wind U to be independent of x and y. Also $\bar{v}^*$ is independent of y. Also terms containing vertical wind shear do not contribute to the kinetic energy. Again using the continuity equation and hydrostatic approximation one can show that

$$u'\frac{\partial\phi'}{\partial x}+v'\frac{\partial\phi'}{\partial y} \equiv \underline{V}'\cdot\nabla\phi'$$
$$= \nabla\cdot(\underline{V}'\phi') + \frac{\partial}{\partial p}(\phi'\omega') + \omega'\alpha'$$

Integrating the above equation over one wavelength in both x and y directions and over the depth of the atmosphere the flux terms will vanish. Thus the rate of change of perturbation kinetic energy is given by

$$\frac{\partial}{\partial t}\int\frac{f}{2}(u'^2+v'^2)\,d\tau = -\int\rho\,u'v'\frac{\partial\bar{v}^*}{\partial x}\,d\tau - \int\rho\,\omega'\alpha'\,d\tau$$

where $d\tau \equiv dx\,dy\,dz$

In (x, y, p) co-ordinates the above equation can be rewritten as

$$\frac{1}{2g}\iiint \frac{\partial}{\partial t}(u'^2+v'^2)\,dx\,dy\,dp$$

$$= -\frac{1}{g}\iiint u'v'\frac{\partial \bar{v}^*}{\partial x}\,dx\,dy\,dp - \frac{1}{g}\iiint \omega'\alpha'\,dx\,dy\,dp \qquad (4.24)$$

The integrations are over the domain $0 \leq x \leq 2\pi/k_0$,

$$0 \leq y \leq 2\pi/l \quad \text{and} \quad 0 \leq p \leq p_0 .$$

The perturbation equation for the change of available potential energy will be derived by considering the quasi-geostrophic thermodynamic energy equation (3.2) in the absence of heating. As in Section 4.2 this equation is linearised to get

$$\frac{\partial \alpha'}{\partial t} + U\frac{\partial \alpha'}{\partial x} + u'\frac{\partial \bar{\alpha}^*}{\partial x} + \bar{v}^*\frac{\partial \alpha'}{\partial y}$$

$$+ v'\frac{\partial [\bar{\alpha}]}{\partial y} - \sigma\omega' = 0 . \qquad (4.25)$$

Multiplying (4.25) by α'/σ and integrating over a complete wavelength in x and y, the flux terms vanish. Finally we get the equation for the rate of change of perturbation

available potential energy as follows.

$$\frac{1}{2\sigma g}\iiint \frac{\partial \alpha'^2}{\partial t}\,dx\,dy\,dp$$

$$= -\frac{1}{\sigma g}\iiint \left(v'\alpha' \frac{\partial[\bar{\alpha}]}{\partial y} + u'\alpha' \frac{\partial \bar{\alpha}^*}{\partial x}\right) dx\,dy\,dp$$

$$+ \frac{1}{g}\iiint \omega'\alpha'\,dx\,dy\,dp \qquad (4.26)$$

The integration is over the same domain as in case of (4.24). Adding (4.24) and (4.26) we get the equation for the rate of change of total energy of the perturbation. The last terms on the right hand side of (4.24) and (4.26) cancel each other, as they represent conversion from eddy available potential energy to eddy kinetic energy. We have not calculated this conversion in the present study. From (4.24) and (4.26) we get

$$\frac{1}{2g}\iiint \left\{\frac{\partial}{\partial t}(u'^2+v'^2) + \frac{1}{\sigma}\frac{\partial \alpha'^2}{\partial t}\right\} dx\,dy\,dp$$

$$= \frac{1}{g}\iiint \left\{-u'v'\frac{\partial \bar{v}^*}{\partial x} - \frac{1}{\sigma}v'\alpha'\frac{\partial[\bar{\alpha}]}{\partial y} - \frac{1}{\sigma}u'\alpha'\frac{\partial \bar{\alpha}^*}{\partial x}\right\} dx\,dy\,dp. \qquad (4.27)$$

On the right hand side of (4.27), the first term represents the rate of conversion of kinetic energy of the basic wave

to perturbation kinetic energy $C(K_w, K')$ through the Reynold stress $(-u'v')$. The second term represents the rate of conversion from the available potential energy of the zonal flow $C(A_z, A')$ and the last term is the conversion from the available potential energy of the stationary baroclinic Rossby wave $C(A_w, A')$. The relative magnitudes of these different conversion rates are calculated by using the following relations.

$$C(K_w, K') = -\frac{1}{g}\iiint u'v' \frac{\partial \bar{v}^*}{\partial x} dx\, dy\, dp \qquad (4.28)$$

$$C(A_w, A') = -\frac{1}{g\sigma}\iiint u'\alpha' \frac{\partial \bar{\alpha}^*}{\partial x} dx\, dy\, dp \qquad (4.29)$$

$$C(A_z, A') = -\frac{1}{g\sigma}\iiint v'\alpha' \frac{\partial [\bar{\alpha}]}{\partial y} dx\, dy\, dp \qquad (4.30)$$

4.3.1 Conversion from kinetic energy of the basic wave:

In two-level model we calculate the rate of conversion from kinetic energy of the basic wave to perturbation kinetic energy by considering both the levels 1 and 3. Hence (4.28) is rewritten as

$$C(K_w, K') = -\frac{1}{g}\iiint \left(u_1' v_1' \frac{\partial \bar{v}_1^*}{\partial x} + u_3' v_3' \frac{\partial \bar{v}_3^*}{\partial x}\right) dx\, dy\, dp \qquad (4.31)$$

where the integration over p is from 0 to Δp. Using geostrophic wind relations and (4.11), the above relation can be expressed in terms of geopotential perturbations as follows.

$$C(K_W, K') = i \frac{k_0 \Delta p}{2g f_0^2} \iint \left\{ \bar{v}_1 \frac{\partial \phi_1'}{\partial y} \frac{\partial \phi_1'}{\partial x} + \bar{v}_3 \frac{\partial \phi_3'}{\partial y} \frac{\partial \phi_3'}{\partial x} \right\} \left(e^{ik_0 x} - e^{-ik_0 x} \right) dx\, dy \qquad (4.32)$$

For stability analysis in Section 4.2 we had not used the complex conjugate terms in (4.13), because finally we collected the co-efficients of $\exp[i(nk_0x + ly + \lambda t)]$ to get (4.14) and (4.15). The inclusion of complex conjugate terms in (4.13) could not have changed (4.14) and (4.15) But for calculating the rate of energy conversion we will have to integrate over certain volume and hence the complex conjugate terms are to be considered.

Hence we write

$$\phi_1' = \sum_{n=-\infty}^{\infty} \left\{ \phi_n^{(1)} e^{i(nk_0x + ly + \lambda t)} + \tilde{\phi}_n^{(1)} e^{-i(nk_0x + ly + \tilde{\lambda} t)} \right\} \qquad (4.33)$$

$$\phi_3' = \sum_{n=-\infty}^{\infty} \left\{ \phi_n^{(3)} e^{i(nk_0x + ly + \lambda t)} + \tilde{\phi}_n^{(3)} e^{-i(nk_0x + ly + \tilde{\lambda} t)} \right\}$$

where ϕ_n and λ are complex and $\tilde{\phi}_n$ and $\tilde{\lambda}_n$ are the respective complex conjugates i.e. $\phi_n = \phi_n^r + i\,\phi_n^i$;

$\tilde{\phi}_n = \phi_n^r - i\,\phi_n^i$; $\lambda = \lambda_r + i\,\lambda_i$ and $\tilde{\lambda} = \lambda_r - i\,\lambda_i$

Let us consider the first integral on the right hand side of (4.32). Substituting for ϕ_1' from (4.33) we get

$$\iint \frac{\partial \phi_1'}{\partial y}\,\frac{\partial \phi_1'}{\partial x}\left(e^{ik_0x} - e^{-ik_0x}\right)dx\,dy$$

$$= -lk_0 \iint \sum_{n=-\infty}^{\infty} \left\{\phi_n^{(1)} e^{i(nk_0x+ly+\lambda t)} - \tilde{\phi}_n^{(1)} e^{-i(nk_0x+ly+\tilde{\lambda}t)}\right\}$$

$$\times \sum_{m=-\infty}^{\infty} m \left\{\phi_m^{(1)} e^{i(mk_0x+ly+\lambda t)} - \tilde{\phi}_m^{(1)} e^{-i(mk_0x+ly+\tilde{\lambda}t)}\right\}$$

$$\times \left(e^{ik_0x} - e^{-ik_0x}\right)dx\,dy$$

$$= -lk_0\, e^{-2\lambda_i t} \int_x \sum_{n,m}{}' m \Big[\phi_n^{(1)}\phi_m^{(1)} e^{i\{(n+m)k_0x + 2\lambda_r t\}} \int_0^{2\pi/l} e^{i2ly}\,dy$$

$$- \phi_n^{(1)}\tilde{\phi}_m^{(1)} e^{i(n-m)k_0x} \int_0^{2\pi/l} dy - \tilde{\phi}_n^{(1)}\phi_m^{(1)} e^{i(m-n)k_0x} \int_0^{2\pi/l} dy$$

$$+ \tilde{\phi}_n^{(1)}\tilde{\phi}_m^{(1)} e^{-i\{(n+m)k_0x + 2\lambda_r t\}} \int_0^{2\pi/l} e^{-i2ly}\,dy\Big]$$

$$\times \left(e^{ik_0x} - e^{-ik_0x}\right)dx \,.$$

The first and last integrals on the right hand side vanish

after integration over y so that

$$\iint \frac{\partial \phi_1'}{\partial y} \frac{\partial \phi_1'}{\partial x} \left(e^{ik_0x} - e^{-ik_0x}\right) dx\, dy$$

$$= 2\pi k_0 e^{-2\lambda_i t} \int_0^{2\pi/k_0} \sum_{n,m}^{m} \Big[\phi_n^{(1)} \tilde{\phi}_m^{(1)} \left\{ e^{i(n-m+1)k_0x} - e^{i(n-m-1)k_0x} \right\} + \tilde{\phi}_n^{(1)} \phi_m^{(1)} \left\{ e^{i(m-n+1)k_0x} - e^{i(m-n-1)k_0x} \right\} \Big] dx$$

While integrating over x it can be shown that terms with $m = n+1$ from the first series; with $m = n-1$ from the second; with $m = n-1$ from the third and with $m = n+1$ from the last series contribute. Other terms vanish. Hence we get

$$\iint \frac{\partial \phi_1'}{\partial y} \frac{\partial \phi_1'}{\partial x} \left(e^{ik_0x} - e^{-ik_0x}\right) dx\, dy = 4\pi^2 e^{-2\lambda_i t} \sum_{n=-\infty}^{\infty} \left\{ (n+1) \times \phi_n^{(1)} \tilde{\phi}_{n+1}^{(1)} - (n-1) \phi_n^{(1)} \tilde{\phi}_{n-1}^{(1)} + (n-1) \tilde{\phi}_n^{(1)} \phi_{n-1}^{(1)} - (n+1) \tilde{\phi}_n^{(1)} \phi_{n+1}^{(1)} \right\}$$

$$= 4\pi^2 e^{-2\lambda_i t} \sum_{n=-\infty}^{\infty} \Big[(n+1) \left(\phi_n^{(1)} \tilde{\phi}_{n+1}^{(1)} - \tilde{\phi}_n^{(1)} \phi_{n+1}^{(1)} \right) - (n-1) \left\{ \phi_n^{(1)} \tilde{\phi}_{n-1}^{(1)} - \tilde{\phi}_n^{(1)} \phi_{n-1}^{(1)} \right\} \Big]$$

Similarly the second integral on the right hand side of (4.32) can be evaluated as

$$\iint \frac{\partial \phi_3'}{\partial y}\frac{\partial \phi_3'}{\partial x}\left(e^{ik_0x}-e^{-ik_0x}\right)dx\,dy$$

$$= 4\pi^2 e^{-2\lambda_i t}\sum_{n=-\infty}^{\infty}\Big\{(n+1)\left(\phi_n^{(3)}\tilde{\phi}_{n+1}^{(3)}-\tilde{\phi}_n^{(3)}\phi_{n+1}^{(3)}\right)$$

$$-(n-1)\left(\phi_n^{(3)}\tilde{\phi}_{n-1}^{(3)}-\tilde{\phi}_n^{(3)}\phi_{n-1}^{(1)}\right)\Big\}.$$

Substituting for these integrals in (4.32) we get

$$C(K_W,K') = i\,\frac{2\pi^2 k_0 \Delta p}{g f_0^2}\,e^{-2\lambda_i t}$$

$$\times\sum_{n=-\infty}^{\infty}\Big[\bar{v}_1\Big\{(n+1)\left(\phi_n^{(1)}\tilde{\phi}_{n+1}^{(1)}-\tilde{\phi}_n^{(1)}\phi_{n+1}^{(1)}\right)$$

$$-(n-1)\left(\phi_n^{(1)}\tilde{\phi}_{n-1}^{(1)}-\tilde{\phi}_n^{(1)}\phi_{n-1}^{(1)}\right)\Big\}$$

$$+\bar{v}_3\Big\{(n+1)\left(\phi_n^{(3)}\tilde{\phi}_{n+1}^{(3)}-\tilde{\phi}_n^{(3)}\phi_{n+1}^{(3)}\right)$$

$$-(n-1)\left(\phi_n^{(3)}\tilde{\phi}_{n-1}^{(3)}-\tilde{\phi}_n^{(3)}\phi_{n-1}^{(3)}\right)\Big\}\Big]. \qquad (4.34)$$

Expressing ϕ_n and $\tilde{\phi}_n$ in terms of the real and imaginary parts ϕ_n^r and ϕ_n^i of the eigenfunctions we can get

$$C(K_W,K') = \frac{4k_0\Delta p\,\pi^2}{g f_0^2}\,e^{-2\lambda_i t}$$

$$\times\sum_{n=-\infty}^{\infty}\Big[\bar{v}_1\Big\{(n+1)\left(\phi_n^{1r}\phi_{n+1}^{1i}-\phi_n^{1i}\phi_{n+1}^{1r}\right).$$

$$-(n-1)\left(\phi_n^{1r}\phi_{n-1}^{1i}-\phi_n^{1i}\phi_{n-1}^{1r}\right)\Big\}$$
$$+\bar{v}_3\left\{(n+1)\left(\phi_n^{3r}\phi_{n+1}^{3i}-\phi_n^{3i}\phi_{n+1}^{3r}\right)\right.$$
$$\left.-(n-1)\left(\phi_n^{3r}\phi_{n-1}^{3i}-\phi_n^{3i}\phi_{n-1}^{3r}\right)\Big\}\right] . \qquad (4.35)$$

4.3.2 Conversion from available potential energy of basic wave:

Now we will consider (4.29) to calculate the rate of conversion from available potential energy of the basic wave to that of perturbation.

We have
$$\frac{\partial\bar{\alpha}^*}{\partial x}=\frac{\partial}{\partial x}\left(-\frac{\partial\bar{\phi}^*}{\partial p}\right)=-\frac{\partial}{\partial p}\left(\frac{\partial\bar{\phi}^*}{\partial x}\right)$$
$$=-f_0\frac{\partial\bar{v}^*}{\partial p} .$$

Using finite difference approximation

$$\left(\frac{\partial\bar{\alpha}^*}{\partial x}\right)_2=-f_0\frac{\bar{v}_3^*-\bar{v}_1^*}{\Delta p}=-\frac{f_0(\bar{v}_3-\bar{v}_1)}{2\Delta p}\left(e^{ik_0x}+e^{-ik_0x}\right)$$

Similarly
$$\alpha_2'=-\left(\frac{\partial\phi'}{\partial p}\right)_2=-\frac{\phi_3'-\phi_1'}{\Delta p}$$
$$u_2'=-\frac{1}{f_0}\frac{\partial\phi_2'}{\partial y}=-\frac{1}{2f_0}\frac{\partial}{\partial y}\left(\phi_3'+\phi_1'\right)$$

Hence from (4.29), after integration over p from 0 to p_0 we get

$$C(A_w, A') = \frac{P_0(\bar{v}_3 - \bar{v}_1)}{4\sigma g (\Delta p)^2} \iint \left(\frac{\partial \phi_3'}{\partial y} \phi_3' - \frac{\partial \phi_3'}{\partial y} \phi_1' + \frac{\partial \phi_1'}{\partial y} \phi_3' - \frac{\partial \phi_1'}{\partial y} \phi_1' \right) \left(e^{ik_0 x} + e^{-ik_0 x} \right) dx\, dy \qquad (4.36)$$

Let us consider the third integral on the right hand side of (4.36). Substituting for ϕ_1' and ϕ_3' from (4.33) we get

$$\iint \frac{\partial \phi_1'}{\partial y} \phi_3' \left(e^{ik_0 x} + e^{-ik_0 x} \right) dx\, dy$$

$$= il \iint \sum_m' \left\{ \phi_m^{(1)} e^{i(mk_0 x + ly + \lambda t)} - \tilde{\phi}_m^{(1)} e^{-i(mk_0 x + ly + \tilde{\lambda} t)} \right\}$$

$$\times \sum_n \left\{ \phi_n^{(3)} e^{i(nk_0 x + ly + \lambda t)} + \tilde{\phi}_n^{(3)} e^{-i(nk_0 x + ly + \tilde{\lambda} t)} \right\}$$

$$\times \left(e^{ik_0 x} + e^{-ik_0 x} \right) dx\, dy$$

Integrating over y the right hand side can be simplified to get

$$\iint \frac{\partial \phi_1'}{\partial y} \phi_3' \left(e^{ik_0 x} + e^{-ik_0 x} \right) dx\, dy$$

$$= i 2\pi e^{-2\lambda_i t} \int_0^{2\pi/k_0} \sum_{n,m}' \left\{ \phi_m^{(1)} \tilde{\phi}_n^{(3)} \left(e^{i(m-n+1)k_0 x} + e^{i(m-n-1)k_0 x} \right) - \tilde{\phi}_m^{(1)} \phi_n^{(3)} \left(e^{i(n-m+1)k_0 x} + e^{i(n-m-1)k_0 x} \right) \right\} dx$$

While integrating over X , terms with $m = n-1$ from the first series; with $m = n+1$ from the second, with $m = n+1$ from the third and with $m = n-1$ from the last series contribute and others vanish.

Hence,

$$\iint \frac{\partial \phi_1'}{\partial y} \phi_3' \left(e^{ik_0 x} + e^{-ik_0 x}\right) dx\,dy$$

$$= i \frac{4\pi^2}{k_0} e^{-2\lambda_i t} \sum_{n=-\infty}^{\infty}{}' \left\{ \phi_{n-1}^{(1)} \tilde{\phi}_n^{(3)} + \phi_{n+1}^{(1)} \tilde{\phi}_n^{(3)} \right.$$

$$\left. - \tilde{\phi}_{n+1}^{(1)} \phi_n^{(3)} - \tilde{\phi}_{n-1}^{(1)} \phi_n^{(3)} \right\}$$

Similarly we can evaluate the other integrals.

$$\iint \frac{\partial \phi_3'}{\partial y} \phi_3' \left(e^{ik_0 x} + e^{-ik_0 x}\right) dx\,dy$$

$$= i \frac{4\pi^2}{k_0} e^{-2\lambda_i t} \sum_{n=-\infty}^{\infty}{}' \left\{ \phi_{n-1}^{(3)} \tilde{\phi}_n^{(3)} + \phi_{n+1}^{(3)} \tilde{\phi}_n^{(3)} \right.$$

$$\left. - \tilde{\phi}_{n+1}^{(3)} \phi_n^{(3)} - \tilde{\phi}_{n-1}^{(3)} \phi_n^{(3)} \right\} ,$$

$$-\iint \frac{\partial \phi_3'}{\partial y} \phi_1' \left(e^{ik_0 x} + e^{-ik_0 x}\right) dx\,dy$$

$$= -i \frac{4\pi^2}{k_0} e^{-2\lambda_i t} \sum_{n=-\infty}^{\infty}{}' \left\{ \phi_{n-1}^{(3)} \tilde{\phi}_n^{(1)} + \phi_{n+1}^{(3)} \tilde{\phi}_n^{(1)} \right.$$

$$\left. - \tilde{\phi}_{n+1}^{(3)} \phi_n^{(1)} - \tilde{\phi}_{n-1}^{(3)} \phi_n^{(1)} \right\}$$

and

$$-\iint \frac{\partial \phi_1'}{\partial y}\,\phi_1'\left(e^{ik_0x}+e^{-ik_0x}\right)dx\,dy$$
$$=-i\,\frac{4\pi^2}{k_0}\,e^{-2\lambda_i t}\sum_{n=-\infty}^{\infty}\Big\{\phi_{n-1}^{(1)}\,\tilde{\phi}_n^{(1)}+\phi_{n+1}^{(1)}\,\tilde{\phi}_n^{(1)}$$
$$-\tilde{\phi}_{n+1}^{(1)}\,\phi_n^{(1)}-\tilde{\phi}_{n-1}^{(1)}\,\phi_n^{(1)}\Big\}$$

Substituting for all these integrals in (4.36) and rearranging the terms we get

$$C(A_W,A')=i\,\frac{\pi^2 k_0(\bar{v}_3-\bar{v}_1)}{\sigma g k_0(\Delta\rho)^2}\,e^{-2\lambda_i t}$$
$$\times\sum_{n=-\infty}^{\infty}\Big[\left(\tilde{\phi}_{n+1}^{(1)}+\tilde{\phi}_{n+1}^{(3)}+\tilde{\phi}_{n-1}^{(1)}+\tilde{\phi}_{n-1}^{(3)}\right)\left(\phi_n^{(1)}-\phi_n^{(3)}\right)$$
$$-\left(\phi_{n+1}^{(1)}+\phi_{n+1}^{(3)}+\phi_{n-1}^{(1)}+\phi_{n-1}^{(3)}\right)\left(\tilde{\phi}_n^{(1)}-\tilde{\phi}_n^{(3)}\right)\Big]. \tag{4.37}$$

Expressing the right hand side in terms of the eigenfunctions ϕ_n^r and ϕ_n^i we can get

$$C(A_W,A')=-\frac{2\pi^2 k_0(\bar{v}_3-\bar{v}_1)}{\sigma g k_0(\Delta\rho)^2}\,e^{-2\lambda_i t}$$
$$\times\sum_{n=-\infty}^{\infty}\Big[\left(\phi_n^{1i}-\phi_n^{3i}\right)\left(\phi_{n+1}^{1r}+\phi_{n+1}^{3r}+\phi_{n-1}^{1r}+\phi_{n-1}^{3r}\right)$$
$$-\left(\phi_n^{1r}-\phi_n^{3r}\right)\left(\phi_{n+1}^{1i}+\phi_{n+1}^{3i}+\phi_{n-1}^{1i}+\phi_{n-1}^{3i}\right)\Big]. \tag{4.38}$$

4.3.3 Conversion from available potential energy of zonal flow:

Let us consider (4.30) to calculate the rate of change of available potential energy of zonal flow.

We have

$$\frac{\partial[\bar{\alpha}]}{\partial y} = -\frac{\partial}{\partial y}\left(\frac{\partial[\bar{\phi}]}{\partial p}\right) = \frac{\partial}{\partial p}\left(-\frac{\partial[\bar{\phi}]}{\partial y}\right) = f_0 \frac{\partial U}{\partial p}$$

Using finite difference approximation

$$\left(\frac{\partial[\bar{\alpha}]}{\partial y}\right)_2 = \frac{f_0}{\Delta p}(U_3 - U_1)$$

and

$$\alpha_2' = -\left(\frac{\partial \phi'}{\partial p}\right)_2 = -\frac{\phi_3' - \phi_1'}{\Delta p}$$

and

$$v_2' = \frac{1}{2}(v_3' + v_1') = \frac{1}{2f_0}\left(\frac{\partial \phi_3'}{\partial x} + \frac{\partial \phi_1'}{\partial x}\right)$$

Substituting for $\left(\frac{\partial[\bar{\alpha}]}{\partial y}\right)_2$, α_2' and v_2' in (4.30) and integrating over p,

$$C(A_z, A') = \frac{p_0 (U_3 - U_1)}{2\sigma g (\Delta p)^2}$$

$$\times \iint \left(\frac{\partial \phi_3'}{\partial x}\phi_3' - \frac{\partial \phi_3'}{\partial x}\phi_1' + \frac{\partial \phi_1'}{\partial x}\phi_3' - \frac{\partial \phi_1'}{\partial x}\phi_1' \right) dx\, dy .$$

(4.39)

Substituting for ϕ_1' and ϕ_3' from (4.33) the second integral on the right hand side of (4.39) becomes

$$-\iint \frac{\partial \phi_3'}{\partial x}\,\phi_1'\,dx\,dy = -ik_0 \iint \sum_{m=-\infty}^{\infty}{}' m \left\{ \phi_m^{(3)} e^{i(mk_0x+ly+\lambda t)} - \tilde{\phi}_m^{(3)} e^{-i(mk_0x+ly+\tilde{\lambda}t)} \right\} \sum_{n=-\infty}^{\infty}{}' \left\{ \phi_n^{(1)} e^{i(nk_0x+ly+\lambda t)} + \tilde{\phi}_n^{(1)} e^{-i(nk_0x+ly+\tilde{\lambda}t)} \right\} dx\,dy .$$

Integrating over y from 0 to $2\pi/l$ we get

$$-\iint \frac{\partial \phi_3'}{\partial x}\,\phi_1'\,dx\,dy = -i\,\frac{2\pi k_0}{l}\, e^{-2\lambda_i t} \times \int_0^{2\pi/k_0} \sum_{n,m}{}' m \left\{ \phi_m^{(3)} \tilde{\phi}_n^{(1)} e^{i(m-n)k_0x} - \tilde{\phi}_m^{(3)} \phi_n^{(1)} e^{i(n-m)k_0x} \right\} dx .$$

While integrating over x, terms with $m = n$ contribute and others vanish. So we can simplify the right hand side to get

$$-\iint \frac{\partial \phi_3'}{\partial x}\,\phi_1'\,dx\,dy = -i\,\frac{4\pi^2}{l}\, e^{-2\lambda_i t} \sum_{n=-\infty}^{\infty}{}' n \left(\phi_n^{(3)} \tilde{\phi}_n^{(1)} - \tilde{\phi}_n^{(3)} \phi_n^{(1)} \right).$$

Similarly the third integral on the right hand side of (4.39) can be evaluated to get

$$\iint \frac{\partial \phi_1'}{\partial x}\,\phi_3'\,dx\,dy = i\,\frac{4\pi^2}{l}\, e^{-2\lambda_i t} \sum_{n=-\infty}^{\infty}{}' n \left(\phi_n^{(1)} \tilde{\phi}_n^{(3)} - \tilde{\phi}_n^{(1)} \phi_n^{(3)} \right)$$

It can be shown that the first and the last integrals on the right hand side of (4.39) vanish. Substituting for these integrals in (4.39) we get

$$C(A_z, A') = i \frac{2\pi^2 \rho_0 (U_3 - U_1)}{\log (\Delta p)^2} e^{-2\lambda_i t} \times \sum_{n=-\infty}^{\infty}{}' n \left(\phi_n^{(1)} \tilde{\phi}_n^{(3)} - \tilde{\phi}_n^{(1)} \phi_n^{(3)} - \phi_n^{(3)} \tilde{\phi}_n^{(1)} + \tilde{\phi}_n^{(3)} \phi_n^{(1)} \right). \quad (4.40)$$

Expressing ϕ_n and $\tilde{\phi}_n$ in terms of the real and imaginary parts ϕ_n^r and ϕ_n^i respectively, one gets

$$C(A_z, A') = \frac{8\pi^2 \rho_0 (U_3 - U_1)}{\log (\Delta p)^2} e^{-2\lambda_i t} \times \sum_{n=-\infty}^{\infty}{}' n \left(\phi_n^{1r} \phi_n^{3i} - \phi_n^{1i} \phi_n^{3r} \right). \quad (4.41)$$

Calculating the energy conversions from (4.35), (4.38) and (4.41), we found the following ratios for the fastest growing mode when $\overline{v}_3 = 10 \text{ m s}^{-1}$.

$$\frac{C(K_W, K')}{C(A_z, A')} = 3.4 \times 10^3$$

$$\frac{C(K_W, K')}{C(A_W, A')} = 1.3 \times 10^2$$

$$\frac{C(A_W, A')}{C(A_z, A')} = 26$$

Here, $C(K_W, K')$ stands for conversion from the kinetic energy of basic wave, $C(A_W, A')$ for that from the available potential energy of basic wave and $C(A_Z, A')$ for the change of available potential energy of the zonal flow. These ratios have been calculated for the disturbance with the maximum growth rate corresponding to the doubling time of 3.2 days. It was found that for other growing disturbances the ratios do not change very much. From the above ratios it is evident that the disturbances grow mainly by drawing on kinetic energy of the stationary wave.

4.4 Summary and Conclusions:

Calculations show that the realistic zonal winds in the monsoon atmosphere can sustain a finite amplitude baroclinic stationary Rossby wave of wavelength about 30° longitude. The amplitude of the stationary Rossby wave in the lower troposphere is more than 20 times its amplitude in the upper troposphere. Such a stationary wave is in fact observed over Bay of Bengal (Gadgil, 1977). These stationary waves can probably be induced by orographic influences, like the presence of Western Ghats over peninsular India.

By carrying out stability analysis using a two-level quasi-geostrophic model it is seen that the stationary Rossby wave embedded in the monsoon zonal current is unstable to perturbations.

The growth rate of perturbation depends on the amplitude of the Rossby wave as well as on the meridional scale of the perturbation. It is seen that the doubling time decreases as the amplitude of stationary Rossby wave increases but there is a minimum value of $\overline{v}_3$ which can induce the growth. In the present study the minimum value is 9 m s^{-1}. For each value of $\overline{v}_3$ the growth rate attains a maximum value for a particular value of the meridional wavenumber ' l ', which lies between $5k_o/12$ and $7k_o/12$. In other words the maximum growth rate of a disturbance occurs for meridional scalelength lying between 5000 and 7000 km.

The amplitudes of the growing modes are mainly confined to the lower troposphere.

The doubling time of about 3 days corresponding to the value of $\overline{v}_3$ = 10 m s^{-1} is a reasonable doubling time for monsoon disturbances.

The growing modes are Rossby modes and they are almost stationary.

Energy calculations for the fastest growing mode reveals that perturbations grow mainly by drawing on kinetic energy of the basic wave. This is in confirmity with the result that growth rate increases with the amplitude of the stationary Rossby wave.

From this study we conclude that the monsoon zonal flow can sustain a finite amplitude stationary Rossby wave of wavelength about 30° longitude. This stationary wave is unstable to perturbations. Instability of such a stationary Rossby wave is perhaps one of the mechanisms of formation and growth of monsoon disturbances. This will also explain the confinement of monsoon cyclogenesis to eastern India.

CHAPTER FIVE

STABILITY OF A STATIONARY ROSSBY WAVE EMBEDDED IN BAROTROPIC ZONAL FLOW

In the stability analysis of the previous chapter we had considered the monsoon zonal flow having vertical wind shear. The meridional component of wind had also vertical shear. To examine the role of baroclinicity in the growth of perturbations we intend to conduct the stability analysis by superposing a stationary Rossby wave of wavelength 30° longitude on the barotropic basic flow.

5.1 Barotropic zonal flow sustaining a stationary Rossby wave:

First we will calculate the barotropic zonal wind which can sustain a stationary Rossby wave of wavelength 30° longitude along the zonal direction. For that we consider the Rossby wave speed formula

$$C = U - \frac{\beta}{k_o^2} \qquad (5.1)$$

As calculated in Section 4.1 we take $k_o = 1.84 \times 10^{-6} m^{-1}$, corresponding to a stationary Rossby wave of wavelength 30° longitude. Considering a beta-plane centred at 18°N latitude from (5.1) we calculate

$$U_s \equiv \frac{\beta}{k_o^2} \simeq 5.5 \ m \ s^{-1}$$

Thus a zonal wind $U_s = 5.5 \ m \ s^{-1}$ can sustain a stationary Rossby wave of wavelength 30° longitude.

5.2 Stability analysis:

The stability analysis is conducted as in Section 4.2 by putting the vertical shear $U_3 - U_1 = 0$. We use the basic flow

$$\phi = -f_o U_s y + f_o A \sin k_o x \qquad (5.2)$$

and the Rossby wave amplitude

$$\bar{v} \equiv k_o A = 10 \ m \ s^{-1}$$

The stability analysis reveals that the stationary Rossby wave embedded in the barotropic basic flow is also unstable. The growth rate depends on the meridional scale of the perturbation and the fastest growing mode has a doubling time of about 1.5 days (Fig.21). The growth rate is maximum for $l \leq k_o/2$ which agrees with the results of barotropic stability analysis of Lorenz (1972). The frequencies of growing disturbances are small compared to the coriolis parameter (Table 19) which suggest that these are Rossby modes. The meridional scale length of the fastest growing perturbation is the same as in the earlier stability analysis with vertical wind shear. The Fourier co-efficients of geopotential perturbation corresponding to the fastest growing mode are shown in Fig.22. As in the case of two-level quasi-geostrophic model the amplitudes are mainly confined to the first few low order harmonics.

5.3 Energy conversion:

As there are no vertical wind shears, the only source of energy for a perturbation to grow is the kinetic energy of the basic wave. The rate of conversion from kinetic energy of the basic wave to perturbation

Table 19

Characteristics of growing modes in case of barotropic basic flow and $\overline{v} = 10$ m s^{-1} (Meridional scale length of perturbation is $\frac{12}{J}$ times wavelength of the stationary Rossby wave).

$J = \frac{12\,l}{k_o}$	Frequency $\lvert\lambda_r\rvert$ (s^{-1})	Doubling time τ_d (days)
1	2.2×10^{-21}	7.0
2	3.5×10^{-23}	3.6
3	3.3×10^{-22}	2.5
4	3.3×10^{-22}	2.0
5	2.6×10^{-22}	1.7
6	1.0×10^{-22}	1.6
7	8.3×10^{-22}	1.6
8	4.6×10^{-20}	1.6
9	2.9×10^{-22}	1.8
10	8.7×10^{-21}	2.2
11	2.8×10^{-23}	3.8
12	8.5×10^{-22}	2.1×10^{16}

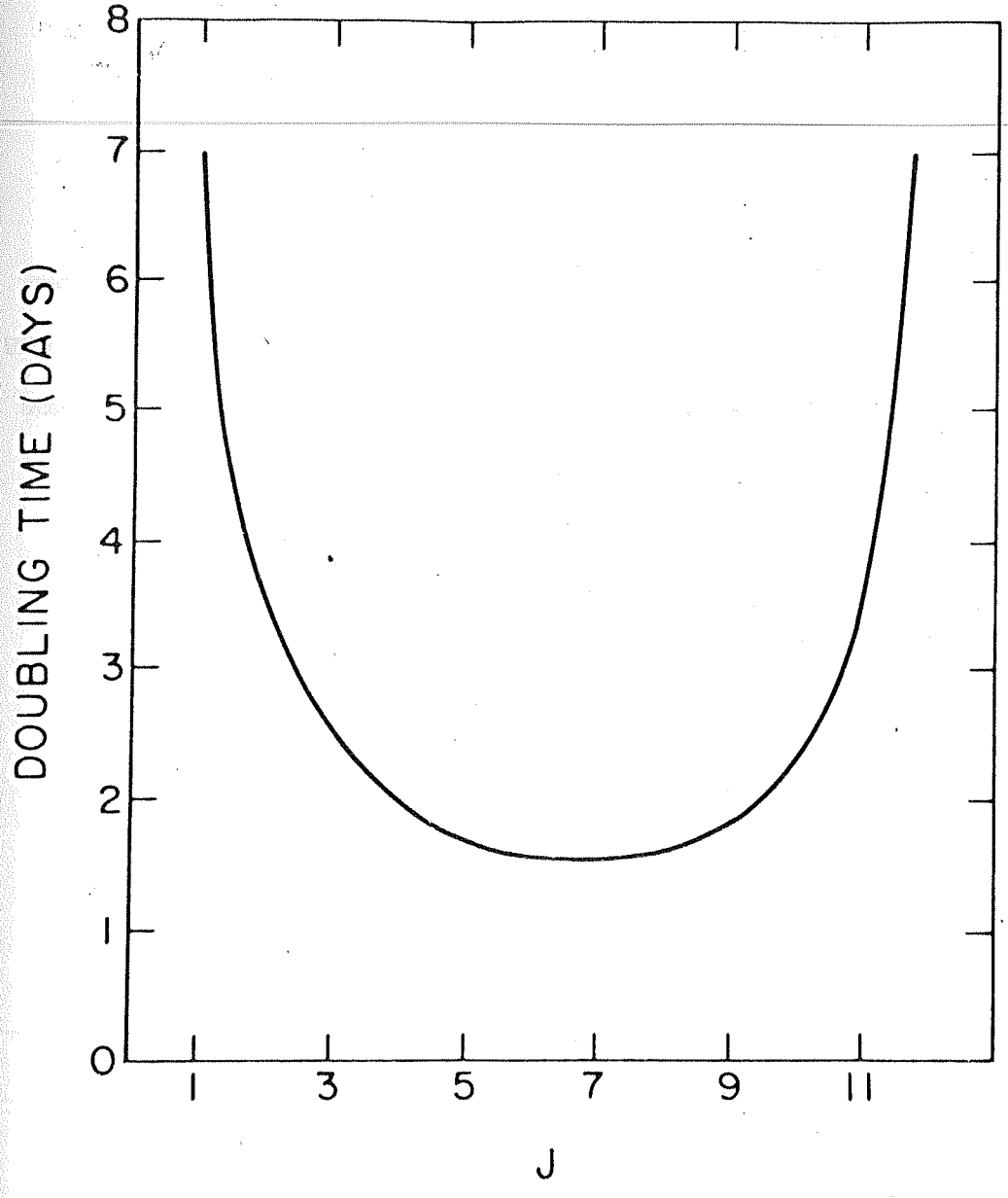

Figure 21: Meridional wavenumber ($l = J k_o/12$) dependence of the growth of Rossby modes in case of barotropic zonal flow for $\overline{v} = 10$ (m s^{-1}).

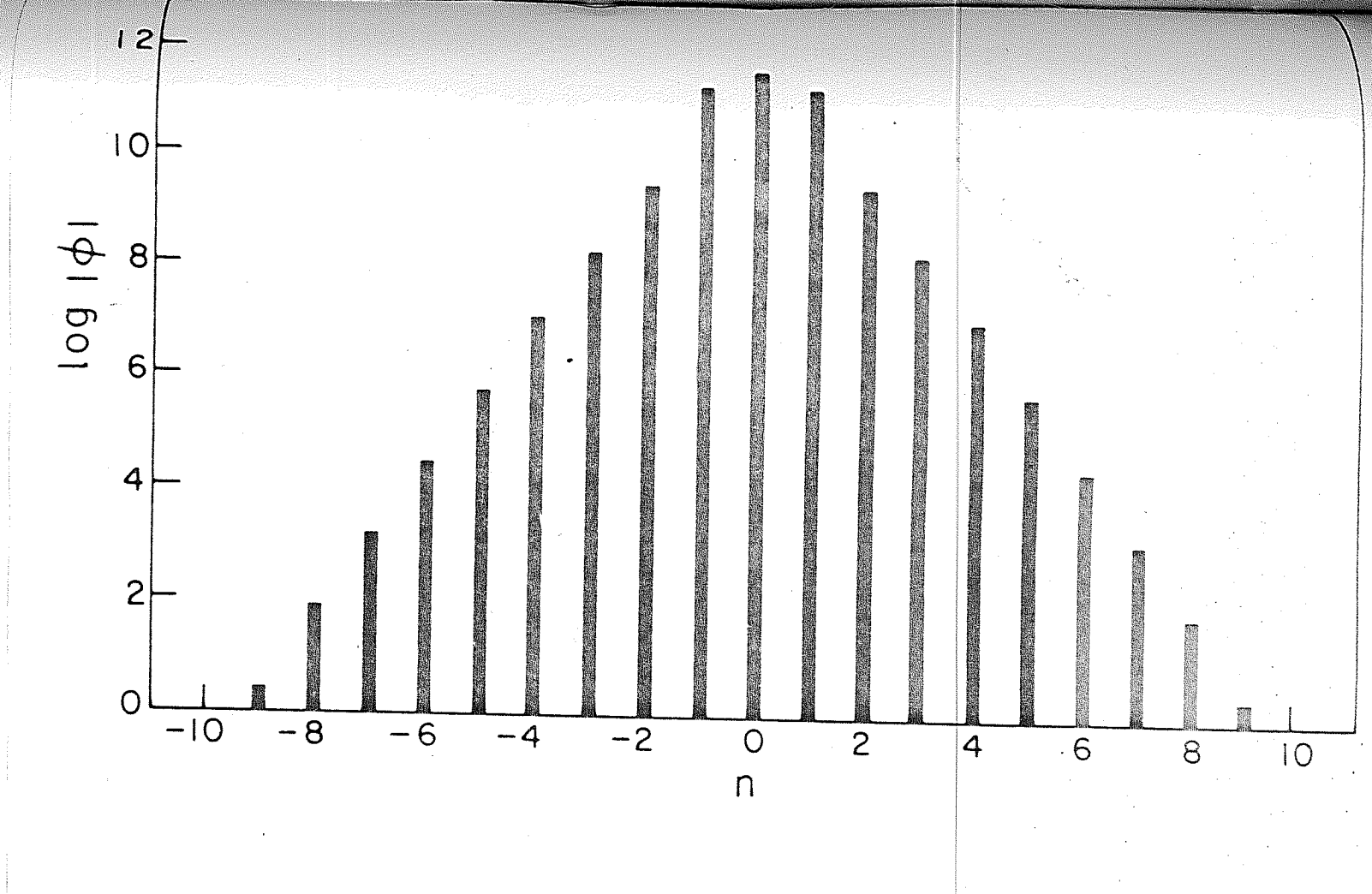

Figure 22: Fourier components of geopotential perturbation of the fastest growing Rossby mode in Fig.21.

kinetic energy, $C(K_w, K')$ is calculated from (4.35). Calculations show that the perturbation grows by drawing on kinetic energy of the stationary Rossby wave.

5.4 Summary:

To examine the role of baroclinicity in the growth of perturbations, the stability analysis is conducted by superposing a stationary Rossby wave of wavelength 30° longitude on the zonal flow without vertical shear. It is found that a stationary Rossby wave embedded in a barotropic zonal flow is also unstable to perturbations. The growing modes are Rossby modes and their growth rates depend on the meridional scales. The fastest growing mode has a doubling time of 1.5 days for $\overline{u} = 10$ m s^{-1}. Perturbations grow by drawing on kinetic energy of the stationary Rossby wave.

CHAPTER SIX

STABILITY OF A STATIONARY ROSSBY WAVE EMBEDDED IN THE MONSOON ZONAL FLOW: TWO-LEVEL PRIMITIVE EQUATION MODEL

In Chapter 4 stability analysis of the stationary Rossby wave embedded in the monsoon zonal flow was conducted using a two-level quasi-geostrophic model. It is the intention of this chapter to reexamine the stability of the finite amplitude stationary Rossby wave superposed on the monsoon zonal flow by using the primitive equation model with a beta-plane centred at 18°N latitude.

The stationary Rossby wave used is the same as that superposed on the monsoon zonal flow in Chapter 4.

It has a wavelength of 30° longitude and its amplitude is maximum in the lower troposphere. The ratio of the relative amplitudes at lower and upper troposphere is given by (4.12).

6.1 Basic equations:

In the primitive equation model we use the following vorticity, divergence and thermodynamic energy equations respectively.

$$\frac{\partial \zeta}{\partial t} = -\underline{V}\cdot\nabla(\zeta+f) - \omega\frac{\partial \zeta}{\partial p} - (\zeta+f)D + \underline{k}\cdot\left(\frac{\partial \underline{V}}{\partial p}\times\nabla\omega\right) \tag{6.1}$$

$$\frac{\partial D}{\partial t} = -\nabla^2\phi - \nabla\cdot(\underline{V}\cdot\nabla)\underline{V} - \nabla\cdot(\underline{k}\times\underline{V}f) - \omega\frac{\partial D}{\partial p} - \frac{\partial \underline{V}}{\partial p}\cdot\nabla\omega \tag{6.2}$$

$$\frac{\partial}{\partial t}\left(\frac{\partial \phi}{\partial p}\right) = -\underline{V}\cdot\nabla\left(\frac{\partial \phi}{\partial p}\right) - \sigma\omega \tag{6.3}$$

where $D \equiv \nabla\cdot\underline{V}$ and we do not include heating in the model. Expanding the vector terms in the above equations, we get,

$$\frac{\partial J}{\partial t} = -u\frac{\partial J}{\partial x} - v\frac{\partial J}{\partial y} - \beta v - \omega\frac{\partial J}{\partial p} - (J+f)D + \frac{\partial u}{\partial p}\frac{\partial \omega}{\partial y} - \frac{\partial v}{\partial p}\frac{\partial \omega}{\partial x} \tag{6.4}$$

$$\frac{\partial D}{\partial t} = -\nabla^2\phi - u\frac{\partial D}{\partial x} - v\frac{\partial D}{\partial y} - \left(\frac{\partial u}{\partial x}\right)^2 - 2\frac{\partial v}{\partial x}\frac{\partial u}{\partial y} - \left(\frac{\partial v}{\partial y}\right)^2 + f\frac{\partial v}{\partial x} - f\frac{\partial u}{\partial y} - \beta u - \omega\frac{\partial D}{\partial p} - \frac{\partial u}{\partial p}\frac{\partial \omega}{\partial x} - \frac{\partial v}{\partial p}\frac{\partial \omega}{\partial y} \tag{6.5}$$

$$\frac{\partial}{\partial t}\left(\frac{\partial \phi}{\partial p}\right) = -u\frac{\partial}{\partial x}\left(\frac{\partial \phi}{\partial p}\right) - v\frac{\partial}{\partial y}\left(\frac{\partial \phi}{\partial p}\right) - \sigma\omega \tag{6.6}$$

In addition to the above three equations we will have to use another equation where the surface boundary condition for ω is incorporated. We have the geopotential tendency

$$\frac{d\phi}{dt} = gW$$

where W is the vertical velocity. Expanding $\frac{d\phi}{dt}$ in isobaric co-ordinates and using hydrostatic approximation we get

$$\frac{\partial \phi}{\partial t} + \underline{V}\cdot\nabla\phi - \alpha\omega = gW$$

when applied to a level lower boundary, $W = 0$. Also at the surface

$$\alpha = \frac{1}{p_0}\theta_4 R$$

Hence

$$\frac{\partial \phi}{\partial t} = -u\frac{\partial \phi}{\partial x} - v\frac{\partial \phi}{\partial y} + \frac{\theta_4 R}{p_0}\omega \qquad (6.7)$$

6.2 Linearisation of the basic equations:

The set of equations (6.4) - (6.7) after linearisation will be used for the stability analysis. The linearisation is done as in Section 4.2 and we get the following perturbation vorticity, divergence, thermodynamic energy equations and bottom boundary condition respectively.

$$\mathcal{L}\zeta' + u'\frac{\partial \bar{\zeta}^*}{\partial x} + \beta v' + (\bar{\zeta}^* + f_0)D' + \omega'\frac{\partial \bar{\zeta}^*}{\partial p} + \frac{\partial \bar{v}^*}{\partial p}\frac{\partial \omega'}{\partial x} - \frac{\partial U}{\partial p}\frac{\partial \omega'}{\partial y} = 0 \qquad (6.8)$$

$$\mathcal{L}D' - f_0\zeta' + \beta u' + \nabla^2\phi' + \frac{\partial U}{\partial p}\frac{\partial \omega'}{\partial x} + \frac{\partial \bar{v}^*}{\partial p}\frac{\partial \omega'}{\partial y} + 2\frac{\partial \bar{v}^*}{\partial x}\frac{\partial u'}{\partial y} = 0 \qquad (6.9)$$

$$\mathcal{L}\frac{\partial \phi'}{\partial p} + f_0 u'\frac{\partial \bar{v}^*}{\partial p} - f_0 v'\frac{\partial U}{\partial p} + \sigma\omega' = 0 \qquad (6.10)$$

$$\mathcal{L}\phi' - \frac{R\theta_4}{p_0}\omega' = 0 \qquad (6.11)$$

where the operator

$$\mathcal{L} \equiv \frac{\partial}{\partial t} + U\frac{\partial}{\partial x} + \bar{v}^*\frac{\partial}{\partial y} .$$

6.3 The model:

As is customary, the vorticity, divergence and the thermodynamic energy equations at levels 1 and 3 and the bottom boundary condition are written down.

100 mb	ϕ_0 , $\omega_0 = 0$	0
325	ψ_1 , χ_1	1
550	ϕ_2 , ω_2	2
775	ψ_3 , χ_3	3
1000	ϕ_4 , ω_4	4

The perturbation vorticity, divergence and thermodynamic energy equations at level 1 can be written as

$$\mathcal{L}_1 J_1' + u_1' \frac{\partial \bar{J}_1^*}{\partial x} + \beta v_1' + (\bar{J}_1^* + f_0) D_1' + \omega_1' \frac{\partial \bar{J}_1^*}{\partial p} + \frac{\partial \bar{v}_1^*}{\partial p}\frac{\partial \omega_1'}{\partial x} - \frac{\partial U_1}{\partial p}\frac{\partial \omega_1'}{\partial y} = 0 \qquad (6.12)$$

$$\mathcal{L}_1 D_1' - f_0 \zeta_1' + \beta u_1' + \nabla^2 \phi_1' + \frac{\partial U_1}{\partial p}\frac{\partial \omega_1'}{\partial x} + \frac{\partial \bar{v}_1^*}{\partial p}\frac{\partial \omega_1'}{\partial y} + 2\frac{\partial \bar{v}_1^*}{\partial x}\frac{\partial u_1'}{\partial y} = 0 \qquad (6.13)$$

and

$$\mathcal{L}_1 \frac{\partial \phi_1'}{\partial p} + f_0 u_1' \frac{\partial \bar{v}_1^*}{\partial p} - f_0 v_1' \frac{\partial U_1}{\partial p} + \sigma_1 \omega_1' = 0 \qquad (6.14)$$

Similarly the perturbation vorticity, divergence and thermodynamic energy equations at level 3 are

$$\mathcal{L}_3 \zeta_3' + u_3' \frac{\partial \bar{\zeta}_3^*}{\partial x} + \beta v_3' + (\bar{\zeta}_3^* + f_0) D_3' + \omega_3' \frac{\partial \bar{\zeta}_3^*}{\partial p} + \frac{\partial \bar{v}_3^*}{\partial p}\frac{\partial \omega_3'}{\partial x} - \frac{\partial U_3}{\partial p}\frac{\partial \omega_3'}{\partial y} = 0 \qquad (6.15)$$

$$\mathcal{L}_3 D_3' - f_0 \zeta_3' + \beta u_3' + \nabla^2 \phi_3' + \frac{\partial U_3}{\partial p}\frac{\partial \omega_3'}{\partial x} + \frac{\partial \bar{v}_3^*}{\partial p}\frac{\partial \omega_3'}{\partial y} + 2\frac{\partial \bar{v}_3^*}{\partial x}\frac{\partial u_3'}{\partial y} = 0 \qquad (6.16)$$

and

$$\mathcal{L}_3 \frac{\partial \phi_3'}{\partial p} + f_0 u_3' \frac{\partial \bar{v}_3^*}{\partial p} - f_0 v_3' \frac{\partial U_3}{\partial p} + \sigma_3 \omega_3' = 0 \qquad (6.17)$$

The bottom boundary condition is

$$\mathcal{L}_4 \phi_4' - \frac{R\theta_4}{p_0}\omega_4' = 0 \qquad (6.18)$$

As defined earlier,

$$\mathcal{L}_i \equiv \frac{\partial}{\partial t} + U_i \frac{\partial}{\partial x} + \bar{v}_i^* \frac{\partial}{\partial y} \quad , \quad i = 1, 3 \text{ and } 4 .$$

Unlike in the quasigeotrophic model the horizontal divergence is not neglected (compared to the vorticity) in the primitive equation model. Hence we have

$$D' = \nabla^2 \chi' = -\frac{\partial \omega'}{\partial p}$$

and (6.19)

$$\zeta' = \nabla^2 \psi'$$

where the perturbation wind components are expressed by

$$u' = -\frac{\partial \psi'}{\partial y} + \frac{\partial \chi'}{\partial x}$$

and (6.20)

$$v' = \frac{\partial \psi'}{\partial x} + \frac{\partial \chi'}{\partial y} .$$

Here ψ' and χ' are the stream function and the velocity potential respectively. For the perturbation fields ψ', χ' and ϕ' we assume solutions of the form

$$\begin{pmatrix} \psi' \\ \chi' \\ \phi' \end{pmatrix} = \sum_{n=-\infty}^{\infty} \begin{pmatrix} \psi_n \\ \chi_n \\ \phi_n \end{pmatrix} \exp\{i(nk_0 x + kx + ly + \lambda t)\} \quad (6.21)$$

For simplicity we take $k = 0$ as in case of the quasi-geostrophic model. Substituting (6.19), (6.20) and (6.21) in the set of Eqs. (6.12) to (6.18) and collecting the co-efficients of $\exp\{i(nk_0x + ly + \lambda t)\}$ we get the following set of linear algebraic equations, after considerable algebra.

$$\frac{1}{2} l \bar{v}_1 (k_0^2 - b_{n-1}) \psi_{n-1}^{(1)} + a_n (\beta - b_n U_1) \psi_n^{(1)} + \frac{1}{2} l \bar{v}_1 (k_0^2 - b_{n+1}) \psi_{n+1}^{(1)} + \left\{ \frac{1}{2} k_0 \bar{v}_1 (-k_0 a_{n-1} - b_{n-1}) + \frac{1}{4} b_{n-1} (\bar{v}_2 - \bar{v}_0)(k_0 + a_{n-1}) \right\} \chi_{n-1}^{(1)} + l \left\{ \beta - \frac{1}{2} b_n (U_2 - U_0) \right\} \chi_n^{(1)} + \left\{ \frac{1}{2} k_0 \bar{v}_1 (b_{n+1} - k_0 a_{n+1}) + \frac{1}{4} b_{n+1} (\bar{v}_2 - \bar{v}_0)(a_{n+1} - k_0) \right\} \chi_{n+1}^{(1)} + i f_0 b_n \chi_n^{(1)} - \lambda b_n \psi_n^{(1)} = 0 \qquad (6.22)$$

$$k_0 l^2 \bar{v}_1 \psi_{n-1}^{(1)} - l\beta \psi_n^{(1)} - k_0 l^2 \bar{v}_1 \psi_{n+1}^{(1)} + \left\{ \frac{1}{2} l b_{n-1} \left(\frac{\bar{v}_2 - \bar{v}_0}{2} - \bar{v}_1 \right) - l k_0 \bar{v}_1 a_{n-1} \right\} \chi_{n-1}^{(1)} + a_n \left\{ \beta + b_n \left(\frac{U_2 - U_0}{2} - U_1 \right) \right\} \chi_n^{(1)} + \left\{ \frac{1}{2} l b_{n+1} \left(\frac{\bar{v}_2 - \bar{v}_0}{2} - \bar{v}_1 \right) + l k_0 \bar{v}_1 a_{n+1} \right\} \chi_{n+1}^{(1)} + i \left\{ -f_0 b_n \psi_n^{(1)} + \frac{1}{2} b_n \phi_n^{(0)} + \frac{1}{2} b_n \phi_n^{(2)} \right\} - \lambda b_n \chi_n^{(1)} = 0 \qquad (6.23)$$

$$-\frac{1}{2} l s_1 (\bar{v}_2 - \bar{v}_0) \psi_{n-1}^{(1)} - a_n s_1 (U_2 - U_0) \psi_n^{(1)}$$
$$-\frac{1}{2} l s_1 (\bar{v}_2 - \bar{v}_0) \psi_{n+1}^{(1)} + \frac{1}{2} a_{n-1} s_1 (\bar{v}_2 - \bar{v}_0) \chi_{n-1}^{(1)}$$
$$- l s_1 (U_2 - U_0) \chi_n^{(1)} + \frac{1}{2} a_{n+1} s_1 (\bar{v}_2 - \bar{v}_0) \chi_{n+1}^{(1)}$$
$$- \frac{l s_1 \bar{v}_1}{2 f_0} \phi_{n-1}^{(0)} - \frac{a_n s_1 U_1}{f_0} \phi_n^{(0)} - \frac{l s_1 \bar{v}_1}{2 f_0} \phi_{n+1}^{(0)}$$
$$+ \frac{l s_1 \bar{v}_1}{2 f_0} \phi_{n-1}^{(2)} + \frac{a_n s_1 U_1}{f_0} \phi_n^{(2)} + \frac{l s_1 \bar{v}_1}{2 f_0} \phi_{n+1}^{(2)}$$
$$- i \frac{1}{2} f_0 b_n \chi_n^{(1)} - \lambda \left\{ \frac{s_1}{f_0} \phi_n^{(0)} - \frac{s_1}{f_0} \phi_n^{(2)} \right\} = 0 \qquad (6.24)$$

$$\frac{1}{2} l \bar{v}_3 (k_0^2 - b_{n-1}) \psi_{n-1}^{(3)} + a_n (\beta - U_3 b_n) \psi_n^{(3)} + \frac{1}{2} l \bar{v}_3 (k_0^2$$
$$- b_{n+1}) \psi_{n+1}^{(3)} + \frac{1}{2} b_{n-1} (\bar{v}_4 - \bar{v}_2)(k_0 + a_{n-1}) \chi_{n-1}^{(1)}$$
$$- l b_n (U_4 - U_2) \chi_n^{(1)} + \frac{1}{2} b_{n+1} (\bar{v}_4 - \bar{v}_2)(a_{n+1} - k_0) \chi_{n+1}^{(1)}$$
$$+ \left\{ \frac{1}{2} k_0 \bar{v}_3 (-k_0 a_{n-1} - b_{n-1}) + \frac{1}{4} b_{n-1} (\bar{v}_4 - \bar{v}_2)(k_0 \right.$$
$$\left. + a_{n-1}) \right\} \chi_{n-1}^{(3)} + l \left(\beta - b_n \frac{U_4 - U_2}{2}\right) \chi_n^{(3)}$$
$$+ \left\{ \frac{1}{2} k_0 \bar{v}_3 (b_{n+1} - k_0 a_{n+1}) + \frac{1}{4} b_{n+1} (\bar{v}_4 - \bar{v}_2)(a_{n+1} \right.$$
$$\left. - k_0) \right\} \chi_{n+1}^{(3)} + i f_0 b_n \chi_n^{(3)} - \lambda b_n \psi_n^{(3)} = 0 \qquad (6.25)$$

$$(l^2 k_o \bar{v}_3 \psi_{n-1}^{(3)} - l\beta \psi_n^{(3)} - l^2 k_o \bar{v}_3 \psi_{n+1}^{(3)} + \frac{1}{2} l b_{n-1} (\bar{v}_4 - \bar{v}_2) \chi_{n-1}^{(1)}$$
$$+ a_n b_n (U_4 - U_2) \chi_n^{(1)} + \frac{1}{2} l b_{n+1} (\bar{v}_4 - \bar{v}_2) \chi_{n+1}^{(1)}$$
$$+ \left\{ \frac{1}{4} l b_{n-1} (\bar{v}_4 - \bar{v}_2) - l \bar{v}_3 \left(k_o a_{n-1} + \frac{1}{2} b_{n-1} \right) \right\} \chi_{n-1}^{(3)}$$
$$+ a_n \left\{ \beta + b_n \left(\frac{U_4 - U_2}{2} - U_3 \right) \right\} \chi_n^{(3)} + \left\{ \frac{1}{4} l b_{n+1} (\bar{v}_4 - \bar{v}_2) \right.$$
$$\left. + l \bar{v}_3 \left(k_o a_{n+1} - \frac{1}{2} b_{n+1} \right) \right\} \chi_{n+1}^{(3)} + i \left\{ -f_o b_n \psi_n^{(3)} \right.$$
$$\left. + \frac{1}{2} b_n \phi_n^{(2)} + \frac{1}{2} b_n \phi_n^{(4)} \right\} - \lambda b_n \chi_n^{(3)} = 0 \qquad (6.26)$$

$$- \frac{1}{2} l s_3 (\bar{v}_4 - \bar{v}_2) \psi_{n-1}^{(3)} - a_n s_3 (U_4 - U_2) \psi_n^{(3)} - \frac{1}{2} l s_3 (\bar{v}_4 - \bar{v}_2) \psi_{n+1}^{(3)}$$
$$+ \frac{1}{2} a_{n-1} (\bar{v}_4 - \bar{v}_2) s_3 \chi_{n-1}^{(3)} - l s_3 (U_4 - U_2) \chi_n^{(3)} + \frac{1}{2} s_3 a_{n+1} (\bar{v}_4$$
$$- \bar{v}_2) \chi_{n+1}^{(3)} - \frac{l s_3 \bar{v}_3}{2 f_o} \phi_{n-1}^{(2)} - \frac{a_n s_3 U_3}{f_o} \phi_n^{(2)} - \frac{l s_3 \bar{v}_3}{2 f_o} \phi_{n+1}^{(2)}$$
$$+ \frac{l s_3 \bar{v}_3}{2 f_o} \phi_{n-1}^{(4)} + \frac{a_n s_3 U_3}{f_o} \phi_n^{(4)} + \frac{l s_3 \bar{v}_3}{2 f_o} \phi_{n+1}^{(4)} + i \left\{ -f_o b_n \chi_n^{(1)} \right.$$
$$\left. - \frac{1}{2} f_o b_n \chi_n^{(3)} \right\} - \lambda \left\{ \frac{s_3}{f_o} \phi_n^{(2)} - \frac{s_3}{f_o} \phi_n^{(4)} \right\} = 0 \qquad (6.27)$$

$$\frac{l f_o \bar{v}_4}{2 B_c \Delta p} \phi_{n-1}^{(4)} + \frac{a_n f_o U_4}{B_c \Delta p} \phi_n^{(4)} + \frac{l f_o \bar{v}_4}{2 B_c \Delta p} \phi_{n+1}^{(4)}$$
$$+ i f_o b_n \left(\chi_n^{(1)} + \chi_n^{(3)} \right) - \lambda \left(- \frac{f_o}{B_c \Delta p} \right) \phi_n^{(4)} = 0 \qquad (6.28)$$

where $$B_c \equiv \frac{R \Theta_4}{P_o}$$

The bracketed superscripts in the above equations denote the levels. As in Chapter 4 truncating (6.21) at n = N one gets 7x(2N + 1) number of algebraic equations from Eqs. (6.22) to (6.28). Rearranging the terms we get matrix equation of the form (4.16). But here the matrix $\underset{\sim}{P}$ is complex. If $\underset{\sim}{P}^{r}$ and $\underset{\sim}{P}^{i}$ denote the real and imaginary parts of $\underset{\sim}{P}$ respectively, the eigenvalue equation can be written as

$$\left(\underset{\sim}{P}^{r}\cdot\underset{\sim}{Q}^{-1}+i\,\underset{\sim}{P}^{i}\cdot\underset{\sim}{Q}^{-1}-\lambda\underset{\sim}{I}\right)\left(\underset{\sim}{Q}\cdot\underset{\sim}{R}\right)=0 \qquad (6.29)$$

Here $\underset{\sim}{P}^{r}$, $\underset{\sim}{P}^{i}$ and $\underset{\sim}{Q}^{-1}$ are real matrices of size 7(2N+1) x 7(2N+1) each. Due to computational limit we could go up to N = 4. However, from our experience with the quasi-geostrophic model in Chaper 4 we know that the Fourier series (6.21) converges very fast. Hence the eigenvalues and eigenvectors are probably not very much different from the true values. With N = 4, we have matrices of size 63 x 63 each.

The nonzero elements p^{r}_{jk}, p^{i}_{jk} and q_{jk} of the matrices $\underset{\sim}{P}^{r}$, $\underset{\sim}{P}^{i}$ and $\underset{\sim}{Q}$ respectively are shown in Figs. 23, 24 and 25.

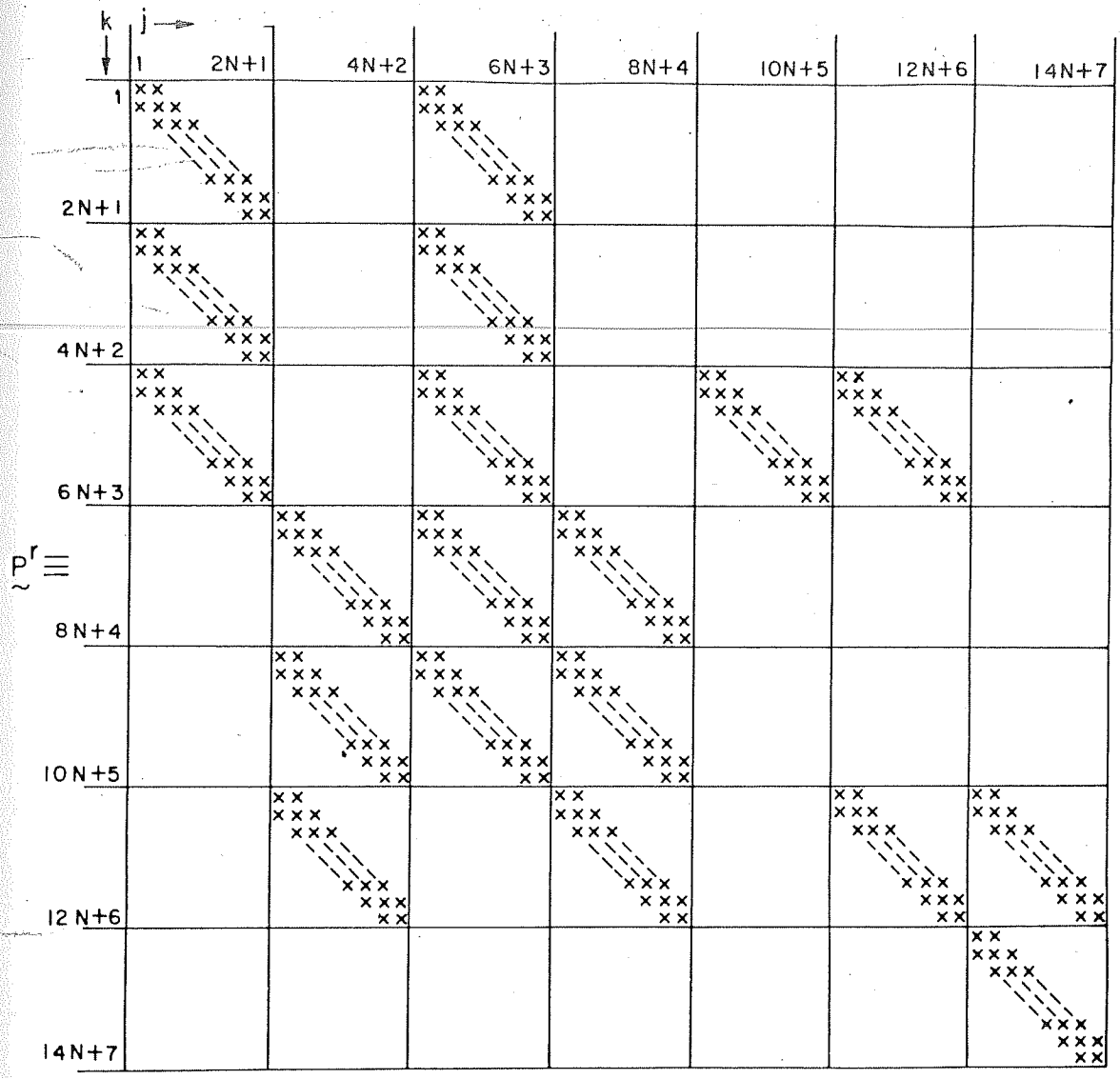

Figure 23: Nonzero elements of matrix $\underset{\sim}{P}^r$ appearing in Eq. (6.29). The cross marks denote the nonzero elements.

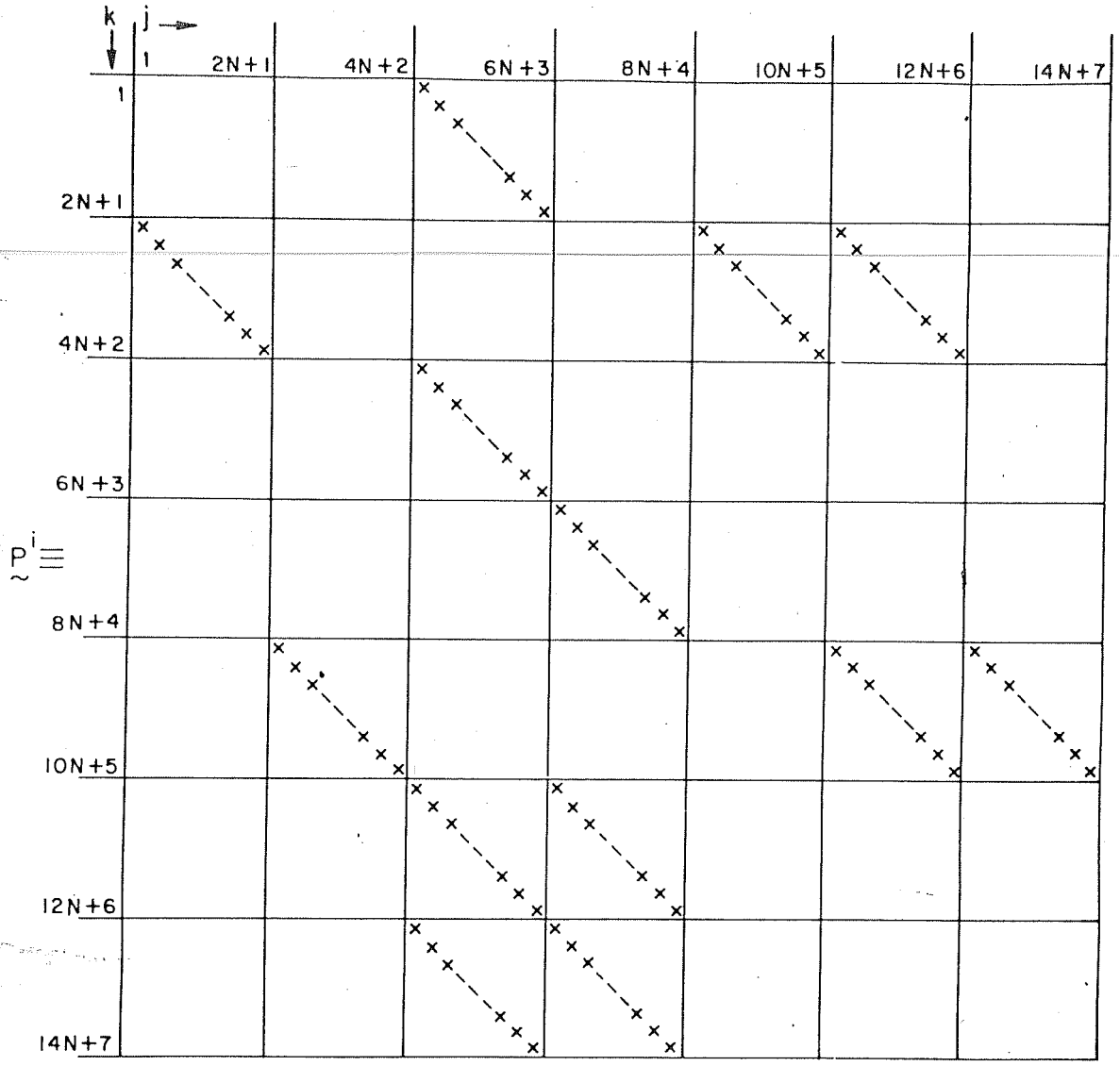

Figure 24: Nonzero elements of matrix $\underset{\sim}{P}^i$ appearing in Eq. (6.29). The cross marks denote the nonzero elements.

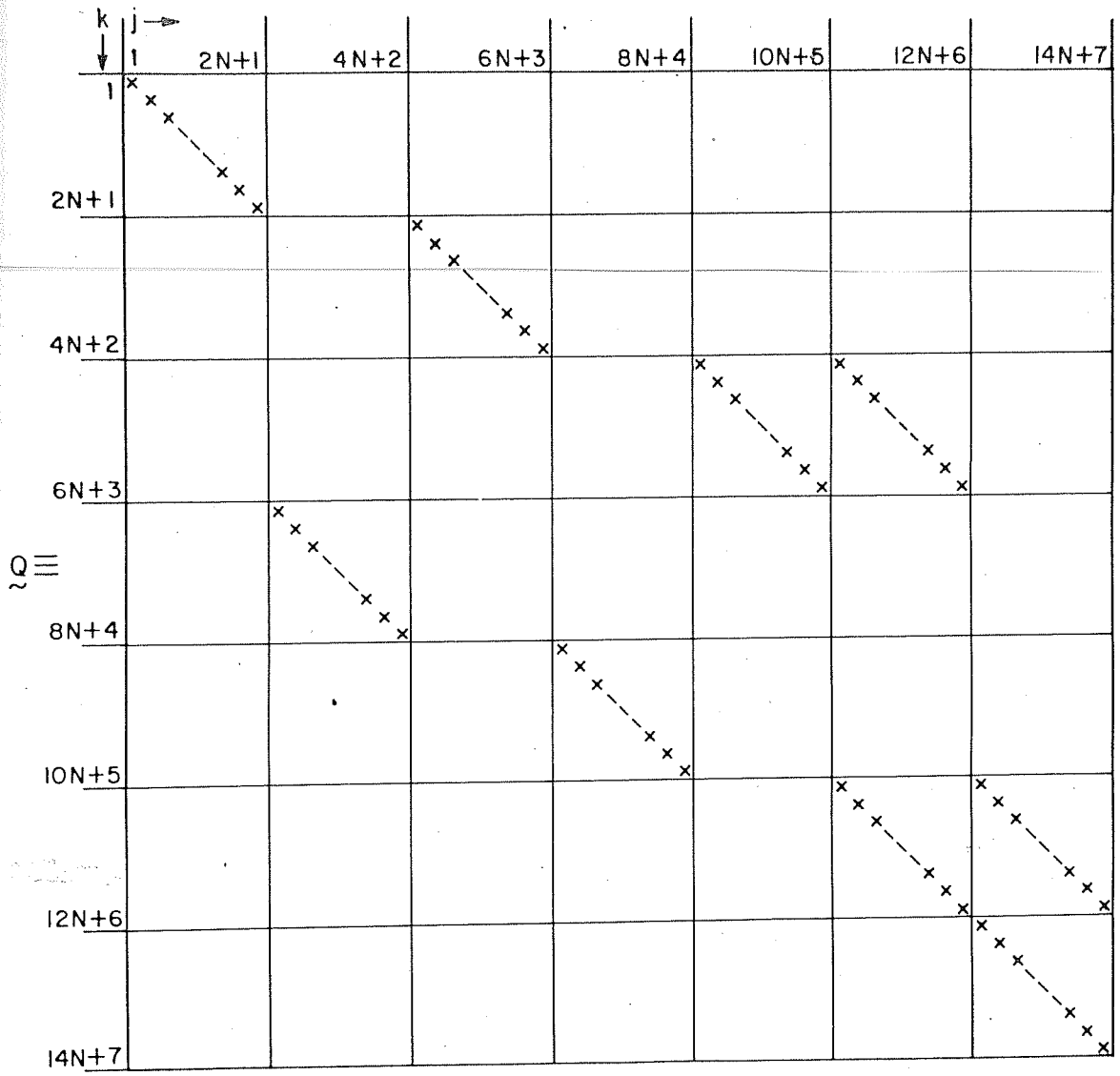

Figure 25: Nonzero elements of matrix $\underset{\sim}{Q}$ appearing in Eq. (6.29). The cross marks denote the nonzero elements.

$\underset{\sim}{R}$ is a column matrix of the form

$$\underset{\sim}{R} = \begin{pmatrix} r_1 \\ r_2 \\ \vdots \\ r_{2N+1} \\ r_{2N+2} \\ \vdots \\ r_{4N+2} \\ r_{4N+3} \\ \vdots \\ r_{6N+3} \\ r_{6N+4} \\ \vdots \\ r_{8N+4} \\ r_{8N+5} \\ \vdots \\ r_{10N+5} \\ r_{10N+6} \\ \vdots \\ r_{12N+6} \\ r_{12N+7} \\ \vdots \\ r_{14N+7} \end{pmatrix}$$

The nonzero elements $\overset{r}{p}_{jk}$, $\overset{i}{p}_{jk}$ and q_{jk} are defined below. For conveneince let $n = m - (N + 1)$.

When m varies from 1 to (2N + 1)

$$\overset{r}{p}_{m,m} = a_n(\beta - b_n U_1)$$

$$\overset{r}{p}_{m,\,4N+m+2} = l\left\{\beta - \frac{1}{2} b_n (U_2 - U_0)\right\}$$

$$\overset{r}{p}_{2N+m+1,\,m} = -l\beta$$

$$\overset{r}{p}_{2N+m+1,\,4N+m+2} = a_n\left\{\beta + b_n\left(\frac{U_2 - U_0}{2} - U_1\right)\right\}$$

$$\overset{r}{p}_{4N+m+2,\,m} = -a_n s_1 (U_2 - U_0)$$

$$\overset{r}{p}_{4N+m+2,\,4N+m+2} = -l s_1 (U_2 - U_0)$$

$$\overset{r}{p}_{4N+m+2,\,8N+m+4} = -\frac{a_n s_1 U_1}{f_0}$$

$$\overset{r}{p}_{4N+m+2,\,10N+m+5} = \frac{a_n s_1 U_1}{f_0}$$

$$\overset{r}{p}_{6N+m+3,\,2N+m+1} = a_n(\beta - b_n U_3)$$

$$\overset{r}{p}_{6N+m+3,\,4N+m+2} = -l b_n (U_4 - U_2)$$

$$\overset{r}{p}_{6N+m+3,\,6N+m+3} = l\left(\beta - b_n \frac{U_4 - U_2}{2}\right)$$

$$\overset{r}{p}_{8N+m+4,\,2N+m+1} = -l\beta$$

$$\overset{r}{p}_{8N+m+4,\,4N+m+2} = a_n b_n (U_4 - U_2)$$

$$\overset{r}{p}_{8N+m+4,\,6N+m+3} = a_n \left\{ \beta + b_n \left(\frac{U_4 - U_2}{2} - U_3 \right) \right\}$$

$$\overset{r}{p}_{10N+m+5,\,2N+m+1} = -a_n s_3 (U_4 - U_2)$$

$$\overset{r}{p}_{10N+m+5,\,6N+m+3} = -1 s_3 (U_4 - U_2)$$

$$\overset{r}{p}_{10N+m+5,\,10N+m+5} = -\frac{a_n s_3 U_3}{f_o}$$

$$\overset{r}{p}_{10N+m+5,\,12N+m+6} = \frac{a_n s_3 U_3}{f_o}$$

$$\overset{r}{p}_{12N+m+6,\,12N+m+6} = \frac{a_n f_o U_4}{\Delta p \, B_c}$$

$$\dot{\overset{i}{p}}_{m,\,4N+m+2} = f_o b_n$$

$$\dot{\overset{i}{p}}_{2N+m+1,\,m} = -f_o b_n$$

$$\dot{\overset{i}{p}}_{2N+m+1,\,8N+m+4} = \frac{1}{2} b_n$$

$$\dot{\overset{i}{p}}_{2N+m+1,\,10N+m+5} = \frac{1}{2} b_n$$

$$\dot{\overset{i}{p}}_{4N+m+2,\,4N+m+2} = -\frac{1}{2} f_o b_n$$

$$\dot{\overset{i}{p}}_{6N+m+3,\,6N+m+3} = f_o b_n$$

$$\dot{p}^i_{8N+m+4,\,2N+m+1} = -f_o b_n$$

$$\dot{p}^i_{8N+m+4,\,10N+m+5} = \frac{1}{2} b_n$$

$$\dot{p}^i_{8N+m+4,\,12N+m+6} = \frac{1}{2} b_n$$

$$\dot{p}^i_{10N+m+5,\,4N+m+2} = -f_o b_n$$

$$\dot{p}^i_{10N+m+5,\,6N+m+3} = -\frac{1}{2} f_o b_n$$

$$\dot{p}^i_{12N+m+6,\,4N+m+2} = f_o b_n$$

$$\dot{p}^i_{12N+m+6,\,6N+m+3} = f_o b_n$$

$$q_{m,m} = b_n$$

$$q_{2N+m+1,\,4N+m+2} = b_n$$

$$q_{4N+m+2,\,8N+m+4} = \frac{s_1}{f_o}$$

$$q_{4N+m+2,\,10N+m+5} = -\frac{s_1}{f_o}$$

$$q_{6N+m+3,\,2N+m+1} = b_n$$

$$q_{8N+m+4,\,6N+m+3} = b_n$$

$$q_{10N+m+5,\,10N+m+5} = \frac{s_3}{f_o}$$

$$q_{10N+m+5,\,12N+m+6} = -\frac{s_3}{f_o}$$

$$q_{12N+m+6,\,12N+m+6} = -\frac{f_o}{\Delta p\, B_c}$$

When m varies from 1 to 2N

$$p^r_{m,\,m+1} = \frac{1}{2} l\, \bar{v}_1 (k_o^2 - b_{n+1})$$

$$p^r_{m,\,4N+m+3} = \frac{1}{2} k_o \bar{v}_1 (b_{n+1} - k_o a_{n+1}) + \frac{1}{4} b_{n+1} (\bar{v}_2 - \bar{v}_o)(a_{n+1} - k_o)$$

$$p^r_{2N+m+1,\,m+1} = -k_o l^2 \bar{v}_1$$

$$p^r_{2N+m+1,\,4N+m+3} = \frac{1}{2} l\, b_{n+1} \left(\frac{\bar{v}_2 - \bar{v}_o}{2} - \bar{v}_1 \right) + l\, k_o \bar{v}_1 a_{n+1}$$

$$p^r_{4N+m+2,\,m+1} = -\frac{1}{2} l\, s_1 (\bar{v}_2 - \bar{v}_o)$$

$$p^r_{4N+m+2,\,4N+m+3} = \frac{1}{2} a_{n+1} s_1 (\bar{v}_2 - \bar{v}_o)$$

$$p^r_{4N+m+2,\,8N+m+5} = -\frac{s_1 \bar{v}_1 l}{2 f_o}$$

$$p^r_{4N+m+2,\,10N+m+6} = \frac{s_1 \bar{v}_1 l}{2 f_o}$$

$$p^r_{6N+m+3,\,2N+m+2} = \frac{1}{2} l\, \bar{v}_3 (k_o^2 - b_{n+1})$$

$$p^r_{6N+m+3,\,4N+m+3} = \frac{1}{2} b_{n+1} (\bar{v}_4 - \bar{v}_2)(a_{n+1} - k_o)$$

$$b^r_{6N+m+3,\,6N+m+4} = \frac{1}{4} k_0 \bar{v}_3 (b_{n+1} - k_0 a_{n+1}) + \frac{1}{4} b_{n+1} (\bar{v}_4 - \bar{v}_2)(a_{n+1} - k_0)$$

$$b^r_{8N+m+4,\,2N+m+2} = -l^2 k_0 \bar{v}_3$$

$$b^r_{8N+m+4,\,4N+m+3} = \frac{1}{2} l\, b_{n+1} (\bar{v}_4 - \bar{v}_2)$$

$$b^r_{8N+m+4,\,6N+m+4} = \frac{1}{4} l\, b_{n+1} (\bar{v}_4 - \bar{v}_2) + l \bar{v}_3 \left(k_0 a_{n+1} - \frac{1}{2} b_{n+1}\right)$$

$$b^r_{10N+m+5,\,2N+m+2} = -\frac{1}{2} l s_3 (\bar{v}_4 - \bar{v}_2)$$

$$b^r_{10N+m+5,\,6N+m+4} = \frac{1}{2} a_{n+1} s_3 (\bar{v}_4 - \bar{v}_2)$$

$$b^r_{10N+m+5,\,10N+m+6} = -\frac{l s_3 \bar{v}_3}{2 f_0}$$

$$b^r_{10N+m+5,\,12N+m+7} = \frac{l s_3 \bar{v}_3}{2 f_0}$$

$$b^r_{12N+m+6,\,12N+m+7} = \frac{l f_0 \bar{v}_4}{2 \Delta p B_c}$$

When m varies from 2 to (2N + 1)

$$b^r_{m,m-1} = \frac{1}{2} l \bar{v}_1 (k_0^2 - b_{n-1})$$

$$b^r_{m,4N+m+1} = \frac{1}{2} k_0 \bar{v}_1 (-k_0 a_{n-1} - b_{n-1}) + \frac{1}{4} b_{n-1} (\bar{v}_2 - \bar{v}_0)(k_0 + a_{n-1})$$

$$b^r_{2N+m+1,m-1} = k_0 l^2 \bar{v}_1$$

$$b^r_{2N+m+1,4N+m+1} = \frac{1}{2} l b_{n-1} \left(\frac{\bar{v}_2 - \bar{v}_0}{2} - \bar{v}_1 \right) - l k_0 \bar{v}_1 a_{n-1}$$

$$b^r_{4N+m+2,m-1} = -\frac{1}{2} l s_1 (\bar{v}_2 - \bar{v}_0)$$

$$b^r_{4N+m+2,4N+m+1} = \frac{1}{2} a_{n-1} s_1 (\bar{v}_2 - \bar{v}_0)$$

$$b^r_{4N+m+2,8N+m+3} = -\frac{l s_1 \bar{v}_1}{2 f_0}$$

$$b^r_{4N+m+2,10N+m+4} = \frac{l s_1 \bar{v}_1}{2 f_0}$$

$$b^r_{6N+m+3,2N+m} = \frac{1}{2} l \bar{v}_3 (k_0^2 - b_{n-1})$$

$$b^r_{6N+m+3,4N+m+1} = \frac{1}{2} b_{n-1} (\bar{v}_4 - \bar{v}_2)(k_0 + a_{n-1})$$

$$p^r_{6N+m+3,\,6N+m+2} = \frac{1}{2}k_0\bar{v}_3(-k_0 a_{n-1} - b_{n-1}) + \frac{1}{4}b_{n-1}(\bar{v}_4 - \bar{v}_2)(k_0 + a_{n-1})$$

$$p^r_{8N+m+4,\,2N+m} = l^2 k_0 \bar{v}_3$$

$$p^r_{8N+m+4,\,4N+m+1} = \frac{1}{2} l\, b_{n-1}(\bar{v}_4 - \bar{v}_2)$$

$$p^r_{8N+m+4,\,6N+m+2} = \frac{1}{4} l\, b_{n-1}(\bar{v}_4 - \bar{v}_2) - l\bar{v}_3\left(k_0 a_{n-1} + \frac{1}{2} b_{n-1}\right)$$

$$p^r_{10N+m+5,\,2N+m} = -\frac{1}{2} l\, s_3(\bar{v}_4 - \bar{v}_2)$$

$$p^r_{10N+m+5,\,6N+m+2} = \frac{1}{2} s_3\, a_{n-1}(\bar{v}_4 - \bar{v}_2)$$

$$p^r_{10N+m+5,\,10N+m+4} = -\frac{l s_3 \bar{v}_3}{2 f_0}$$

$$p^r_{10N+m+5,\,12N+m+5} = \frac{l s_3 \bar{v}_3}{2 f_0}$$

$$p^r_{12N+m+6,\,12N+m+5} = \frac{l f_0 \bar{v}_4}{2 \Delta p\, B_c}$$

The elements r_j of $\underset{\sim}{R}$ are defined as follows. Let $n = m - (N + 1)$ and m varies from 1 to $(2N + 1)$. Then

$$r_{m,n} = \psi_n^{(1)}$$

$$r_{2N+m+1} = \psi_n^{(3)}$$

$$r_{4N+m+2} = \chi_n^{(1)}$$

$$r_{6N+m+3} = \chi_n^{(3)}$$

$$r_{8N+m+4} = \phi_n^{(0)}$$

$$r_{10N+m+5} = \phi_n^{(2)}$$

$$r_{12N+m+6} = \phi_n^{(4)}$$

The eigenvalue equation (6.29) is solved by standard numerical algorithms. The imaginary parts of these eigenvalues give the growth rates and the real parts give the frequencies of the disturbances. The amplitudes of disturbances corresponding to different harmonics are obtained from the eigenfunctions.

We have conducted the stability analysis for a typical value of the Rossby wave amplitude $\overline{v}_3 = 10 \text{ m s}^{-1}$. The corresponding amplitude in the upper troposphere $\overline{v}_1$ is calculated from (4.12). We also need the meridional winds at levels 2 and 4. $\overline{v}_2$ is calculated by numerical interpolation using the values of $\overline{v}_1$ and $\overline{v}_3$ whereas $\overline{v}_4$ is assumed to be equal to $\overline{v}_3$. The latter assumption is made with a view to neglect the effect of friction at the boundary layer. Similarly the zonal wind at level 4 is made equal to that at level 3 i.e. $U_4 = U_3$. Also U_2 is interpolated from the values of U_1 and U_3, which are the same realistic winds used in the quasi-geostrophic model in Chapter 4.

With the above values of zonal and meridional winds at different levels the characteristics of perturbations are obtained for different values of meridional perturbation wave number 'l'. As described in the previous chapter, to satisfy cyclic boundary conditions both in

x and y directions we write $l = \frac{J}{12} k_0$ and vary J from 1 to 12 by steps of one.

6.4 Results:

Unlike in the quasi-geostrophic model we get two distinct types of growing modes in the primitive equation model. The characteristics of growing modes are reported in Table 20. There are growing modes with frequencies much less than the coriolis parameter which are Rossby modes. In addition to these modes we also find inertia-gravity modes whose frequencies are either comparable to the corioles parameter or greater. The classification of these separate growing modes will be further justified later on.

The Rossby modes grow with almost the same doubling time as in the case of quasi-geostrophic model. These growing modes are almost stationary and the fastest mode corresponds to $l \leq k_0/2$ with doubling time of 3.1 days (Fig. 26). Comparing the characteristics of these Rossby modes with those of the quasi-geostrophic model we do not find marked difference. Amplitudes of stream functions $|\psi|$ for different harmonics shown in Figs. 28 and 29 (note the log scale) indicate that these Rossby modes

Table 20

Characteristics of growing modes in primitive equation model for $\bar{v}_3 = 10$ m s^{-1} (Meridional scale length of perturbation is $\frac{12}{J}$ times wavelength of the stationary Rossby wave)

$J = \frac{12l}{k_o}$	Rossby modes		Inertia-gravity modes	
	$\lvert\lambda_r\rvert$ (s^{-1})	τ_d (days)	$\lvert\lambda_r\rvert$ (s^{-1})	τ_d (days)
1	1.1×10^{-6}	31.3	4.8×10^{-5}	0.1
2	6.9×10^{-7}	7.5	4.6×10^{-5}	0.1
3	6.5×10^{-7}	6.2	1.4×10^{-4}	0.6
4	9.8×10^{-7}	4.6	1.9×10^{-4}	1.0
5	1.2×10^{-6}	3.6	2.4×10^{-4}	1.6
6	1.3×10^{-6}	3.1	2.9×10^{-4}	2.3
7	1.4×10^{-6}	3.1	3.7×10^{-4}	3.2
8	1.5×10^{-6}	3.7	3.8×10^{-4}	4.1
9	2.0×10^{-6}	5.9	4.3×10^{-4}	5.2
10	3.1×10^{-6}	12.3	4.8×10^{-4}	6.5
11	6.4×10^{-6}	16.0	5.2×10^{-4}	7.8
12	5.4×10^{-6}	51.3	5.7×10^{-4}	9.3

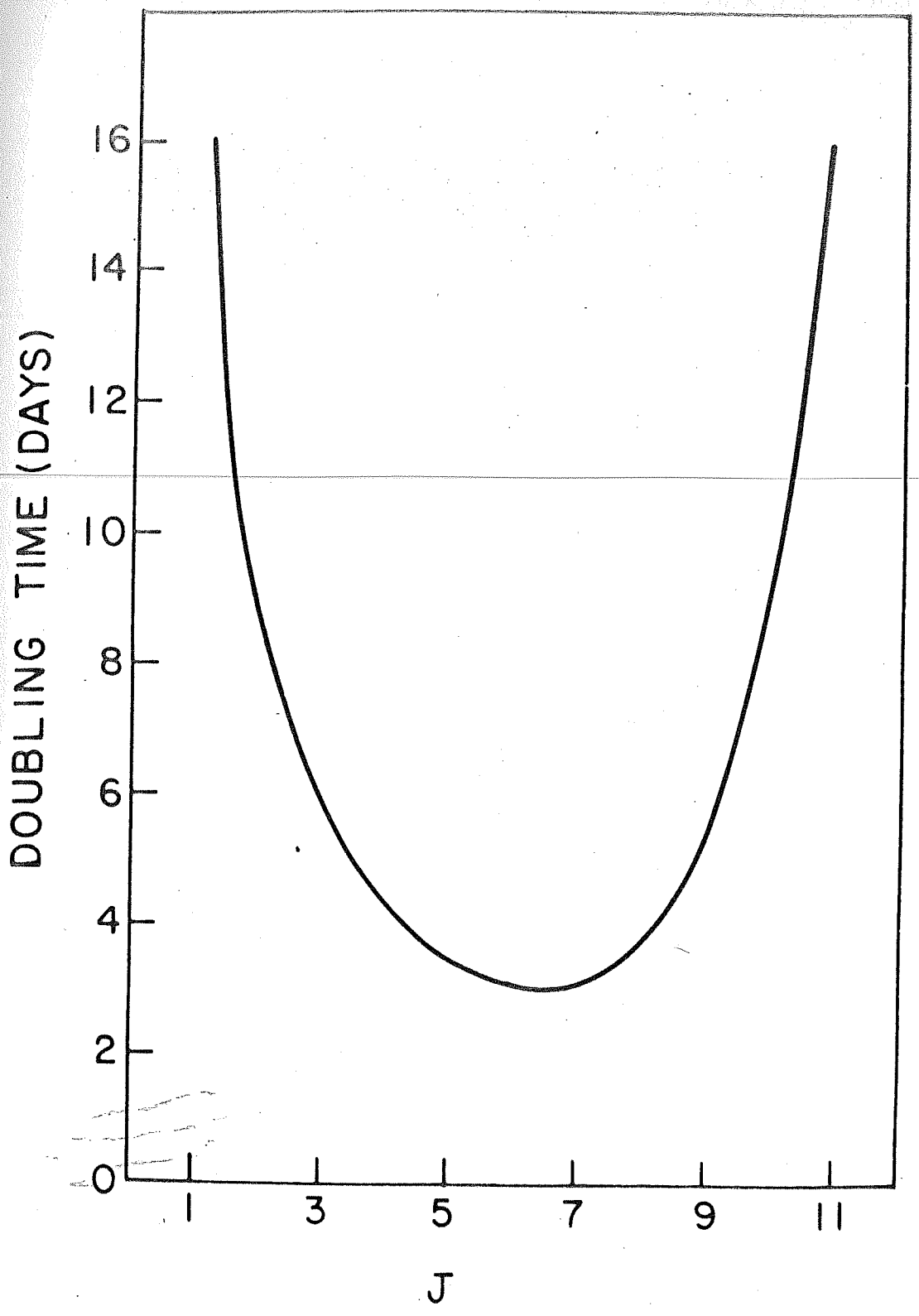

Figure 26: Meridional wavenumber ($l = Jk_0/12$) dependence of the growth of Rossby modes in primitive-equation model for $\overline{v}_3 = 10$ (m s^{-1}).

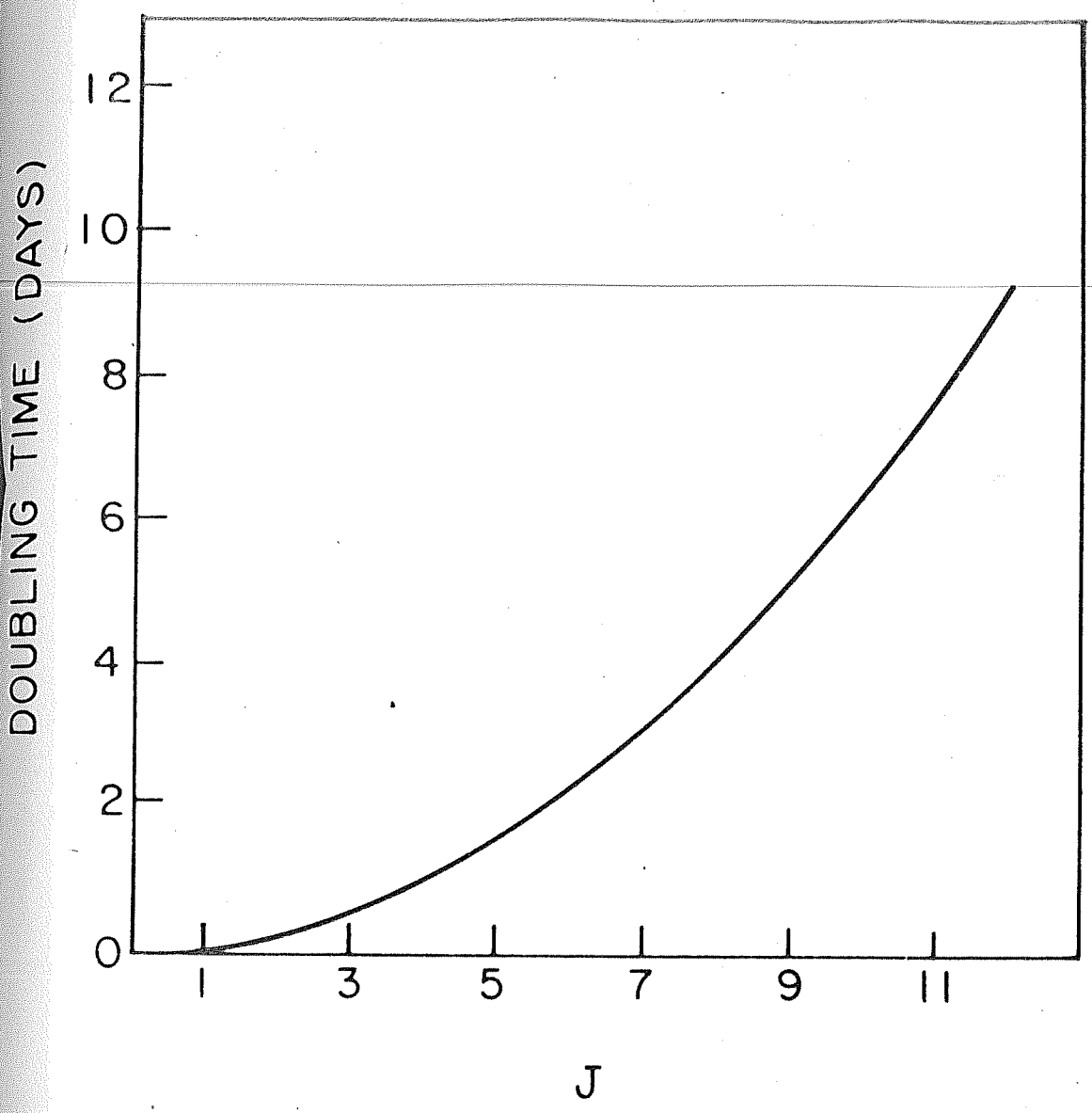

Figure 27: Meridional wavenumber ($l = J k_0 / 12$) dependence of the growth of inertia-gravity modes in primitive-equation model for $\overline{v}_3 = 10$ (m s^{-1}).

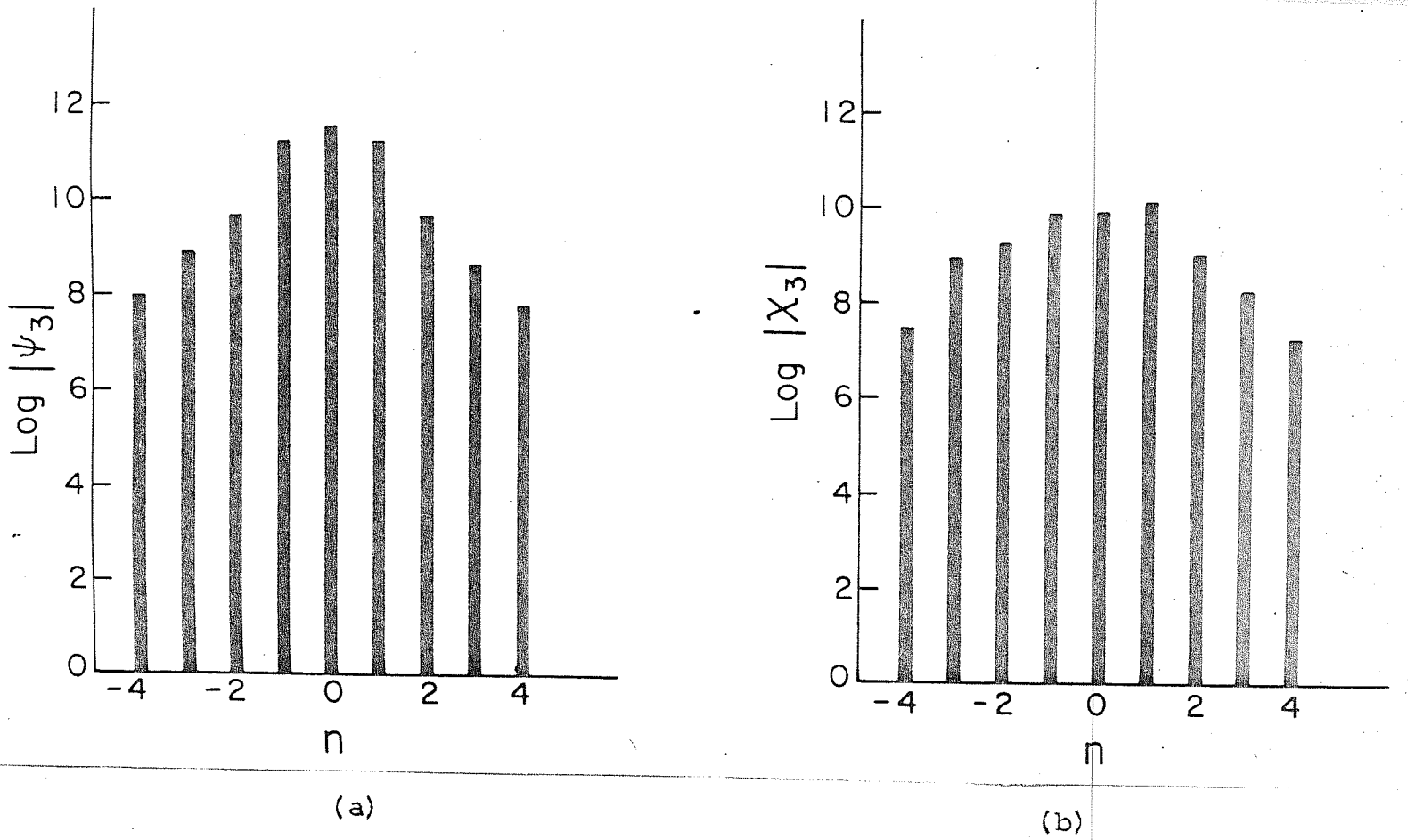

Figure 28: Fourier components of lower tropospheric perturbation stream function (a) and velocity potential (b) of the fastest growing Rossby mode in Fig. 26.

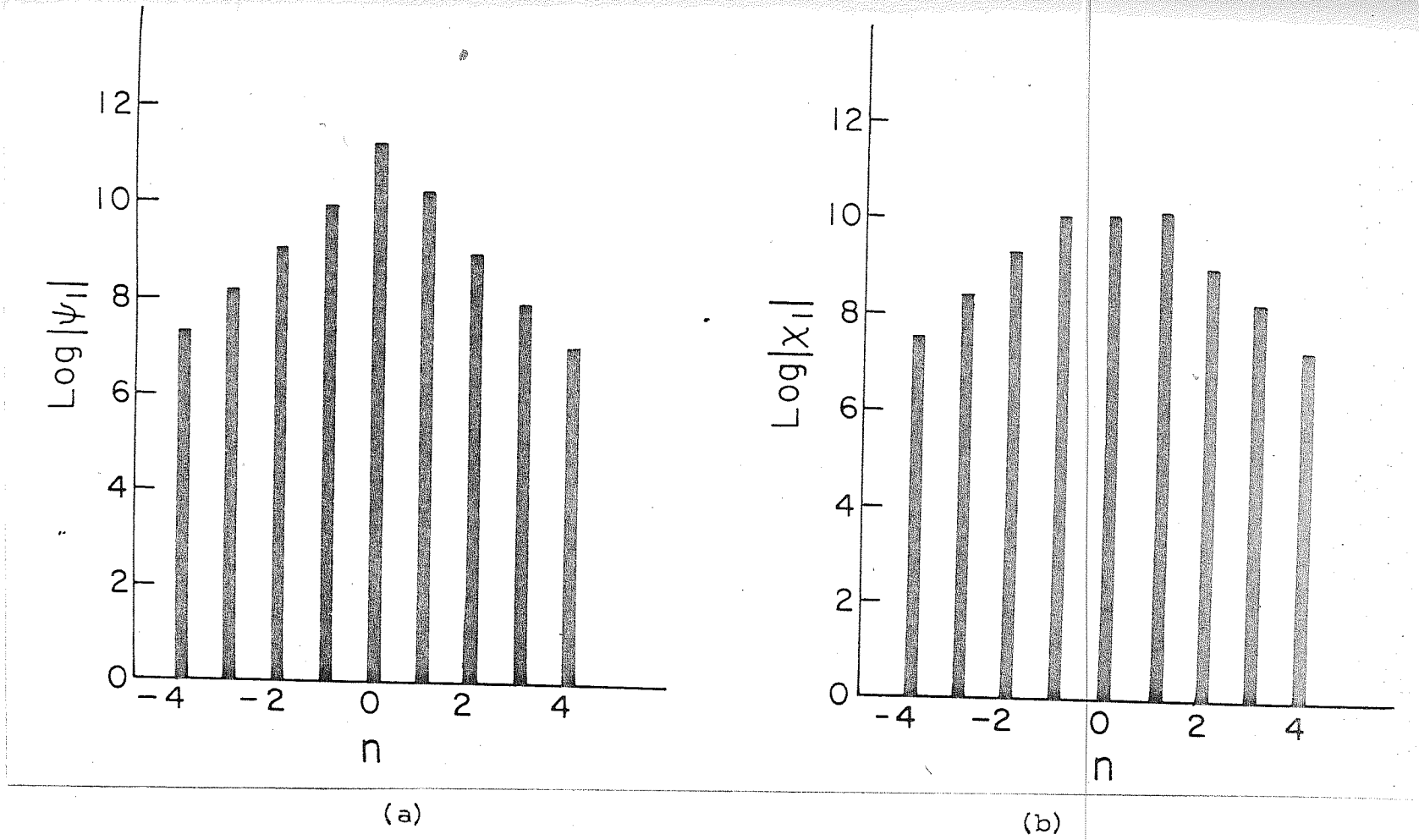

Figure 29: Fourier components of upper tropospheric perturbation stream function (a) and velocity potential (b) of the fastest growing Rossby mode in Fig. 26.

have greater magnitude in the lower troposphere than in the upper troposphere.

The inertia-gravity modes also grow (Table 20), but there is no preferred scale for maximum growth rate. The growth rate increases with the meridional scale ... length of the disturbance (Fig. 27). Figures 30 and 31 (note the log scale) show that the magnitudes of velocity potentials $|\chi|$ in the lower troposphere is also greater than that at the upper troposphere.

Looking at Figs. 32 and 33, the identification of Rossby and inertia-gravity modes are further justified. In Fig. 32 the stream function $|\psi|$ is larger than the velocity potential $|\chi|$. This shows that the contribution due to divergence is less and these are Rossby modes. Similarly from Fig. 33 it is clear that the divergence component is greater than the rotational component and these are inertia-gravity modes.

Both in Rossby and inertia-gravity modes the Fourier components of stream functions and velocity potentials decrease very fast with the order of harmonics (Figs. 28 to 31). The magnitudes are mainly confined to the first few lower order harmonics. Thus the truncation of the series (6.21) at $N = 4$ seems reasonable.

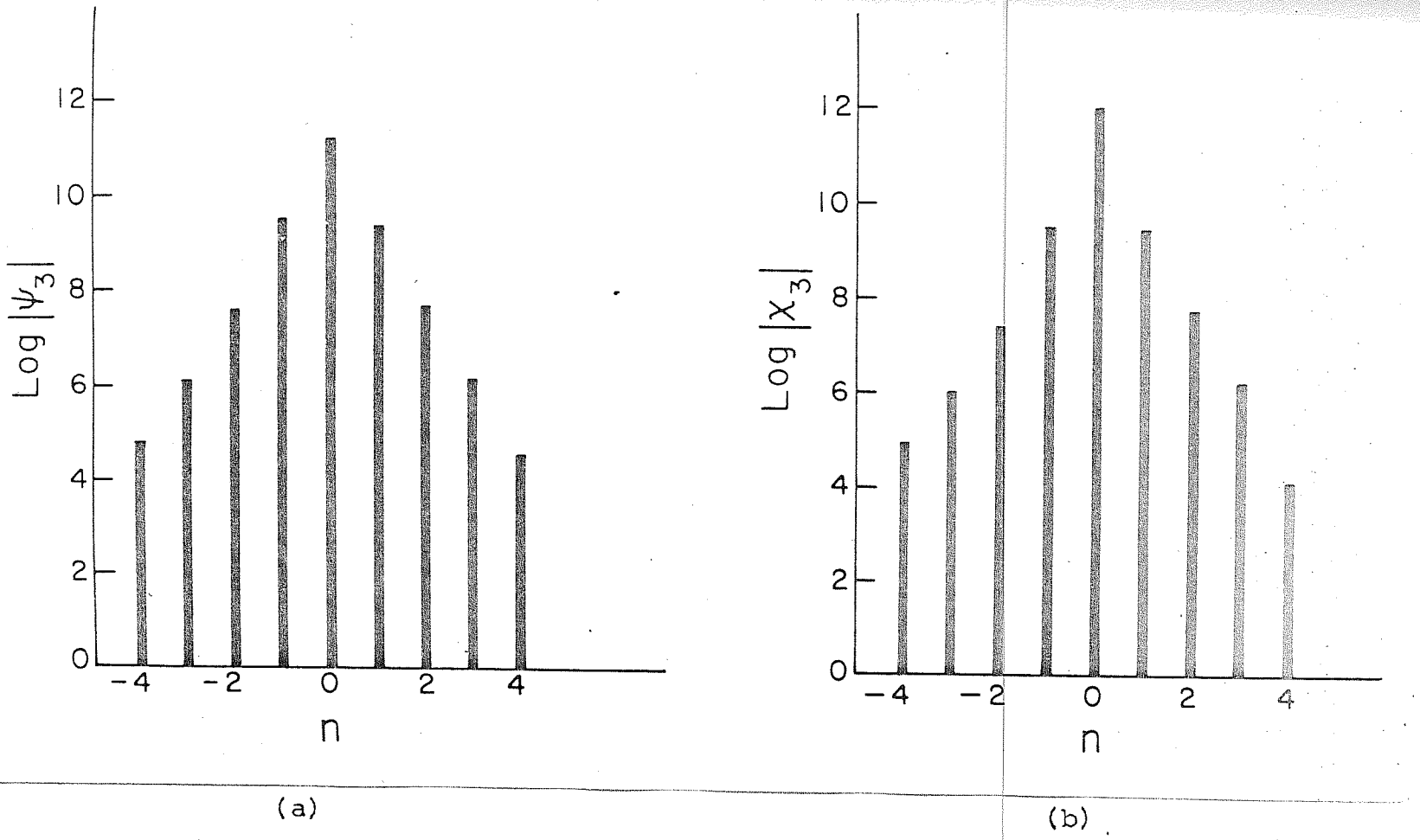

Figure 30: Fourier components of lower tropospheric perturbation stream function (a) and velocity potential (b) of inertia-gravity mode for $l = R_0/2$ (m^{-1}) in Fig. 27.

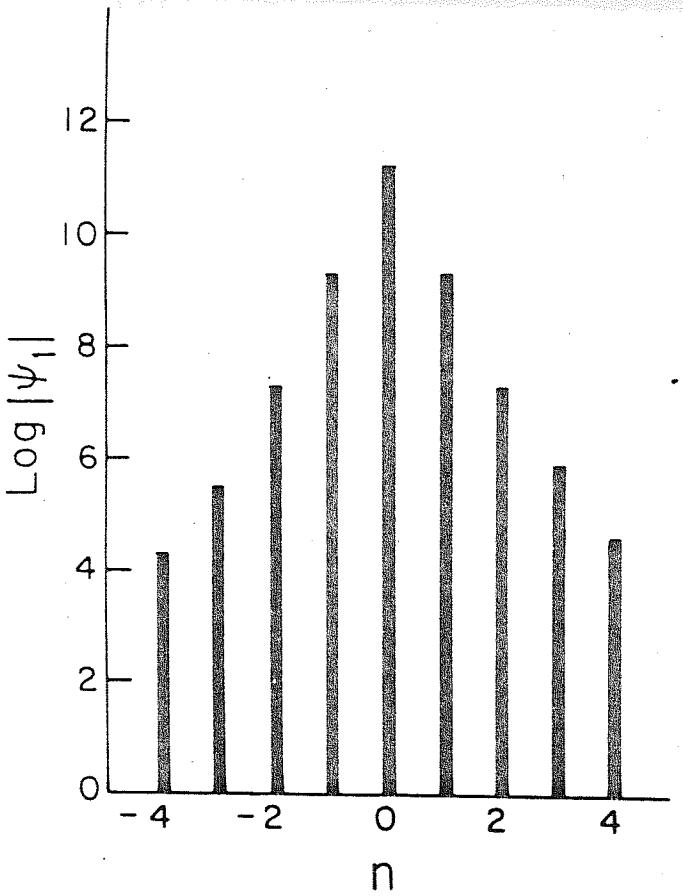

(a)

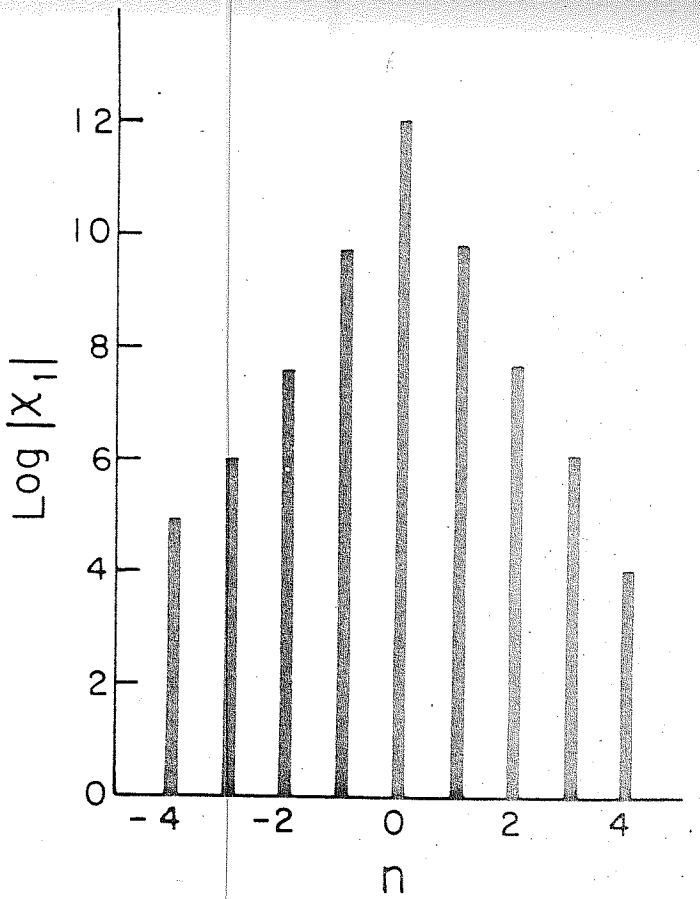

(b)

Figure 31: Fourier components of upper tropospheric perturbation stream function (a) and velocity potential (b) of inertia-gravity mode for $l = k_0/2$ (m^{-1}) in Fig.27

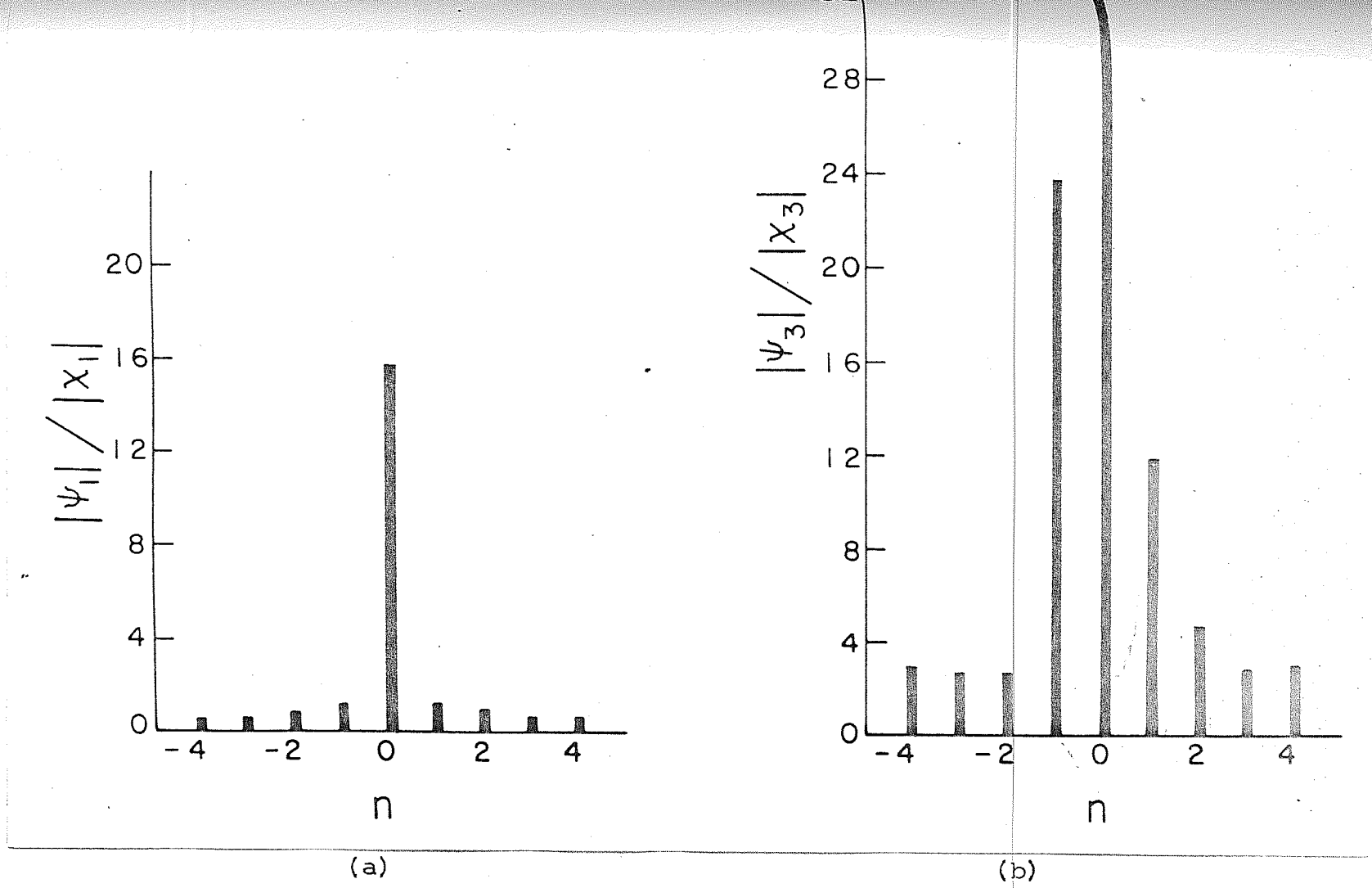

Figure 32: Ratios of Fourier components of perturbation stream function and velocity potential at upper (a) and lower (b) troposphere of the fastest growing Rossby mode in Fig. 26.

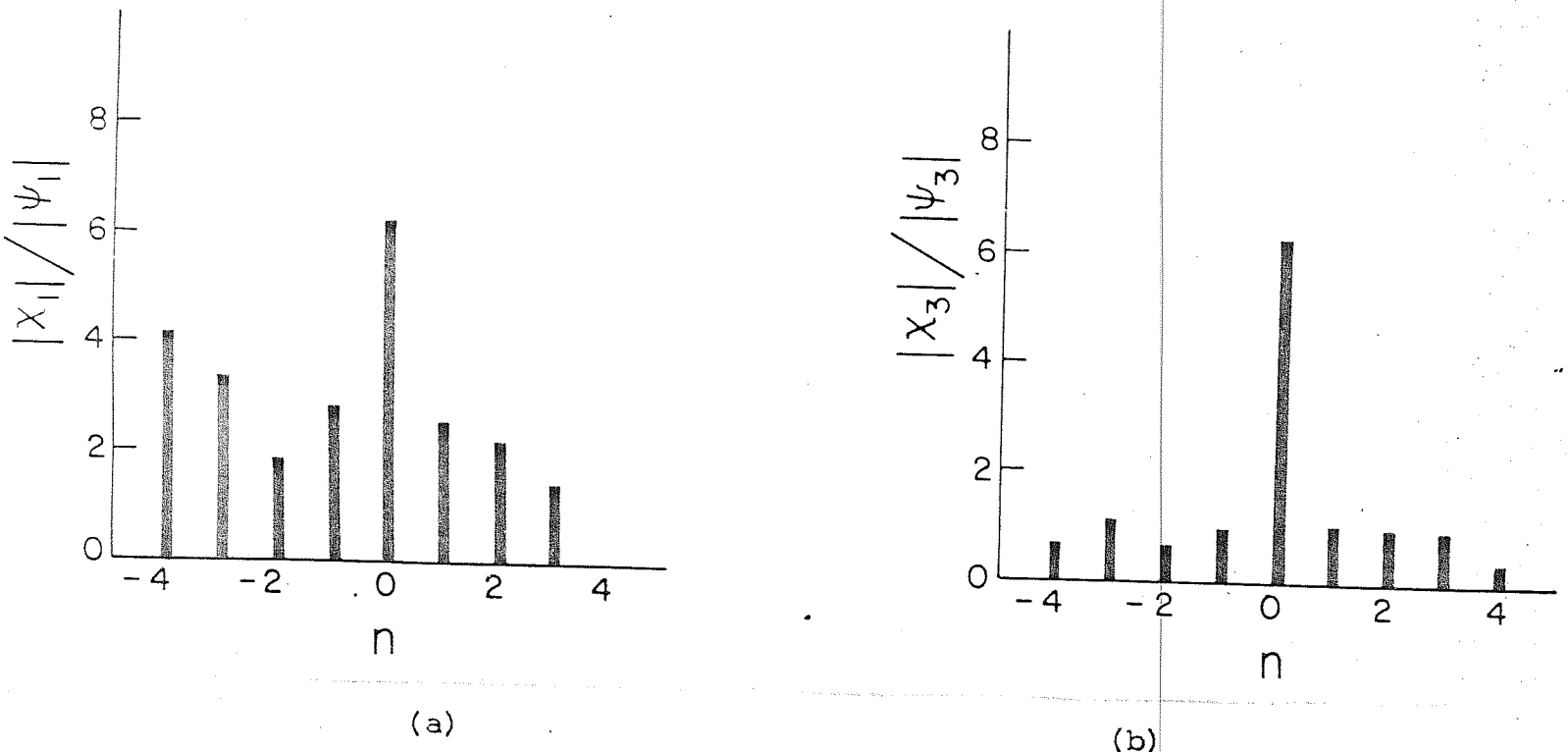

(a) (b)

Figure 33: Ratios of Fourier components of perturbation velocity potential and stream function at upper (a) and lower (b) troposphere of inertia-gravity mode for $l = k_0/2$ (m^{-1}) in Fig. 27.

6.5 Summary and conclusions:

In this chapter we have studied the stability of a stationary Rossby wave superposed on the monsoon zonal flow using a primitive equation model. The stationary Rossby wave used is the same as used in the quasi-geostrophic model. It has a wavelength of 30° longitude and its amplitude in the lower troposphere is much larger than that at the upper troposphere.

As in quasi-geostrophic model, in primitive equation model also the stationary Rossby wave is unstable to perturbations. But unlike in the former model here two different types of growing modes are identified. The classification is done by considering the frequency and the relative magnitudes of stream functions and velocity potentials.

Growing modes with frequencies less than the corilis parameter are Rossby modes. These have stream functions with greater magnitudes than the velocity potentials. The characteristics of these Rossby modes are almost the same as those found in the quasi-geostrophic model. The maximum growth rate occurs for the meridional wavenumber $l \leq k_0/2$. It has maximum amplitude in the lower troposphere.

There are growing modes whose frequencies are either comparable to or greater than the coriolis

parameter. These modes have velocity potentials greater than the magnitudes of stream functions. Thus the divergence components are more dominant than the rotational components and these are inertia-gravity modes. It is found that there is no preferred scale for the maximum growth. The growth rate increases with the meridional scale length of the disturbance.

The finding that inertia-gravity modes can grow by drawing on the energy of a basic Rossby wave superposed on a zonal shear flow is of intriguing significance for numerical weather prediction where we generally try to eliminate gravity waves.

CHAPTER SEVEN

STABILITY OF A STATIONARY ROSSBY WAVE EMBEDDED IN THE MONSOON ZONAL FLOW: WITH A GENERAL PERTURBATION WAVE NUMBER

In Chapters 4,5 and 6 the zonal wave number of the perturbation fields were taken to be multiples of zonal wavenumber of the basic Rossby wave by assuming $k = 0$ in (4.13). In this chapter we intend to take a more general perturbation zonal wavenumber by allowing nonzero values of k. The stability analysis using a two-level primitive equation model in Chapter 6 does not give any additional information regarding the Rossby modes.

The characteristics of growing Rossby modes obtained from the quasi-geostrophic model in Chapter 4 are not changed considerably when we extend the study to primitive equation model. Hence in this chapter we will consider a two-level quasi-geostrophic model with a beta-plane centred at 18°N. The basic zonal flow and the stationary Rossby wave are the same as used in Chapter 4. The stationary Rossby wave has a wavelength of 30° longitude and its amplitude is predominantly large in the lower troposphere.

7.1 Conditions for resonant interaction:

Before conducting the stability analysis we will mention about the conditions for resonant interaction. It is known that the basic wave and perturbation can be regarded as weakly interacting waves and perturbation can grow when the condition for resonant interaction is satisfied or nearly satisfied. Essentially two waves combine to force a third wave to form a 'triad' for resonance. Longuet-Higgins and Gill (1967) have shown that all wave vectors can participate in a resonant triad with a family of wave vectors. In this case there is nonlinear coupling and strong energy transfer between the

waves. However, two waves of either the same wavelength or parallel wave vectors will not resonate as in that case the interaction co-efficient vanishes. In order for resonance to occur the triad must satisfy the condition

$$\theta_j + \theta_m + \theta_n = 0 \qquad (7.1)$$

where the m^{th} and n^{th} waves combine to produce a phase, $(\theta_m + \theta_n)$ which is equal to the phase angle of a third free mode θ_j. If $\theta_i = k_i x + l_i y + \lambda_i t$, then the resonance conditions can be given by

$$\begin{aligned} k_j + k_m + k_n &= 0 \\ l_j + l_m + l_n &= 0 \qquad (7.2) \\ \lambda_j(k_j, l_j) + \lambda_m(k_m, l_m) + \lambda_n(k_n, l_n) &= 0 \end{aligned}$$

We are considering the basic Rossby wave to be directed eastward i.e. $k_j \equiv k_o$ and $l_j = 0$. In Chapters 4,5 and 6 we had taken $k\,(\equiv k_m) = 0$. This implies that the basic Rossby wave and the perturbation wave vectors are parallel and hence there should not be any instability. However, for small 'l', this perturbation can be as close as desired to satisfying a resonance condition (Gill, 1974).

Under present circumstances it can be shown (Pedlosky, 1979) that the two wavevectors k_m and k_n lie on the locus at opposite ends of the line passing

through $k = -k_0/2$ and intersecting the locus. Hence we assume the zonal wavenumber of a perturbation to be equal to $(nk_0 + k)$ i.e. multiples of the basic wavenumber k_0 plus a constant wave number. 'k', which is constrained to satisfy a resonant condition is taken to be equal to $-k_0/2$.

7.2 Stability analysis:

The linearised potential vorticity equations at levels 1 and 3 are given by (4.9) and (4.10). The basic flow for the stability analysis is the same as in Chapter 4 given by (4.3). We assume solutions (4.13) for the perturbation geopotential fields. In previous three chapters we had limited the stability analysis to the case $k = 0$. But here we put $k = -k_0/2$. Using (4.11), (4.12) and (4.13) equations (4.9) and (4.10) can be simplified. Finally collecting the co-efficients of $\exp[i(nk_0x + kx + ly + \lambda t)]$ we get algebraic equations identical to (4.14) and (4.15), but here the parameters a_n and b_n are redefined as follows.

$$a_n \equiv nk_0 + k \quad \text{and} \quad b_n \equiv (nk_0 + k)^2 + l^2$$

Truncating the series (4.13) at n = N and rearranging the

the terms we get eigenvalue equation(4.16) as in Chapter 4. Here also we truncate the series (4.13) at N = 10.

For different values of $\bar{v}_3$ the corresponding values of $\bar{v}_1$ are calculated from (4.12). For each set of values of $\bar{v}_3$ and $\bar{v}_1$, doubling times, frequencies and amplitudes of disturbances are obtained by varying the meridional wavenumber of perturbation. As explained in Chapter 4, we write $l = \frac{J}{12} k_0$ and vary J from 1 to 12 by steps of one to satisfy cyclic boundary conditions both in x and y directions. The characteristics of growing modes are reported in Tables 21 to 24. It is seen that the frequencies of growing modes are smaller than the coriolis parameter and hence they are Rossby modes. For each value of $\bar{v}_3$ there is a meridional scale length of the disturbance for which the growth rate is maximum (Fig.34). In agreement with Gill (1974), and Duffy (1975) the most unstable mode has a growth rate less than that of the case $k = 0$. This is evident by comparing Figs.17 and 34. Also, disturbances do not grow unless $\bar{v}_3 = 15$ m s^{-1}, as compared to $\bar{v}_3 = 9$ m s^{-1} when $k = 0$.

The growing modes are almost stationary (Tables 21 to 24). But for each growing mode there are two frequencies.

The eigenfunctions corresponding to different

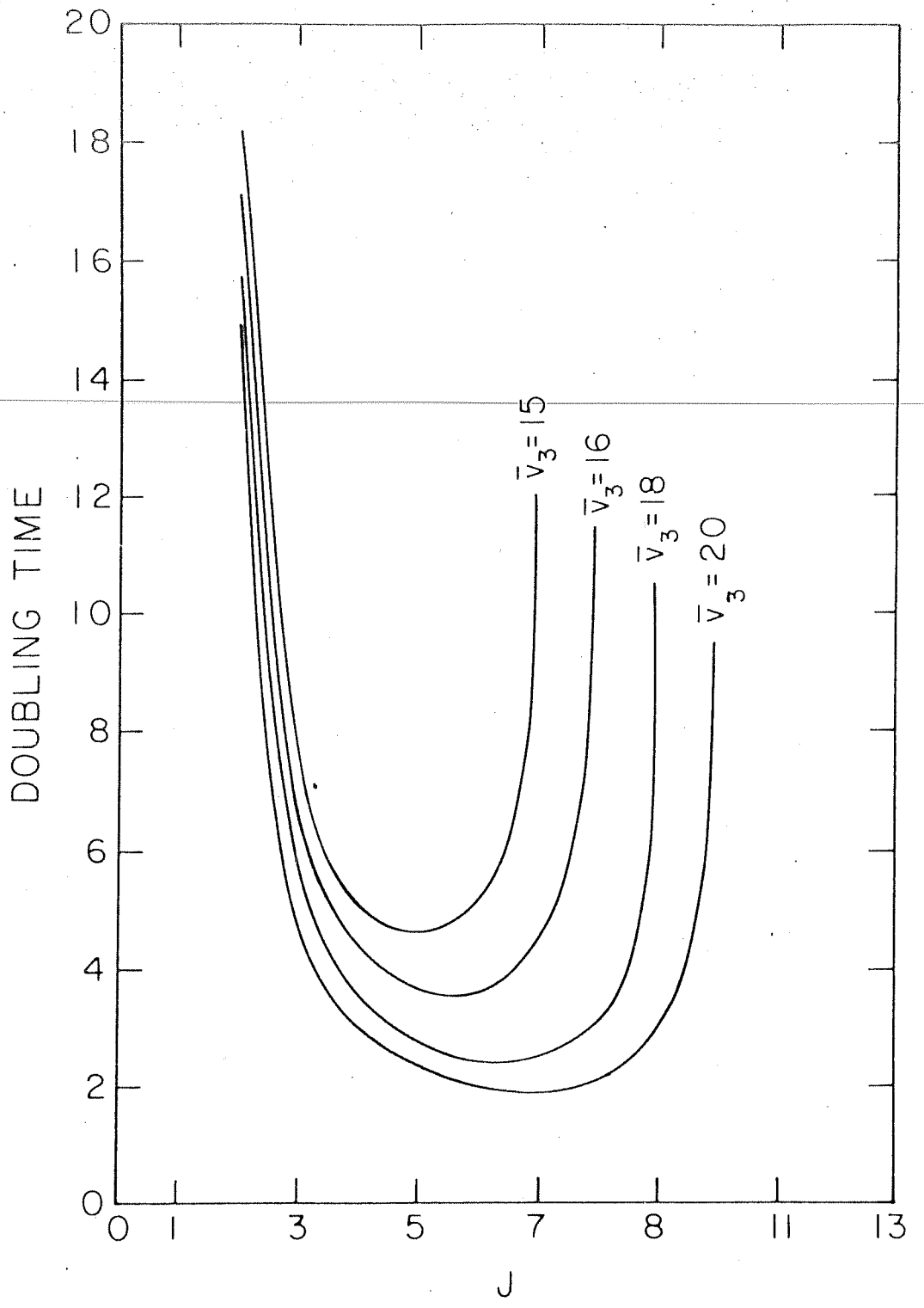

Figure 34: Meridional wavenumber ($l = J k_0/12$) dependence of the growth of Rossby modes in quasi-geostrophic model when $k = -k_0/2$.

Table 21

Characteristics of growing modes in quasi-geostrophic model for $k = -k_0/2$ and $\bar{v}_3 = 15$ m s^{-1} (Meridional scale length of perturbation is $\frac{12}{J}$ times wavelength of the stationary Rossby wave).

$J = \frac{12L}{k_0}$	Frequency λ_r (s^{-1})	Doubling time τ_d (days)
1	-1.4×10^{-5}	6.8×10^{15}
2	$\pm 1.3 \times 10^{-5}$	18.2
3	$\pm 1.3 \times 10^{-5}$	7.4
4	$\pm 1.2 \times 10^{-5}$	5.2
5	$\pm 1.1 \times 10^{-5}$	4.6
6	$\pm 9.4 \times 10^{-6}$	5.2
7	7.8×10^{-6}	1.7×10^{13}

Table 22

Characteristics of growing modes in quasi-geostrophic model for $k = -k_o/2$ and $\bar{v}_3 = 16$ m s^{-1} ($L_y = \frac{12}{J} L_s$).

$J = \frac{12l}{k_o}$	Frequency λ_r (s^{-1})	Doubling time τ_d (days)
1	-1.4×10^{-5}	7.6×10^{15}
2	$\pm 1.3 \times 10^{-5}$	17.1
3	$\pm 1.3 \times 10^{-5}$	6.6
4	$\pm 1.2 \times 10^{-5}$	4.4
5	$\pm 1.1 \times 10^{-5}$	3.7
6	$\pm 9.4 \times 10^{-6}$	3.6
7	$\pm 8.2 \times 10^{-6}$	4.5
8	6.1×10^{-6}	6.2×10^{14}

Table 23

Characteristics of growing modes in quasi-geostrophic model for $k = -k_0/2$ and $\overline{\vartheta}_3 = 18$ m s^{-1} ($L_y = \frac{12}{J} L_s$).

$J = \frac{12\,l}{k_0}$	Frequency λ_r (s^{-1})	Doubling time τ_d (days)
1	-1.4×10^{-5}	1.3×10^{16}
2	$\pm 1.3 \times 10^{-5}$	15.7
3	$\pm 1.3 \times 10^{-5}$	5.5
4	$\pm 1.2 \times 10^{-5}$	3.5
5	$\pm 1.1 \times 10^{-5}$	2.7
6	$\pm 9.4 \times 10^{-6}$	2.5
7	$\pm 8.1 \times 10^{-6}$	2.5
8	$\pm 6.9 \times 10^{-6}$	3.1
9	5.7×10^{-6}	31.0
10	7.9×10^{-6}	2.2×10^{16}

Table 24

Characteristics of growing modes in quasi-geostrophic model for $k = -k_0/2$ and $\bar{\vartheta}_3 = 20$ m s^{-1} ($L_y = \frac{12}{J} L_s$).

$J = \frac{12 l}{k_0}$	Frequency λ_r (s^{-1})	Doubling time τ_d (days)
1	-1.4×10^{-5}	5.7×10^{16}
2	$\pm 1.3 \times 10^{-5}$	14.9
3	$\pm 1.3 \times 10^{-5}$	4.8
4	$\pm 1.2 \times 10^{-5}$	3.0
5	$\pm 1.1 \times 10^{-5}$	2.3
6	$\pm 9.3 \times 10^{-6}$	2.0
7	$\pm 7.9 \times 10^{-6}$	1.9
8	$\pm 6.6 \times 10^{-6}$	2.1
9	$\pm 5.3 \times 10^{-6}$	3.0
10	-2.2×10^{-6}	2.8×10^{16}

harmonics are shown in Figures 35 and 36. Comparing these two figures it is evident that the disturbances are mainly confined to the lower troposphere. Also the amplitude has considerable magnitude for the first few lower harmonics only. Thus it is reasonable to truncate the series (4.13) at N = 10.

7.3 Energy conversions:

The rates of conversion from kinetic energy of the basic wave, available potential energies of the basic wave and zonal flow are same as given by (4.28), (4.29) and (4.30) respectively. However, here the perturbation fields are redefined as

$$\phi_1' = \sum_{n=-\infty}^{\infty} \left\{ \phi_n^{(1)} e^{i(nk_0x+kx+ly+\lambda t)} + \tilde{\phi}_n^{(1)} e^{-i(nk_0+kx+ly+\tilde{\lambda}t)} \right\}$$

$$\phi_3' = \sum_{n=-\infty}^{\infty} \left\{ \phi_n^{(3)} e^{i(nk_0x+kx+ly+\lambda t)} + \tilde{\phi}_n^{(3)} e^{-i(nk_0x+kx+ly+\tilde{\lambda}t)} \right\} \qquad (7.3)$$

where $k = -k_0/2$.

Hence the rates of conversion from different energies

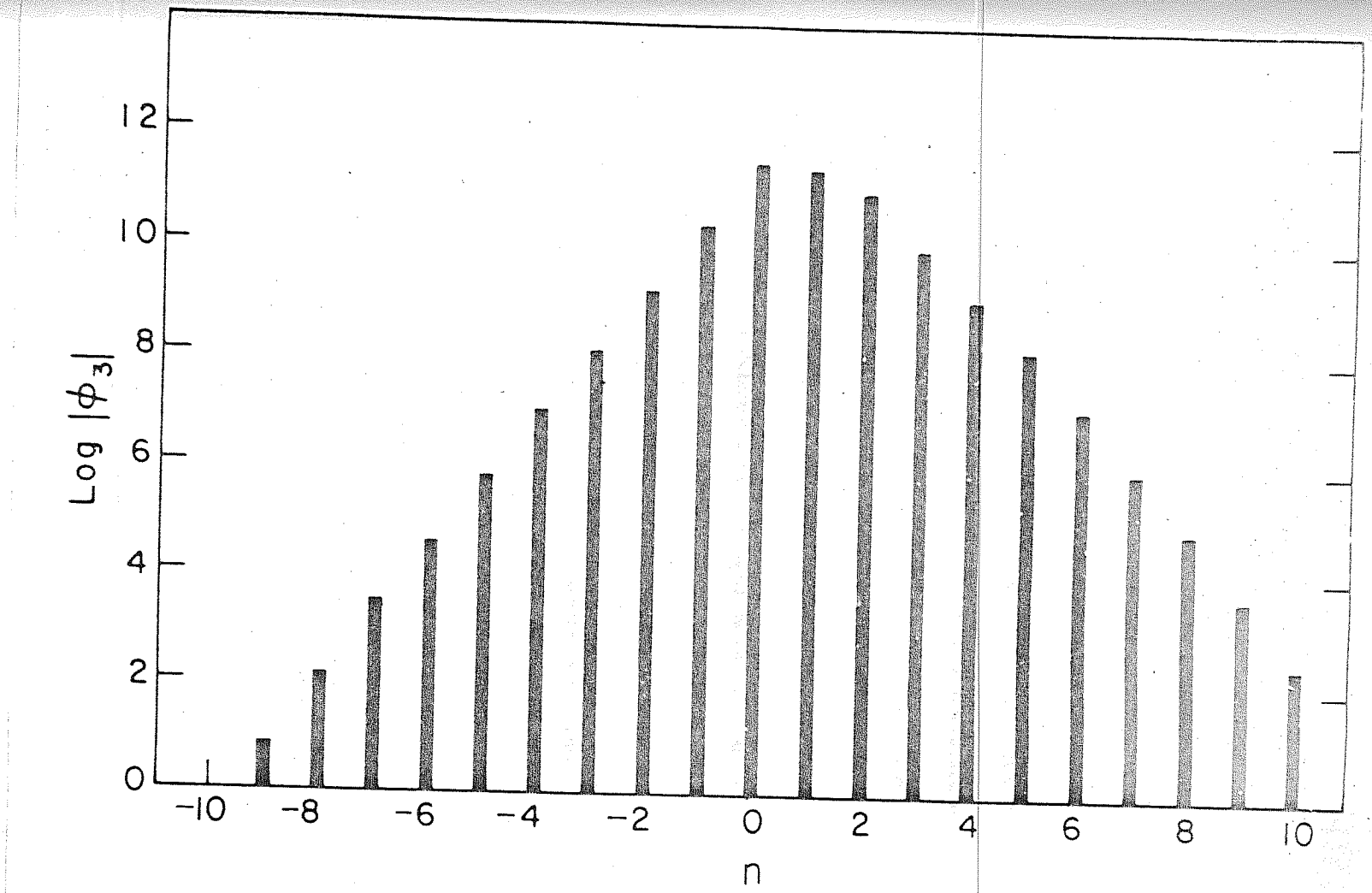

Figure 35: Fourier components of lower tropospheric geopotential perturbation of the fastest growing Rossby mode in Fig. 34.

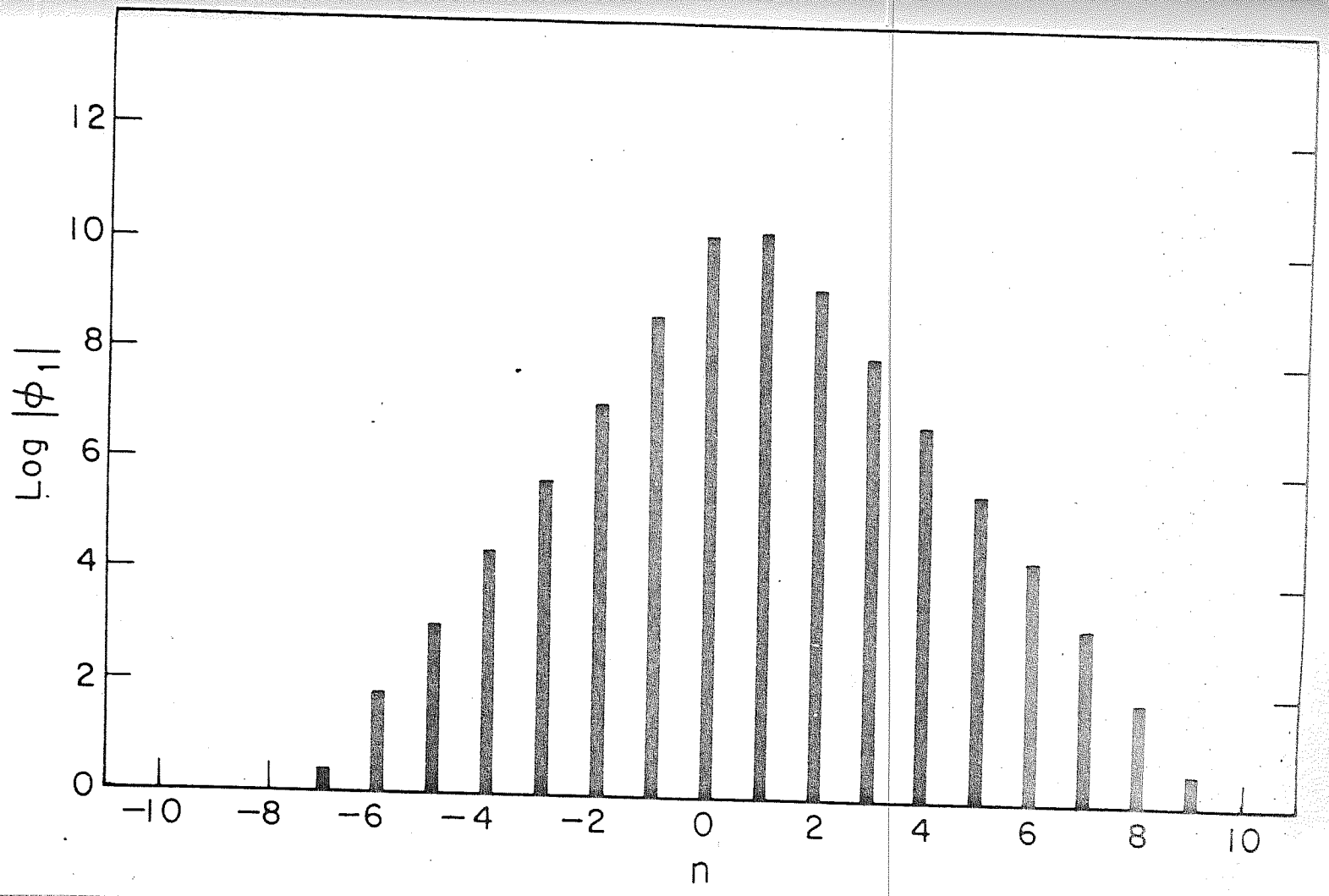

Figure 36: Fourier components of upper tropospheric geopotential perturbation of the fastest growing Rossby mode in Fig. 34.

may be different from those obtained in Chapter 4 where $k = 0$.

7.3.1 Conversion from kinetic energy of the basic wave:

From (4.32) we can calculate the rate of conversion from kinetic energy of the basic wave to perturbation kinetic energy. We have

$$C(K_w, K') = i \frac{k_0 \Delta p}{2 g f_0^2} \iint \left\{ \bar{v}_1 \frac{\partial \phi_1'}{\partial y} \frac{\partial \phi_1'}{\partial x} + \bar{v}_3 \frac{\partial \phi_3'}{\partial y} \frac{\partial \phi_3'}{\partial x} \right\} (e^{i k_0 x} - e^{-i k_0 x}) \, dx \, dy \tag{7.4}$$

Let us consider the first integral on the right hand side of (7.4). Using (7.3) we can write

$$\iint \frac{\partial \phi_1'}{\partial y} \frac{\partial \phi_1'}{\partial x} (e^{i k_0 x} - e^{-i k_0 x}) \, dx \, dy$$

$$= -l \iint \sum_n' \left\{ \phi_n^{(1)} e^{i(n k_0 x + k x + l y + \lambda t)} - \tilde{\phi}_n^{(1)} e^{-i(n k_0 x + k x + l y + \tilde{\lambda} t)} \right\} \sum_m' (m k_0 + k)$$

$$\times \left\{ \phi_m^{(1)} e^{i(m k_0 x + k x + l y + \lambda t)} - \tilde{\phi}_m^{(1)} e^{-i(m k_0 x + k x + l y + \tilde{\lambda} t)} \right\}$$

$$\times (e^{i k_0 x} - e^{-i k_0 x}) \, dx \, dy$$

Integrating over y we get

$$\iint \frac{\partial \phi_1'}{\partial y} \frac{\partial \phi_1'}{\partial x} \left(e^{ik_0x} - e^{-ik_0x}\right) dx\, dy$$

$$= 2\pi e^{-2\lambda_i t} \int_0^{2\pi/k_0} \sum_{n,m}' (mk_0 + k) \left[\Phi_n^{(1)} \tilde{\Phi}_m^{(1)} \left\{e^{i(n-m+1)k_0x} - e^{i(n-m-1)k_0x}\right\} + \tilde{\Phi}_n^{(1)} \Phi_m^{(1)} \left\{e^{i(m-n+1)k_0x} - e^{i(m-n-1)k_0x}\right\}\right] dx$$

While integrating over x, terms with $m = n + 1$ from the first series, with $m = n - 1$ from the second, with $m = n - 1$ from the third and terms with $m = n + 1$ from the last series contribute. Other terms vanish.

Hence

$$\iint \frac{\partial \phi_1'}{\partial y} \frac{\partial \phi_1'}{\partial x} \left(e^{ik_0x} - e^{-ik_0x}\right) dx\,dy$$

$$= \frac{4\pi^2}{k_0} e^{-2\lambda_i t} \sum_{n=-\infty}^{\infty}{}' \Big[\{k+(n+1)k_0\}\left(\phi_n^{(1)} \tilde{\phi}_{n+1}^{(1)} - \tilde{\phi}_n^{(1)} \phi_{n+1}^{(1)}\right) - \{k+(n-1)k_0\}\left(\phi_n^{(1)} \tilde{\phi}_{n-1}^{(1)} - \tilde{\phi}_n^{(1)} \phi_{n-1}^{(1)}\right)\Big]$$

Similarly the second integral on the right hand side of (7.4) can be evaluated.

$$\iint \frac{\partial \phi_3'}{\partial y} \frac{\partial \phi_3'}{\partial x} \left(e^{ik_0x} - e^{-ik_0x}\right) dx\,dy$$

$$= \frac{4\pi^2}{k_0} e^{-2\lambda_i t} \sum_{n=-\infty}^{\infty}{}' \Big[\{k+(n+1)k_0\}\left(\phi_n^{(3)} \tilde{\phi}_{n+1}^{(3)} - \tilde{\phi}_n^{(3)} \phi_{n+1}^{(3)}\right) - \{k+(n-1)k_0\}\left(\phi_n^{(3)} \tilde{\phi}_{n-1}^{(3)} - \tilde{\phi}_n^{(3)} \phi_{n-1}^{(3)}\right)\Big]$$

Expressing ϕ_n and $\tilde{\phi}_n$ in terms of ϕ_n^r and ϕ_n^i and substituting for the above integrals in (7.4) we get

$$C(K_w, K') = \frac{4\pi^2 \Delta p}{g f_o^2} e^{-2\lambda_i t} \sum_{n=-\infty}^{\infty}{}' \bar{v}_1 \Big[\{k+(n+1)k_o\} \times \left(\phi_n^{1r}\phi_{n+1}^{1i} - \phi_n^{1i}\phi_{n+1}^{1r}\right) - \{k+(n-1)k_o\}\left(\phi_n^{1r}\phi_{n-1}^{1i} - \phi_n^{1i}\phi_{n-1}^{1r}\right)\Big] + \sum_{n=-\infty}^{\infty}{}' \bar{v}_3 \Big[\{k+(n+1)k_o\}\left(\phi_n^{3r}\phi_{n+1}^{3i} - \phi_n^{3i}\phi_{n+1}^{3r}\right) - \{k+(n-1)k_o\}\left(\phi_n^{3r}\phi_{n-1}^{3i} - \phi_n^{3i}\phi_{n-1}^{3r}\right)\Big]$$

For $k = -k_o/2$

$$C(K_w, K') = \frac{4\pi^2 \Delta p\, k_o}{g f_o^2} e^{-2\lambda_i t} \times \sum_{n=-\infty}^{\infty}{}' \Big[\bar{v}_1 \Big\{ (n+\tfrac{1}{2})\left(\phi_n^{1r}\phi_{n+1}^{1i} - \phi_n^{1i}\phi_{n+1}^{1r}\right) - (n-\tfrac{3}{2})\left(\phi_n^{1r}\phi_{n-1}^{1i} - \phi_n^{1i}\phi_{n-1}^{1r}\right)\Big\} + \bar{v}_3 \Big\{ (n+\tfrac{1}{2})\left(\phi_n^{3r}\phi_{n+1}^{3i} - \phi_n^{3i}\phi_{n+1}^{3r}\right) - (n-\tfrac{3}{2})\left(\phi_n^{3r}\phi_{n-1}^{3i} - \phi_n^{3i}\phi_{n-1}^{3r}\right)\Big\}\Big] \quad (7.5)$$

7.3.2 Conversion from available potential energy of the basic wave:

Using (4.36) we can calculate the rate of conversion from available potential energy of the basic wave to perturbation available potential energy. We have

$$C(A_W, A') = \frac{k_0(\bar{v}_3 - \bar{v}_1)}{4\sigma g(\Delta\rho)^2} \iint \left(\frac{\partial \phi_3'}{\partial y} \phi_3' - \frac{\partial \phi_3'}{\partial y} \phi_1' + \frac{\partial \phi_1'}{\partial y} \phi_3' - \frac{\partial \phi_1'}{\partial y} \phi_1' \right) \left(e^{ik_0 x} + e^{-ik_0 x} \right) dx\, dy \tag{7.6}$$

As in Section 4.3.2 the integrals on the right hand side of (7.6) can be evaluated to get

$$C(A_W, A') = -\frac{2\pi^2 k_0 (\bar{v}_3 - \bar{v}_1)}{\sigma g k_0 (\Delta\rho)^2} e^{-2\lambda_i t} \times \sum_{n=-\infty}^{\infty} \left[(\phi_n^{1i} - \phi_n^{3i}) (\phi_{n+1}^{1r} + \phi_{n+1}^{3r} + \phi_{n-1}^{1r} + \phi_{n-1}^{3r}) - (\phi_n^{1r} - \phi_n^{3r}) (\phi_{n+1}^{1i} + \phi_{n+1}^{3i} + \phi_{n-1}^{1i} + \phi_{n-1}^{3i}) \right] \tag{7.7}$$

This is identical to (4.38).

7.3.3 Conversion from available potential energy of the zonal flow:

Using (4.39) the rate of change of available potential energy of zonal flow can be calculated. We have

$$C(A_z, A') = \frac{p_0 (U_3 - U_1)}{2\sigma g (\Delta p)^2} \iint \left(\frac{\partial \phi_3'}{\partial x} \phi_3' - \frac{\partial \phi_3'}{\partial x} \phi_1' + \frac{\partial \phi_1'}{\partial x} \phi_3' - \frac{\partial \phi_1'}{\partial x} \phi_1' \right) dx\, dy \tag{7.8}$$

Let us consider the second integral on the right hand side of (7.8). Substituting for ϕ_1' and ϕ_3' from (7.3) first we integrate over y. Then integrating over x, terms with m = n contribute.

Thus

$$-\iint \frac{\partial \phi_3'}{\partial x} \phi_1' \, dx\, dy$$

$$= -\frac{i 4\pi^2}{l k_0} e^{-2\lambda_i t} \sum_{n=-\infty}^{\infty}{}' (k + n k_0) \left(\phi_n^{(3)} \tilde{\phi}_n^{(1)} - \tilde{\phi}_n^{(3)} \phi_n^{(1)} \right)$$

For $k=-k_0/2$,

$$-\iint \frac{\partial \phi_3'}{\partial x}\phi_1' \, dx\,dy = -i\frac{4\pi^2}{l}e^{-2\lambda_i t}\sum_{n=-\infty}^{\infty}{}'(n-\tfrac{1}{2})\left(\phi_n^{(3)}\tilde{\phi}_n^{(1)} - \tilde{\phi}_n^{(3)}\phi_n^{(1)}\right).$$

Similarly

$$\iint \frac{\partial \phi_1'}{\partial x}\phi_3' \, dx\,dy = i\frac{4\pi^2}{l}e^{-2\lambda_i t}\sum_{n=-\infty}^{\infty}{}'(n-\tfrac{1}{2})\left(\phi_n^{(1)}\tilde{\phi}_n^{(3)} - \tilde{\phi}_n^{(1)}\phi_n^{(3)}\right).$$

It can be shown that first and last integrals on the right hand side of (7.8) vanish.

Hence

$$C(A_z, A') = \frac{8\pi^2 p_0 (U_3 - U_1)}{l\sigma g(\Delta p)^2} e^{-2\lambda_i t} \times \sum_{n=-\infty}^{\infty}{}'(n-\tfrac{1}{2})\left(\phi_n^{1r}\phi_n^{3i} - \phi_n^{1i}\phi_n^{3r}\right). \tag{7.9}$$

The rates of conversion from the kinetic energy and available potential energy of the basic wave and rate of change of available potential energy of the zonal

flow are calculated from (7.5), (7.7) and (7.9) respectively, for a typical case $\overline{v}_3 = 20$ m s^{-1}. The rate of conversion from kinetic energy of the basic wave to perturbation kinetic energy is the maximum as in Chapter 4 where $k = 0$. Following ratios give some idea about the magnitudes of different energy conversion rates.

$$\frac{C(K_W, K')}{C(A_Z, A')} = 2 \times 10^2$$

$$\frac{C(K_W, K')}{C(A_W, A')} = 7 \times 10^2$$

$$\frac{C(A_W, A')}{C(A_Z, A')} = 0.3$$

Comparing these results with those of the case $k = 0$ in Chapter 4, it is seen that the rate of change of available potential energy of the zonal flow is more in case of $k = -k_0/2$ than in the case $k = 0$.

7.4 Summary and Conclusions:

In this chapter the stability analysis is extended to the case where the perturbation has a zonal wavenumber equal to $(nk_0 + k)$ and $k = -k_0/2$ satisfying conditions for resonant interaction. In other words we have

studied the stability of a stationary Rossby wave of zonal wavenumber k_0 (corresponding to wavelength of 30° longitude) superposed on the monsoon zonal flow to a perturbation having a zonal wavenumber equal to the sum of the multiples of the basic wavenumber and a constant wavenumber i.e. nk_0+k where $k=-k_0/2$.

The stability analysis is conducted for different values of meridional velocity at lower and upper troposphere satisfying the relation $\bar{v}_3=22\bar{v}_1$. For each pair of values of $\bar{v}_3$ and $\bar{v}_1$ the meridional wavenumber of the perturbation is varied using the equality $l=\frac{J}{12}k_0$ and varying J from 1 to 12 by steps of one.

It is found that as in the previous case of $k = 0$, here for each value of Rossby amplitude there is a meridional wavenumber for which the growth rate of perturbation is maximum. It is also seen that the maximum shifts towards higher value of l. The maxima lie in the range

$$\frac{5}{12}k_0 < l < \frac{7}{12}k_0.$$

There is a threshold value of Rossby amplitude for which perturbations grow. Increasing $\bar{v}_3$ from 5 m s^{-1} to 20 m s^{-1} it is seen that perturbations do not grow unless $\bar{v}_3$ = 15 m s^{-1}. In comparison with k = 0 case, it is found that the minimum value of $\bar{v}_3$ for the growth of perturbations is more in case of $k=-k_0/2$.

The magnitudes of disturbances are more in the lower troposphere than in the upper troposphere.

For the same value of Rossby wave amplitude the growth rate is found to decrease because of the introduction of nonzero value of k. Thus the fastest growth rate occurs for $k = 0$ case. This is in confirmity with the results of Gill (1974) and Duffy (1975).

Energy calculations show that the perturbations grow mainly by drawing on kinetic energy of the basic wave.

REFERENCES

Brode, R.W. and Mak, M.K., 1978: On the mechanisms of the monsoonal mid-tropospheric cyclone formation. J. Atmos. Sci., 35, 1473-1484.

Charney, J.G., 1947: The dynamics of long waves in a baroclinic westerly current. J. Meteor., 4, 135-162.

Charney, J.G., and Eliassen, A., 1949: A numerical method for predicting the perturbations of the middle latitude westerlies. Tellus, 1, 38-54.

Charney, J.G. and Eliassen, A., 1964: On the growth of the Hurricane depression. J. Atmos. Sci., 21, 68-75.

Charney, J.G. and Stern, M.E., 1962: On the stability of internal baroclinic jets in a rotating atmosphere. J. Atmos. Sci., 19, 159-172.

Desai, B.N. and Koteswaram, P., 1951: Air masses and fronts in the monsoon depressions in India. Ind. J. Met. Geophys., 2, 250-265.

Duffy, D.G., 1975: The barotropic instability of Rossby wave motion: A re-examination. J. Atmos. Sci., 32, 1271-1277.

Eady, E.T., 1949: Long waves and cyclone waves. Tellus, Vol.1, No.2, 33-52.

Gadgil, S., 1977: Orographic effects on the Southwest monsoon: A review. Pure Appl. Geophys., 115, 1413-1430.

Gill, A.E., 1974: The stability of planetary waves on an infinite beta-plane. Geophys. Fluid Dyn. 6, 29-47.

Godbole, R.V., 1977: The composite structure of the monsoon depression. Tellus, 29, 25-40.

Goswami, B.N., Keshavamurty, R.N. and Satyan, V., 1980: Role of barotropic, baroclinic and combined barotropic-baroclinic instability for the growth of monsoon depressions and mid-tropospheric cyclones. Proc. Indian Acad. Sci. (Earth and Planet. Sci.), 89, 79-97.

India Meteorological Department, 1979: Tracks of Storms and Depressions in the Bay of Bengal and the Arabian Sea, 1877-1970.

Keshavamurty, R.N., 1971: On the maintenance of the mean Indian Southwest monsoon circulation and the structure and energetics of the monsoon disturbances. Ph.D. Thesis, Mysore University, India.

Keshavamurty, R.N., 1972: On the vertical tilt of monsoon disturbances. J. Atmos. Sci., 29, 993-995.

Keshavamurty, R.N., Asnani, G.C., Pillai, P.V. and Das, S.K., 1978: Some studies of the growth of monsoon disturbances. Proc. Indian Acad. Sci. (Earth and Planet. Sci.), 87A, 61-75.

Keshavamurty, R.N., Satyan, V., Dash, S.K. and Sinha, H.S.S., 1980: Shift of quasi-stationary flow features during active and break monsoons. Proc. Indian Acad. Sci. (Earth and Planet. Sci.), 89, 209-214.

Krishnamurti, T.N., Kanamitsu, M., Godbole, R., Chang, C.B., Carr, F. and Chow, J.H., 1975: Study of a monsoon depression (I), synoptic structure. J. Met. Soc. Japan, 53, 227-240.

Krishnamurti, T.N., Kanamitsu, M., God bole, R., Chang, C.B., C rr, F. and Chow, J.H., 1976: Study of a monsoon depression (II) Dynamical structure. J. Met. Soc. Japan, 54, 208-224.

Koteswaram, P. and George, C.A., 1958: On the formation of monsoon depressions in the Bay of Bengal. Ind. J. Met. Geophys., 9, 9-22.

Kuo, H.L., 1949: Dynamic instability of two-dimensional nondivergent flow in a barotropic atmosphere. J. Meteor., 6, 105-122.

Lin, C.A., 1980: Eddy heat fluxes and stability of planetary waves: Part I and II. J. Atmos. Sci., 37, 2353 - 2380.

Longuet-Higgins, M.S. and Gill, A.E., 1967: Resonant interactions between planetary waves. Proc. Roy. Soc. A. 299, 120-140.

Lorenz, E.N., 1972: Barotropic instability of Rossby wave motion. J. Atmos. Sci., 29, 258-264.

Mak, M.K., 1975: The monsoonal mid-tropospheric cyclogenesis. J. Atmos. Sci., 32, 2246-2253.

Merkine, L.O. and Israeli, M., 1978: The stability of a stationary Rossby wave in a baroclinic zonal flow. J. Atmos. Sci., 35, 1388-1394.

Miller, F.R. and Keshavamurty, R.N., 1968: Structure of an Arabian sea summer monsoon system. IIOE Met. Monograph No.1, East-West Center Press.

Mishra, S.K. and Salvekar, P.S., 1980: Role of baroclinic instability in the development of monsoon disturbances. J. Atmos. Sci., 37, 383-394.

Ogura, Y., 1964: Frictionally controlled, thermally driven circulations in a circular vortex with application to Tropical cyclones. J. Atmos. Sci., 21, 610-621.

Pedlosky, J., 1964: The stability of currents in the atmosphere and the ocean: Part I. J. Atmos. Sci., 21, 201-219.

Pedlosky, J., 1979: Geophysical fluid dynamics. Springer-Verlag.

Petterssen, S., 1955: J. Meteor., 12, 36.

Pisharoty, P.R. and Asnani, G.C., 1957: Rainfall around monsoon depressions over India. Ind. J. Met. Geophys., 8, 15-20.

Phillips, N.A., 1954: Energy transformations and meridional circulations associated with simple baroclinic waves in a two-level quasi-geostrophic model. Tellus, 6, 273-286.

Raman, C.R.V. and Banerjee, A.K., 1970: A kinematic attempt to forecast summer-time heavy rain in central India. Proc. Symp. Tropical Meteorology, Hawaii, pp.H-VIII - 1-6.

Ramanathan, K.R. and Ramakrishnan, K.P., 1933: The Indian south-west monsoon and the structure of depressions associated with it. Mem. Ind. Met. Dept., 26, 13-36.

Ramanna, G.R. 1969: Relationship between depressions of Bay of Bengal and tropical storms of the China Sea. Ind. J. Met. Geophys., 20, 148-150.

Rao, Y.P., 1976: Southwest monsoon. India Meteorological Department.

Roy, S.C. and Roy, A.K., 1930: Structure and movement of cyclones in Indian Seas. Beitr. Phys. Frei. Atmos., 26, 224-234.

Satyan, V., Keshavamurty, R.N. and Goswami, B.N., 1977: The stability of the monsoon zonal flow with a superposed stationary monsoon wave. Joint IUTAM/IUGG International symposium on monsoon dynamics, Delhi. (Monsoon dynamics. Cambridge University Press, 403-413).

Satyan, V., Keshavamurty, R.N., Goswami, B.N., Dash, S.K. and Sinha, H.S.S., 1980: Monsoon cyclogenesis and large-scale flow patterns over South Asia. Proc. Indian Acad. Sci. (Earth and Planet. Sci.), 89, 277-292.

Sikka, D.R. and Paul, D.K., 1975: A diagnostic study on the structure of monsoon depressions. Geophys. Fluid Dynamics Workshop, Monsoon Meteorology, I.I.Sc., 136-182.

Sharma, M.C. and Srinivasan, V., 1971: Centres of monsoon depressions as seen in satellite pictures. Ind. J. Met. Geophys., 22, 357-359.

Shukla, J., 1977: Barotropic-baroclinic instability of mean zonal wind during summer monsoon. Pure Appl. Geophys., 115, 1449-1461.

Shukla, J., 1978: CISK-Barotropic-baroclinic instability and the growth of monsoon depressions. J. Atmos. Sci., 35, 495-508.

Srinivasan, V., Raman, S. and Mukherji, S., 1971: South-west monsoon - Typical situations over Madhya Pradesh and Vidarbha. I.M.D. FNU Report III- 3.4.

LIST OF PUBLICATIONS

1. The Indian Monsoon: Its Cyclonic Activity and Variability. R.N. Keshavamurty, V. Satyan, B.N. Goswami, S.K. Dash and H.S.S. Sinha, Nuclear India, Vol.17, Nos.3 and 4, 1978, p.6.

2. Shift of Quasi-Stationary Flow Features during Active and Break Monsoons. R.N. Keshavamurty, V. Satyan, S.K. Dash and H.S.S. Sinha. Proc.Indian Acad. Sci.(Earth Planet. Sci.), Vol.89, 1980, p.209-214.

3. Monsoon Cyclogenesis and Large-Scale Flow Patterns over South Asia. V. Satyan, R.N. Keshavamurty, B.N. Goswami, S.K. Dash and H.S.S. Sinha. Proc. Indian Acad. Sci. (Earth Planet. Sci.), Vol. 89, 1980, p.277-292.

4. Stability Analysis of Mean Monsoonal Zonal Flow over North Bay of Bengal. V. Satyan, R.N. Keshavamurty, B.N. Goswami and S.K. Dash. GARP Report No.20, February 1980, p.107.

5. Stability Analysis of Mean Monsoonal Flow over North Bay of Bengal: An Alternative Approach. S.K. Dash, R.N. Keshavamurty and V. Satyan. GARP Report No.20, February 1980, p.108.

6. A Note on the Meridional Temperature Gradients in the Upper Stratosphere at Balasore during Monsoon of 1979. S.K. Dash. Mausam, 1981, Vol. 32, p.322-324.

7. Stability of Mean Monsoon Zonal Flow. S.K. Dash and R.N. Keshavamurty (accepted for publication in Beitr. Phys. Atmosph.).

8. Stability of a Stationary Rossby Wave Embedded in the Monsoon Zonal Flow. S.K. Dash and R.N. Keshavamurty. (sent for publication).

9. Stability of a Stationary Rossby Wave Superposed on Barotropic Zonal Flow. S.K. Dash and R.N. Keshavamurty. (sent for publication)

10. Stability of a Stationary Rossby Wave Embedded in the Monsoon Zonal Flow: Further Studies. S.K. Dash and R.N. Keshavamurty (sent for publication).